Does dynamically modeled leaf area improve predictions of land surface water and carbon fluxes? - Insights into dynamic vegetation modules

Sven A. Westermann[1], Anke Hildebrandt[1,2], Souhail Bousetta[3], and Stephan Thober[1]

[1]Helmholtz Centre for Environmental Research GmbH - UFZ, Computational Hydrosystems, Leipzig, Germany
[2]Friedrich Schiller University Jena, Institute for Geosciences, Jena, Germany
[3]European Centre for Medium-Range Weather Forecasts, Reading, UK

Correspondence: Sven Westermann (sven.westermann@ufz.de)

Abstract. Land-surface models represent exchange processes between soil and atmosphere via the land surface by coupling water, energy and carbon fluxes. As a strong mediator between these cycles, vegetation is an important component of land surface models. Some ~~of these~~ land surface models include modules for vegetation dynamics, which allow the adjustment of vegetation biomass, especially leaf area index, to environmental conditions. Here, we conducted a model-data comparison to investigate whether and how vegetation dynamics in the models improve the representation of vegetation processes and related surface fluxes in two specific models, ECLand and Noah-MP, in contrast to using prescribed values from look-up tables or satellite-based products. We compared model results with observations across a range of climate and vegetation types from the FLUXNET2015 dataset ~~,~~ and the MODIS leaf area product, and used ~~more detailed information regarding~~ on-site measured leaf area from an additional site. Yet, switching on the dynamic vegetation did not enhance representativeness of leaf area index and net ecosystem exchange in ECLand, while it improved performance in Noah-MP only for some sites. The representation of energy fluxes and soil moisture was almost unaffected for both models. Interestingly, the performance regarding ~~vegetation- and hydrology-related variables~~ variables of the carbon and water cycle was unrelated for both models, such that the weak performance of e.g. leaf area index did not deteriorate the performance of e.g. latent heat flux. We show that one potential reason for this could be that the implemented ecosystem processes diverge from the observations in their seasonal patterns and variability. Noah-MP includes a seasonal hysteresis in the relationship between leaf area index and gross primary production that is not found in observations. The same relationship is represented by a strong linear response in ECLand, which substantially underestimates the observed variability. For both water and carbon fluxes, the currently implemented dynamic vegetation modules in these two models did not result in better model performance compared to runs with static vegetation and prescribed leaf area climatology.

Copyright statement.

1 Introduction

Land-surface models (LSMs) represent the energy, water and biogeochemical cycles at the land surface. Traditionally, their main purpose has been to provide a surface component in coupled atmosphere-land models. LSMs are applied in meteorological models, reanalysis products or in the Coupled Model Intercomparison Project (CMIP). However, their scope is widening and new fields of application like historical land cover change simulations (Lawrence et al., 2018) or flood alert services (Harrigan et al., 2020) are arising. There is active development within the land surface modeling community, with more and more features being added to existing models to make them more realistic (Blyth et al., 2021).

Given the wide use of these models and the implications of their results, extensive model validation has been done already. Model validation covers a wide range of water, energy and carbon fluxes at global, regional and site scale (e.g. Niu et al., 2011; Haverd et al., 2018; Lawrence et al., 2019; Boussetta et al., 2021). Such works that introduce individual evaluation schemes are often accompanied by studies that perform comparisons between models (e.g. Best et al., 2015; Krinner et al., 2018). Comparisons like those are conducted for different reasons. For example, one aim is to create a ranking between models that allows the assessment against alternative schemes. Using this method, Best et al. (2015) reported that simple statistical methods achieve a higher performance in energy partitioning at eddy-covariance sites than any single LSM tested. One limitation of that study is that they did not report metrics of individual model performance, but only normalized ones. This procedure does not allow to judge whether the investigated methods have achieved a (dis-)satisfactory performance, since all methods might have a poor individual model performance. Other challenges in these activities are to maintain a standard protocol for model comparison, while not creating a superficial performance contest among them, and to minimize human errors (Menard et al., 2021).

Haughton et al. (2016) more closely explored the cause of poor model performance of LSMs shown in the PLUMBER study by Best et al. (2015), which they presented as the bias for the evaporative fraction (EF) derived from various tower sites exemplarily. From all investigated aspects they concluded that mismatches between modeled and observed heat fluxes are most likely caused by calculations within the models and not related to errors in the observations. Yet, specific reasons for this mismatch, for example over-parameterization, missing processes, calibration issues etc., cannot be identified by benchmarking studies or model rankings alone, but requires further investigation of individual model performance. At the same time, the causes of poor model performance can be multifaceted, rendering their identification challenging (Haughton et al., 2018b). Nonetheless, further LSM development needs understanding of how individual process implementation and parameterization affect model performances.

A wealth of studies evaluated different LSMs with respect to radiation, heat fluxes or surface temperature, and carbon fluxes. Carbon fluxes like gross primary production (GPP) are often validated by using global gridded fluxes like FLUXCOM (Ma et al., 2017; Jung et al., 2019; Lawrence et al., 2019). The correct implementation of ecosystem processes and related variables is crucial for using LSMs in assessing impacts due to climate change for example in drought evaluation (Ukkola et al., 2016; Dirmeyer et al., 2021) because plant transpiration directly links the terrestrial carbon and water cycle. For example, a substantial underestimation of evapotranspiration by eight LSMs during drought conditions was shown across different plant communities (Ukkola et al., 2016). De Kauwe et al. (2015) concluded from their simulations of drought responses for the

European FLUXNET sites with the Community Atmosphere Biosphere Land Exchange (CABLE) model that accounting for differing drought sensitivity of plant communities into LSMs may be required to correctly capture drought impacts. Currently, most LSMs are not able to represent direct vegetation control on surface exchange, in part because they under-represent biophysical responses to changing water availability and oversimplify vegetation dynamics, in particular leaf area index (LAI) (Forzieri et al., 2020). LSMs typically work with climatological LAI, e.g. seasonality read from look-up table files, or calculate LAI as a prognostic variable internally. At the same time, LAI has a large impact on both water and carbon fluxes (e.g. Fisher et al., 2014), and an understanding of how its parameterization impacts flux estimates by LSMs would help to shed light on the known discrepancies in representing vegetation.

Here, we investigate model performance for water and carbon fluxes with a focus on vegetation processes. We additionally check the reasons for model-data mismatch, by analysis of the underlying computer source code of the models (as stated by Dirmeyer et al. (2018)), which can only be done for a limited set of models due to the large effort that is needed. For this scope, we chose ECLand and Noah-MP as frequently used and continuously developing LSMs with available modules for vegetation dynamics. In this manuscript, we aim to answer the following research questions: (1) Does the representation of net ecosystem exchange (NEE) and LAI improve, if LSMs represent vegetation dynamically? (2) How does dynamic vegetation in the LSMs impact other variables like heat fluxes and soil moisture? Do improvements in model performance for one variable compromise performance for other variables? (3) What are the mechanics behind modeled temporal patterns in vegetation dynamics and occurring misfits to the observations?

2 Methods

2.1 Data basis

Site selection

The FLUXNET2015 dataset (Pastorello et al., 2020) provides measurements from globally distributed eddy covariance sites. We selected a subset from all ~~the~~ available FLUXNET sites, focusing on sites with long observation periods, covering different vegetation types and a gradient in aridity within each vegetation type. Vegetation types within FLUXNET rely on the IGBP Land Classification (National Center for Atmospheric Research, 2022). The aridity index ~~(AI)~~ of all sites was retrieved from the CGIAR-CSI Global-Aridity and Global-PET Database (Trabucco and Zomer, 2018) and inverted afterwards, bringing it back to the ~~initial~~ definition as the ratio of the long-term mean annual potential evapotranspiration to the long-term mean annual precipitation by Budyko (1974). We excluded sites with observation periods less than six years because they might not represent the local climate (Haughton et al., 2018a) and extreme years could create a systematic bias. Due to the small number of sites per vegetation type with long observation periods, the vegetation types savanna (SAV), woody savanna (WSA) and open shrubland (OSH) were merged into one savanna group before continuing with the selection procedure. For each vegetation type or group, first, we chose the site with the longest observation record. Next, other sites with similar aridity (± 0.1 logarithmic ~~AI~~aridity index) were dropped to avoid an overrepresentation of some vegetation type-aridity combinations due to heterogeneous site

distribution within FLUXNET. We used logarithmic values to create a linear scale of the ~~AI, avoiding an overrepresentation of drier sites within the selection process~~aridity index so that a selection of too many dry sites was prevented. Afterwards, we repeated these steps for the remaining sites and continued until no more sites were available for selection in this vegetation type or group. For the selected sites, we double-checked data availability and quality and replaced with an alternative site if necessary. The most common reasons for discarding sites were missing or poor quality soil moisture data or low-quality gap-filling, which reduced the length of the observation record below the threshold of six years. By doing so, only two sites with mixed forests (MF) were left which is critically few. Thus, we included all MF sites into the deciduous broadleaf forest (DBF) vegetation type and repeated the selection for this group. We were left with 24 sites, covering a ~~range of aridity and vegetation types with varying observation periods , as shown in Figure 1and, thus, we assumed them to be neither very predictable nor very unpredictable in total, as recommended by Haughton et al. (2018a).~~ wide range of site characteristics as recommended by Haughton et al. (2018a) including aridity, vegetation types and observation periods (Fig. 1). Additionally, we also used data of the eddy covariance site "Hohes Holz" (Rebmann and Pohl, 2023) which is part of the TERENO Harz/Central German Lowland Observatory (Wollschläger et al., 2016) and is included in the ICOS network since 2019, because on-site measured LAI data was available for that DBF site.

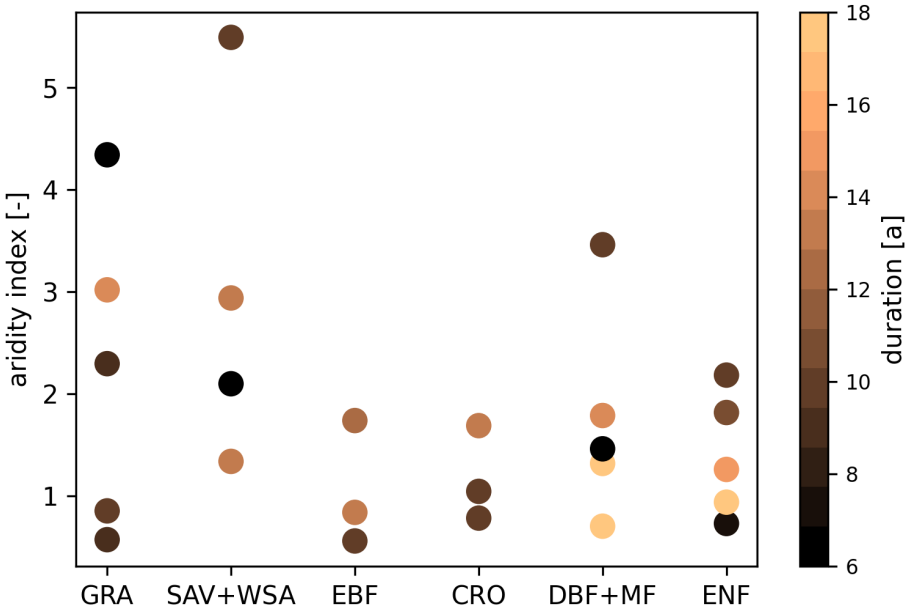

Figure 1. Selected FLUXNET sites grouped by their vegetation type. For each group, sites were chosen to cover a gradient in aridity (y-axis) if available. The vegetation types are: GRA - grassland, SAV - savanna, WSA - woody savanna, EBF - evergreen broadleaf forest, CRO - cropland, MF - mixed forest, DBF - deciduous broadleaf forest, ENF - evergreen needleleaf forest. The color scale represents the duration of the available time series in years.

Variables used and data pre-processing

From the FLUXNET (Pastorello et al., 2020) and Hohes Holz (Rebmann and Pohl, 2023) datasets, air temperature, downward short- and long-wave radiation, wind speed, relative humidity, air pressure and precipitation were used for model forcing. Turbulent fluxes, i.e. latent heat flux (LE) and sensible heat flux (H), as well as net ecosystem exchange (NEE), gross primary production (GPP) and volumetric soil water content in 10 cm depth were used for model evaluation. All data were provided and used at half-hourly resolution. FLUXNET data was retrieved from their website (fluxnet.org, 2020).

LE and H in FLUXNET2015 are available in two different variables: One is a product that corrects the turbulent fluxes for energy balance closure, while the other one provides a continuous time series filled by Marginal Distribution Sampling. We decided to use the first one as long as they were available in the dataset since LSMs also consider for energy balance. Missing data in the "Hohes Holz" meteorological dataset was filled using a Kalman filter (Sayed, 2003) for short gaps up to 3 h, except for precipitation which was set to 0. For longer gaps, the Kalman procedure ~~tent~~ tends to overestimate the observations which resulted in offsets at the end of the filling periods. Thus, filling data for these gaps was retrieved from the ERA5 (Hersbach et al., 2020) data product ~~(via Climate Data Store API from Copernicus, ©2018 ECMWF)~~ (Copernicus, 2018) with 0.1° spatial and 1 h temporal resolution.

For calculation of the evaporative fraction $\frac{LE}{LE+H}$, all time steps with $H \leq 0$ were excluded. The same time steps were left out for LE to focus the comparison of turbulent fluxes on periods with evaporative demand. For estimation of model performance, we excluded gap filled periods that were longer than one month.

2.2 Model description

We investigated how dynamic vegetation affects model outputs in two land-surface models capable of representing both static and dynamic vegetation: ECLand (Balsamo et al., 2009; Dutra et al., 2010; Boussetta et al., 2021) and Noah-MP (Chen and Dudhia, 2001; Ek et al., 2003; Niu et al., 2007, 2011).

ECLand

The European Centre for Medium-range Weather Forecasts (ECMWF) developed a Carbon-Hydrology Tiled Scheme for Surface Exchanges over Land (CHTESSEL) (Balsamo et al., 2009; Dutra et al., 2010; Boussetta et al., 2013) which represents the land component of the Integrated Forecasting System (IFS). As part of the IFS, CHTESSEL has evolved into a more flexible system ECLand (Boussetta et al., 2021), which also allows for several modular extensions. Among these, a dynamic vegetation module simulates the temporal evolution of vegetation. Therein, LAI, vegetation biomass and vegetation coverage are calculated from the daily carbon budget, instead of taking them from the climatological LAI. However, LAI climatology can still be used for fully static or partly dynamic simulations.

In ECLand (IFS version “CY46R1”), each of the 19 vegetation types receives its own parameter values (e.g. for roughness lengths, stomata resistance, root distribution) from look-up tables (Boussetta et al., 2012, 2021). These vegetation types are categorized into high or low vegetation. Each grid-cell has one dominant high and one dominant low vegetation type, together

forming the vegetation of a grid-cell (Balsamo et al., 2009). Surface fluxes are computed for the high and low vegetation tiles separately then merged for the whole grid-cell according to their fractional cover. The vegetation coverage is calculated from a prescribed climatological vegetation fraction (part of input) and a vegetation type dependent density (from look-up table) and corrected by current LAI (Boussetta et al., 2021). Net assimilation results from carbon uptake of atmospheric CO_2 by the current leaf area (defines absorbed radiation) and is restricted by environmental factors such as soil moisture and nitrogen availability (important equations can be found in section A.01). Together with the dark respiration and after scaling with a quantum use efficiency factor, potential gross assimilation is calculated. This value, then, is linearly linked to LAI and the humidity-corrected air density, resulting in gross primary productivity (GPP). With activated vegetation dynamics, a potential net assimilation, together with LAI, forms a damping factor for biomass senescence. Biomass senescence is determined from current biomass, linearly linked to current LAI, and the damping factor. The change in biomass results from this updated biomass and the net assimilation. Then, biomass is updated again and linearly transferred into updated LAI by using specific leaf area from a look-up table (Boussetta et al., 2021). For static ECLand, the prescribed climatological LAI is used. LAI in ECLand determines the canopy resistance for water vapour transport and thus, the evapotranspiration as well as the interception (Boussetta et al., 2012, 2013, 2021).

Noah-MP

Noah-MP is the widely used community Noah land-surface model (Chen and Dudhia, 2001; Ek et al., 2003) with multi-parameterization options (Niu et al., 2007, 2011). Predicted LAI in Noah-MP is calculated based on leaf carbon allocation and specific leaf-area per vegetation type (Ma et al., 2017). In contrast to ECLand, Noah-MP can either use prescribed LAI values per vegetation type or depend solely on dynamic LAI estimates, without the option to mix between the two.

In Noah-MP (version "HRLDAS 3.9"), ~~parameterization~~ parameter values (e.g. value range of stomatal resistance, number of rooted soil layers, specific leaf area) of the 27 vegetation types ~~is~~ are taken from look-up tables. The vegetated sub-grid area of each grid cell is dominated by one vegetation type forming a one-layer canopy. Calculation of canopy interception and transpiration consider aerodynamic and stomatal resistances for the water vapour and carbon fluxes within the canopy and between the canopy and the atmosphere (Ma et al., 2017). Among others, stomatal resistance is predominantly controlled by photosynthesis (Niu et al., 2011) which depends on leaf area, and is limited by light and root zone soil moisture (important equations can be found in section A.02). Assimilation depends on LAI and is constrained by physiology and light availability. Assimilated carbon is allocated to different plant tissues (leaf, stem, wood, root), forming GPP, and reduced by respiration, dying and turnover processes such as drought stress and senescence representing leaf dynamics (Dickinson et al., 1998). Respiration rate is determined by LAI, GPP, temperature and soil moisture stress. Carbon that is allocated to leaves together with biomass losses forming an updated leaf biomass which converts into the LAI by using specific leaf area (Ma et al., 2017). Carbon assimilation and allocation and, thus, also GPP and NEE estimation are usually deactivated for the static Noah-MP since a prescribed LAI is given. We adapted the model code in a way that GPP and NEE for the static simulations are calculated anyways, but resetting all variables that would be dynamically predicted within the same function.

2.3 Model setup and simulations

Simulations with activated modules that predict LAI time series will be *activated vegetation dynamics* or *dynamic ECLand* and *dynamic Noah-MP* hereafter. For both models, the reference height (level of the forcing input) was set to the flux tower height of the sites which depends on the vegetation type. The models were set up as closely as possible to the available site information but there are some technical differences in the structure of the model input, i.e. in the initial files. Forcing and model calculation were done in 30 minutes resolution if available, otherwise, hourly resolution was applied. We used four layered soil representation and used the uppermost layer for evaluation of soil moisture which is 7 cm and 10 cm deep for ECLand and Noah-MP, respectively. Every simulation started with a ten year spin-up phase by recalculating the first year.

ECLand

We used ERA5-based (Hersbach et al., 2020) global initial data for ECLand and selected the grid cells where the flux towers are located. These initial files contain information on albedo, orography, soil type, surface roughness and monthly LAI which is not available in the FLUXNET metadata. For the simulations that use alternative LAI forcing, monthly LAI in the initial files was replaced by the scenario specific alternative values (see section 2.3). We defined the vegetation on that grid-cell to be either high or low vegetation (and not a mixture) depending on the site information. Forests and savannas were treated as high vegetation types while grasslands and croplands were allocated to low vegetation types. The vegetation type that fits most to the FLUXNET characterization was selected (see Tab. 1). The coverage of that vegetation type was set to 100 %. Meteorological forcing was taken from the FLUXNET/TERENO data sets mentioned above (section 2.1). The ECLand simulations were done with van Genuchten soil hydrologic parameters (van Genuchten, 1980), activated sub-grid surface runoff and activated snow parameterization.

Table 1. Assignment of vegetation types used in ECLand and in Noah-MP and referred initial LAI. The values in brackets for Noah-MP initial LAI refer to sites on the Southern Hemisphere due to shifted seasons.

Fluxnet vegetation type	ECLand vegetation type	ECLand vegetation class	Noah-MP USGS	Noah-MP vegetation class	Noah-MP initial LAI
ENF	Evergreen Needleleaf Trees	3 (high)	Evergreen Needleleaf Forest	14	4.0
MF	Mixed Forest/Woodland	18 (high)	Mixed Forest	15	2.0 (4.3)
DBF	Deciduous Broadlead Trees	5 (high)	Deciduous Broadleaf Forest	11	0.0 (4.5)
EBF	Evergreen Broadleaf Trees	6 (high)	Evergreen Broadleaf Forest	13	4.5
SAV	Interrupted Forest	19 (high)	Savanna	10	0.3 (3.8)
WSA	Interrupted Forest	19 (high)	Savanna	10	0.3 (3.8)
CRO	Crops, Mixed Farming	1 (low)	Mixed Dryland/Irrigated Cropland and Pasture	4	0.0 (3.0)
GRA	Tall Grass	7 (low)	Grassland	7	0.4 (3.5)

Noah-MP

Soil type for ~~the~~ Noah-MP was taken from ~~the~~ a global soil grid (Hengl et al., 2014) by selecting the grid cell including the flux tower location. Initial values for temperatures and soil moisture were taken as the FLUXNET/TERENO observations at January 1st 00:00 h in the first year of the simulation period. Vegetation types were chosen to match as closely as possible the USGS vegetation types (University Corporation for Atmospheric Research, 2023) and the initial LAI values were set according to the defaults in the parameter file (see Tab. 1). Vegetation cover fraction was set to 100 % so that the entire grid-cell represents the vegetation type of the observation site. Minimum green vegetation fraction was set to 1 % to ensure that not the whole vegetation cover dies during winter which would hinder temperate short vegetation from growing in spring. For the simulations with alternative LAI forcing, the monthly LAI in the look-up table was replaced by the scenario specific alternative values (see section 2.3). The Noah-MP simulations were done with soil parameterization from look-up tables, Ball-Berry stomatal resistance approach (Ball et al., 1987; Bonan, 1996) ~~and~~ with using matric potential ~~therefor and fully implicit canopy surface temperature time schemes. Other options were used as their defaults.~~ limitation. All other selected options can be found in Table 2.

Table 2. Options chosen for Noah-MP parameterization.

Physical process	Noah-MP Option
Runoff and groundwater	TOPMODEL with groundwater (Niu et al., 2007)
Surface layer roughness	Monin-Obukhov
Supercooled water	no iteration (Yang and Niu, 2006)
Radiative transfer	two-stream (vegetated vs. vegetation-free)
Snow albedo	fresh snow with aging effects
Rain/snow partitioning	threshold temperature at 2.2 $^{\circ}C$
Lower boundary for soil temperature	temperature at 8 m depth (part of input)
Snow/soil temperature time scheme	fully implicit (original Noah)
Surface resistance for evaporation	Sakaguchi and Zeng (2009)
Glacier treatment	phase change of ice included

Leaf area index data and scenarios

Monthly LAI values are part of the initial input of both models via look-up tables. These tables contain annual cycles of LAI for each vegetation type separately. This *default climatology* is already based on values from MODIS. For ECLand, the gridded values of LAI were disaggregated to the high and low vegetation type of the grid cell for the time span 2000-2008 (Boussetta et al., 2013). ~~LAI values in the look-up table of Noah-MP are defined for each plant functional type and were created by disaggregating MODIS observations (Oleson et al., 2010).~~ For alternative LAI inputs, these values in the look-up tables were replaced manually.

LAI values were taken from the MOD15A2H data product from NASA's EarthData portal (Myneni et al., 2015). One grid cell of $500\ m$ x $500\ m$ was selected per eddy covariance tower according to the site coordinates and LAI values with temporal resolution of eight days were extracted for the years 2000 to 2014. To assure reliability of the values, the "MODIS15A2H" data product comes with numeric quality flags. Although Fang et al. (2012) recommend using all values with quality flags less than 64, we excluded data with quality flag 8 because many of these LAI values were extremely low during the vegetation period which is unrealistic. Then again, due to lacking LAI values during winter or wet seasons, values with quality flags of 73 (empirically filled with clouds present), 81 (empirically filled with mixed cloudiness) and 97 (empirically filled for other reasons) were included as a trade-off between excluding as much bad-flagged data as possible and keeping roughly the same amount of data values for each month (see MODIS documentation for more details). Afterwards, we smoothed the remaining values by using a Savgol filter (window length: 11, polyorder: 2) (similarly done by e.g. Xiao et al., 2011; Huang et al., 2021) from the scipy-package (Savitzky and Golay, 1964; Luo et al., 2005) and prepared a mean annual LAI cycle for all available years with monthly resolution, further named *MODIS climatology*. For an additional experiment, the monthly LAI from MODIS of each year within the simulation period separately was used as input, called *MODIS single-year* from this point on. Missing LAI values for a month were filled by the average value of the adjacent months. If LAI values for at least two consecutive months were not available, the LAI values from the default look-up table were used for those months.

For the "Hohes Holz" site, on-site measured LAI data was available from Digital Cover Photography (DCP), which was shown to yield comparable results to established methods (Piayda et al., 2015). For each measurement date, we averaged the values from the whole plot area and, afterwards, calculated monthly means over time span 2014-2019. This alternative LAI forcing will be called *on-site LAI* hereafter. The nomenclature of all LAI scenarios can be found in Table 3.

Table 3. Nomenclature of all model scenarios using LAI data sources.

Term	LAI source
default climatology	default monthly LAI for the dominant high and low vegetation type on respective grid cell (ECLand) or default monthly values per vegetation type from look-up table (Noah-MP)
MODIS climatology	mean annual cycle of monthly LAI values derived from MODIS dataset from 2000 to 2014
MODIS single-year	same as before but without averaging, resulting in an annual cycle for each year separately within the observation period
on-site LAI	mean annual cycle of monthly LAI values based on on-site measured LAI

The MODIS LAI was also applied for model evaluation but in its high temporal resolution of eight days. Due to the usage of single day values, we solely used data with quality flags 0 (no issues) and 32 (saturated) and refrained from smoothing. Gaps were left as they were. For the static runs, comparison with MODIS LAI on daily basis provides the information how well a LAI climatology represents the local LAI evolution and whether an incorporation of more site-specific climatology can improve the representativeness. For the dynamic simulations, comparing modeled LAI with daily MODIS values is used to examine whether the models are able to capture inter- and intra-annual LAI dynamics.

2.4 Performance evaluation

Model outputs and observational data from the flux towers were averaged/summed to daily values for direct comparison. For LAI, we calculated the eight-day mean of the LAI model output to correspond to the temporal resolution of the MODIS LAI estimates. As performance criteria we used the Pearson's correlation coefficient, the normalized standard deviation and a modified relative bias for the model-observation relationship. Pearson's correlation coefficient R describes the fit between model and observation values (Benesty et al., 2009) and is calculated from the numpy-package. The normalized standard deviation s_n is the ratio of the standard deviation of the model predictions and the standard deviation of the observations. It is used to describe the models' ability to reproduce the variability of the observations. The relative bias b applied here was adapted to the domain of the variable to avoid division by zero or by values very close to zero (especially important for NEE). ~~Therefore~~For this purpose, the distribution of the observed values was shifted by their minimum, resulting in only positive values with a minimum of zero:

$$b = \frac{\overline{y - x}}{\overline{x} - \check{x}} \tag{1}$$

whereby y represents the model predictions, x the observations, $\overline{x}$ the mean and $\check{x}$ the minimum of the observed values. To compare the model performance of simulations with static and dynamic vegetation, we determined the change in relative bias as follows:

$$\Delta b = |b_{static}| - |b_{dynamic}| \tag{2}$$

Negative values mean that the relative bias of the dynamic simulation was greater than that of the static simulation and, thus, that the performance was reduced by activating vegetation dynamics.

To investigate the sensitivity of dynamically modelled vegetation on the model performance, we checked how strongly the quality of the model simulation of one target variable (e.g. LE) depends on the model quality of another one (e.g LAI). For this, we used the *elasticity* as a metric. Elasticity is calculated as ratio of the change in one statistical measure (analogous to equation 2) for two different target variables:

$$E = \frac{\Delta m_i}{\Delta m_j} \tag{3}$$

where m is one of the statistical measures mentioned above, i.e. R, s_n or b, while i and j denote different target variables, e.g. GPP or LE. For variables that are strongly related, like LAI and GPP, we expect elasticity to be positive. Two variables are

considered independent if $-0.1 \leq E \leq 0.1$ because the change in m_j then would need to be larger than one order of magnitude to cause a change in m_i. Changes in model performances of the target variables were plotted in Taylor diagrams (Copin, 2021).

3 Results

3.1 Effect of dynamic or prescribed leaf area index on leaf area and carbon uptake prediction

Figure 2 shows the quality metrics for the model performance regarding LAI in a Taylor diagram. The location an optimal model simulation would occupy is indicated with a star. The model performance of the dynamic run is shown with the symbols, while the static runs can be read from the start of each arrow. The direction and length of each arrow highlights the difference in the performance metrics between static and dynamic runs. Shown are simulations started (dynamic) or run (static) with *default* vs. *MODIS climatology*.

While in the Noah-MP simulations with static vegetation the model performance depended on the LAI forcing applied, the simulation results were unaffected by the type of LAI forcing with vegetation dynamics switched on ~~(Fig.~~since the symbols in Figure 2 c ~~+d)~~and d have the same positions. For ECLand, this was also the case for many sites but not all, e.g. *AT-Neu* and *AU-How* (Fig. 2 a+b). Initializing ECLand with *default climatology* (Fig. 2 a) and activating vegetation dynamics generally increased the variance of simulated LAI compared to static simulations but it also decreased model performance, e.g., mean Pearson correlation decreased from 0.72 to 0.62. At the same time, whether the predicted LAI fit better to MODIS observations than *default climatology* was ambiguous, as can be seen by the shift in relative bias which ranged between -0.5 and 1.3. On the contrary, the results for Noah-MP showed a different pattern (Fig. 2 c) because there was no clear shift to higher variances or worse correlation when activating vegetation dynamics. Especially short (GRA+CRO) or sparse (SAV+WSA) vegetation types had the highest changes towards decreased but also enhanced model performance for LAI. For other sites (mostly forests), modelled dynamic LAI correlated well with the observations.

For both models, using *MODIS climatology* instead of *default climatology* in static simulations resulted in the best performances with regard to LAI of all simulations (start of the arrows in Fig. 2 b+d), e.g., the mean correlation coefficient increased to 0.83 and 0.84 and mean relative bias (Tab. A1) improved to -16% and -2% for ECLand and Noah-MP, respectively. This can be expected because MODIS was also used as reference dataset for LAI evaluation. With activated vegetation dynamics, the performance of both models decreased, as all quality metrics shift away from the point indicating best performance in the Taylor diagram (Fig. 2 b+d). The same applied to the relative biases of LAI since their shift was predominantly negative. In other words, switching on vegetation dynamics did not result in improved LAI representation compared to just using *MODIS climatology*.

Forest ecosystems, in general, were better represented by model predictions with vegetation dynamics than short or sparse vegetation. Figure 3 shows the results of the forest site "Hohes Holz" in more detail. Although the representation of LAI variability detoriated when simulating dynamic vegetation with Noah-MP, those runs resulted in LAI predictions that closely match MODIS observations (Fig. 3 d-f), represented by a relative bias of -18% and a correlation coefficient of 0.78. ECLand more generally suffered from larger relative biases in LAI, especially when simulating with vegetation dynamics (-30% on

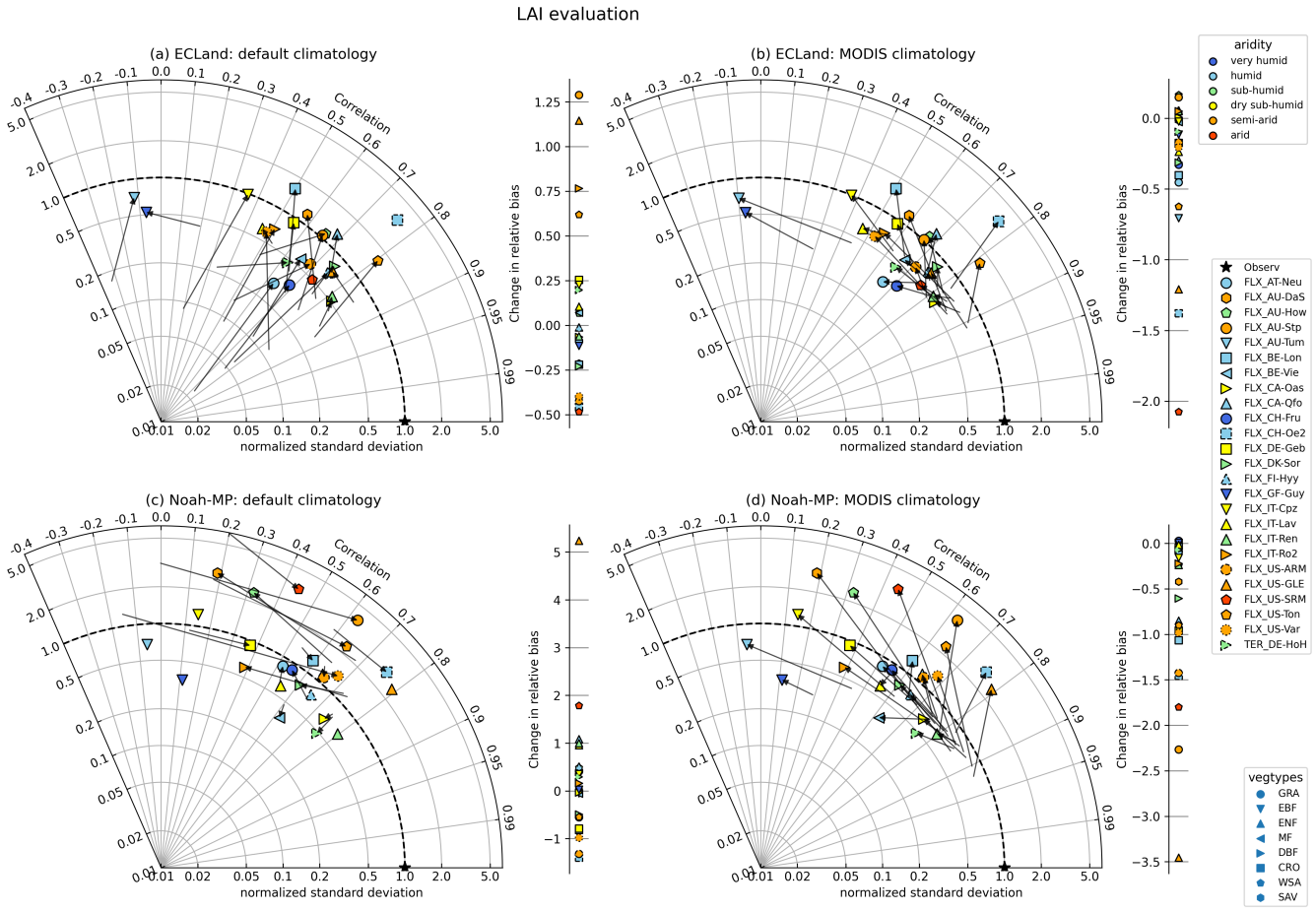

Figure 2. Change of model quality metrics for LAI when switching on vegetation dynamics for all included sites and by using *default climatology* (left) or *MODIS climatology* (right). The star ("Observ") marks the location of the perfect correlation between observation and model and perfect agreement between observed and modelled variance. The model performance of the static runs can be read from the start of each arrow. When no arrow appears, either no correlation could be calculated (e.g. for evergreen forests where default climatological LAI is constant) or values could not be placed on the logarithmic axis. The ~~point~~ symbol colors indicate the site aridity (top right legend) as following: very humid - ~~$AI < 0.6$~~aridity index (AI) < 0.6, humid - $AI < 1.25$, sub-humid - $AI < 1.54$, dry sub-humid - $AI < 2$, semi-arid - $AI < 5$, arid - $AI \geq 5$ (Ashaolu and Iroye, 2018). Vegetation types are symbolized by different marker types (bottom right legend).

average, Fig. 3 c). The only scenario where model performance generally increased for ECLand, was through switching on vegetation dynamics compared to static runs with *default climatology*.~~Statistical measures for die variables LAI, NEE and GPP of the model runs for the site "Hohes Holz". The categories on the y-axis mark the different LAI forcings. Statistical measure of the static and dynamic simulations of the same variable are connected by a horizontal line. The red dotted vertical line marks the optimum of each measure.~~

In contrast to LAI, the model performance of ecosystem exchange variables in ECLand was less affected by activating vege-

tation dynamics. A common feature is that the variance predominantly increased when using dynamic vegetation (Fig. 4 a+b). Mostly, sites with short or sparse vegetation reacted more sensitively to dynamic vegetation modeling in their NEE and GPP representation especially when forcing with *MODIS climatology*, which is indicated by the longer arrows in ~~Fig.~~Figure 4 a and b (for GPP see Fig. A1 in Appendix). For forest ecosystems in general, the changes in the model performance of NEE and GPP were small, as also shown for the site "Hohes Holz" (Fig. 3 a-c). Nevertheless, the performance of NEE (and GPP) decreased when activating vegetation dynamics, mainly driven by lowered correlation coefficients, on average from 0.41 to 0.37 (0.72 to 0.68). Only three sites showed improvements in NEE representation when predicting with dynamic ECLand and just one did so for GPP. Relative bias changed in both directions, towards lower and higher model performance. Dynamic ECLand mainly overestimated NEE by 11% on average, indicating that ecosystems were predicted to be a smaller carbon sink than observed (Tab. A2). Instead, dynamic Noah-MP estimated on average 10% lower NEE compared to the observations for the most sites (Fig. 4 c+d, Fig. 3 c+f).

~~Overall,~~ Activating the dynamic vegetation affected the model performance of NEE and GPP for Noah-MP heterogeneously. Some sites showed very small changes (e.g. *IT-Lav* and *IT-Ren*, Fig 4 c+d) while model performance of NEE was largely impacted by vegetation dynamics for other sites (e.g *US-Var* and *AU-DaS*). In contrast to ECLand, no evidence could be found that certain vegetation types or aridity classes were more sensitive to activated vegetation dynamics in Noah-MP and even forests showed larger changes in model performance (Fig. 3 e). While, for GPP, the variance predominantly enlarged by activating vegetation dynamics in Noah-MP (Fig. A1 c+d), the normalized standard deviation of NEE changed in opposing directions which is another difference compared to ECLand. Despite the higher sensitivity of NEE model performance to Noah-MP vegetation dynamics, the overall model performance was barely affected since relative bias shifted from -12 % to -11 % and correlation coefficient from 0.50 to 0.53 on average. Changes of statistical measures can be in opposing directions as can be seen for normalized standard deviation and relative bias of the forest site "Hohes Holz" (Fig. 3 e+f) which eliminated trends towards improved or reduced model performance. Only the site *AU-Stp* clearly improved regarding NEE representation by activating vegetation dynamics in Noah-MP by initializing with either *default* or *MODIS climatology*. The GPP performance showed small improvements by activating vegetation dynamics in Noah-MP as the mean correlation coefficient shifted from 0.68 to 0.74 and the range of the relative bias was lowered from -32 % $-$ $+69$ % to -28 % $-$ $+42$ %.

In general, Noah-MP seemed to capture NEE representations better as the ~~values scattered more closely to~~ mean deviance from a normalized standard deviation of 1 ~~in the Taylor diagram~~ was 0.33 (ECLand: 0.39) and showed with 0.51 a higher correlation coefficient on average than ECLand (Fig. 4 c). Remarkably, the four and the ~~eight~~ nine best sites regarding NEE ~~representation~~ correlation and variance were forests for ECLand and Noah-MP, respectively. At the same time, all evergreen broadleaf forests suffered from low performance in both models. GPP representation in both models was better than for NEE (Fig. A1, Tab. A3). ~~However, whether switching on vegetation dynamics in Noah-MP improves carbon fluxes cannot be evaluated because they are only calculated for dynamic but not for static simulations (see also section 2.2). Overall,~~ Overall, static and dynamic Noah-MP performed well in representing NEE and GPP for most forest sites apart the evergreen broadleaf forests.~~Same as Taylor diagram before but with NEE evaluation. Since NEE is not generated as variable from Noah-MP when running the model without dynamics, no change in statistical measures can be presented.~~

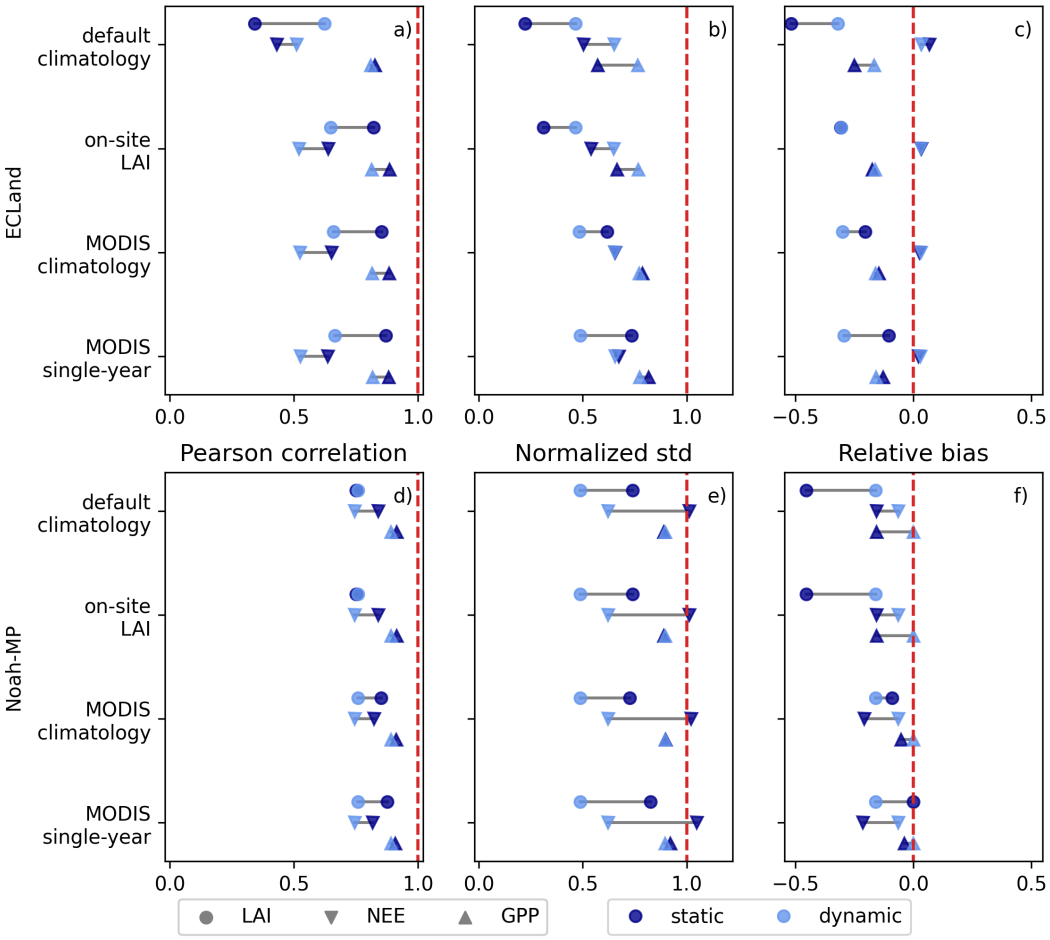

Figure 3. Statistical measures for the variables LAI, NEE and GPP of the model runs for the site "Hohes Holz". The categories on the y-axis mark the different LAI forcings. Statistical measure of the static and dynamic simulations of the same variable are connected by a horizontal line. The red dotted vertical line marks the optimum of each measure.

~~Consistent with~~ In line with the finding that model performances of dynamic Noah-MP ~~being~~ were independent of the prescribed LAI forcing, the availability of *on-site LAI* data for the site "Hohes Holz" yielded no improvement in the representation of NEE or GPP compared to other LAI climatology (Fig. 3). The same appeared for dynamic ECLand. Forcing static ECLand with *on-site LAI* data resulted in NEE and GPP correlation and relative bias comparable to the forcing with *MODIS climatology*, only variability was lower.

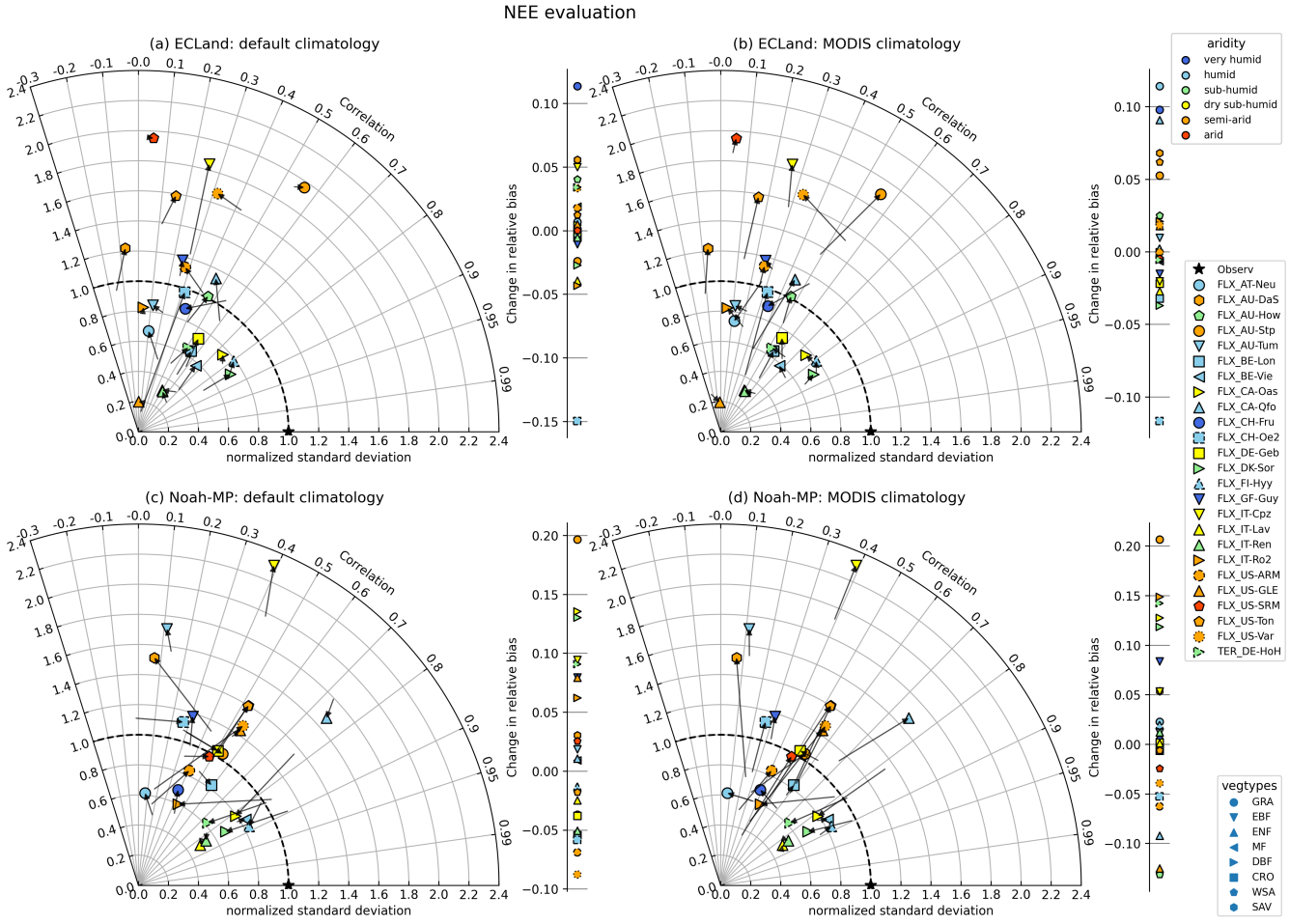

Figure 4. Same as Taylor diagram before but with NEE evaluation.

3.2 On the sensitivity of heat fluxes and soil moisture in LSMs to vegetation dynamics

For both models, activating vegetation dynamics had a small impact on the representation of turbulent fluxes and soil moisture. The strongest changes occurred for short or sparse vegetation types or for drier climates which had the largest arrows in the Taylor diagrams (Fig. 5, Fig. 6). In ECLand, activating vegetation dynamics enhanced the variance of latent heat flux for the most sites (from 0.80 and 0.84 to 0.94 on average for *default* and *MODIS climatology*, respectively), but correlation between simulated and observed values remained unaffected or even diminished (mean change smaller than -0.03). For several sites, LE estimates from dynamic ECLand better represented the observations as shown by the positive shift in relative bias (reduction from -32% to -21%) (Fig. 5 a, Tab. A4), but no relationship regarding vegetation type or site aridity can be seen and changes are small in general~~, except~~ . The big exception appeared for *CH-Oe2* ~~. Change of statistical measures for LE modeling when switching on dynamic vegetation for all included sites and by using *default climatology* (left) or *MODIS climatology* (right) as~~

~~forcing.~~ which was caused by its default LAI climatology that did not fit the vegetation type.

Activating vegetation dynamics in Noah-MP hardly affected model performance of LE (mean change in correlation was 0.02, in standard deviation 0.00 and in relative bias 0.02). Sites that showed some sensitivity predominantly have drier climate (e.g *AU-Stp*, *US-Var*, see Fig. 5 c). Several sites showed less bias in LE predictions when using dynamics vegetation predictions in Noah-MP. When using *MODIS climatology* as LAI forcing, activating vegetation dynamics could be advantageous for some sites regarding LE representation (*AU-Stp*, *CH-Fru*, *US-GLE*), but mostly it would not lead to higher model performance.~~Same as before but for evaporative fraction which represents the turbulent flux partitioning.~~

Model performance regarding the evaporative fraction (EF) was lower compared to LE as points are further away from the point of optimal model performance (Fig. 6). Running ECLand with activated vegetation dynamics lowered the representation of the evaporative fraction which is demonstrated by many points in the Taylor diagram drifting away from the star indicating best performance. Thereby, the mean standard deviation changed from 0.95 to 1.08 and correlation coefficient was reduced slightly from 0.48 to 0.46 on average (Fig. 6 a+b). Exceptions were *BE-Lon*, *US-SRM* and *US-Ton* where model performance slightly improved regarding correlation and variability. Again, relative bias of EF changed in both directions without any trend regarding vegetation type or aridity for both models (see also Tab. A5). For Noah-MP, eight sites showed an improved representation of the evaporative fraction when running the model with vegetation dynamics. This amount was reduced to six when the model was initialized with *MODIS climatology*. But changes were very small on average.

Regarding soil moisture, the model performance was almost insensitive to the used vegetation dynamics option or the type of LAI forcing for both models (Fig. A2). ~~Despite being low, some~~ Some sites showed improvement of soil moisture prediction by activating vegetation dynamics for both models although the improvement was very weak. Interestingly, no humid site was among them. However, the simulation of soil moisture resulted in a broad range of model performances starting with very well-fitting predictions ($R > 0.9$, $b \approx 0\%$) up to very poor-fitting predictions ($R < 0.2$, $b < -40\%$ or $b > 100\%$, see Tab. A6).

To investigate the sensitivity of dynamically modeled vegetation on the model performance, we checked how strongly the quality metrics of NEE, GPP, LE and soil moisture change with the quality metrics of LAI~~and NEE~~. For this, we used the elasticity (defined in equation 3) as a metric which is summarized for all sites in Figure 7. Surprisingly, the quality metrics of those closely related variables were independent from each other, i.e. the elasticity was very low (within grey band) or randomly distributed around zero. The strongest connection of all pairs tested ~~was between GPP and LE in ECLand~~ could be found for the correlation coefficient between LAI and GPP in ECLand when using *MODIS climatology* but without affecting normalized standard deviation or relative bias. Here, the mean elasticity of correlation and normalized standard deviation is positive, meaning that, as expected, an increased model performance in ~~LE~~ LAI co-occurs with enhanced performance for GPP in the same order of magnitude. ~~For the GPP-LE relation, even the elasticity of the relative bias is positive which underlines the co-relation of GPP and LE performances in ECLand. However,~~ In a similar manner, NEE and LAI performance were positively related regarding correlation coefficient in Noah-MP. Other elasticity values that include LAI were small predominantly. ~~Only the correlation coefficient as model performance metric of LAI and GPP or LE in ECLand seems to be coupled when using *MODIS climatology* but without affecting normalized standard deviation or relative bias.~~ In other words, changes in the model

quality for LAI, for most of the sites, do not affect the model performance of LE or soil moisture and even not that of carbon fluxes.

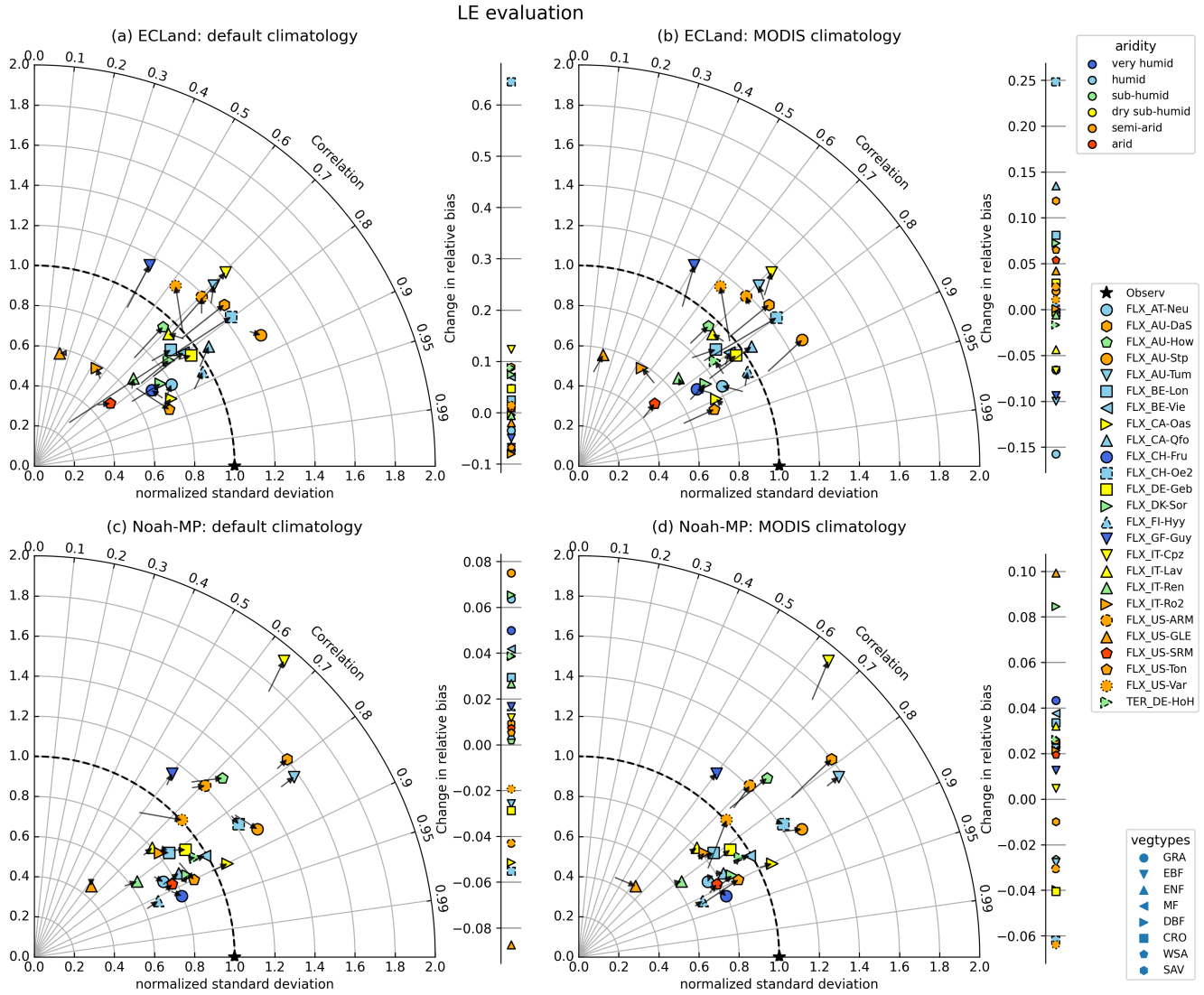

Figure 5. ~~Density plots showing the elasticity~~ Change of ~~correlation (left column), normalized standard deviation (middle column) and relative bias (right column)~~ statistical measures for ~~different variable relationships in both models~~ LE modeling when ~~activating~~ switching on dynamic vegetation for all included sites and by using *default climatology* (~~blue~~left) or *MODIS climatology* (~~orange~~right) as forcing.~~For reasons of practicability, elasticity is used reciprocal. Accordingly, the explanatory variable is the first one of each relationship showed on the y-axis. The grey shaded area marks the range between the thresholds of independence.~~

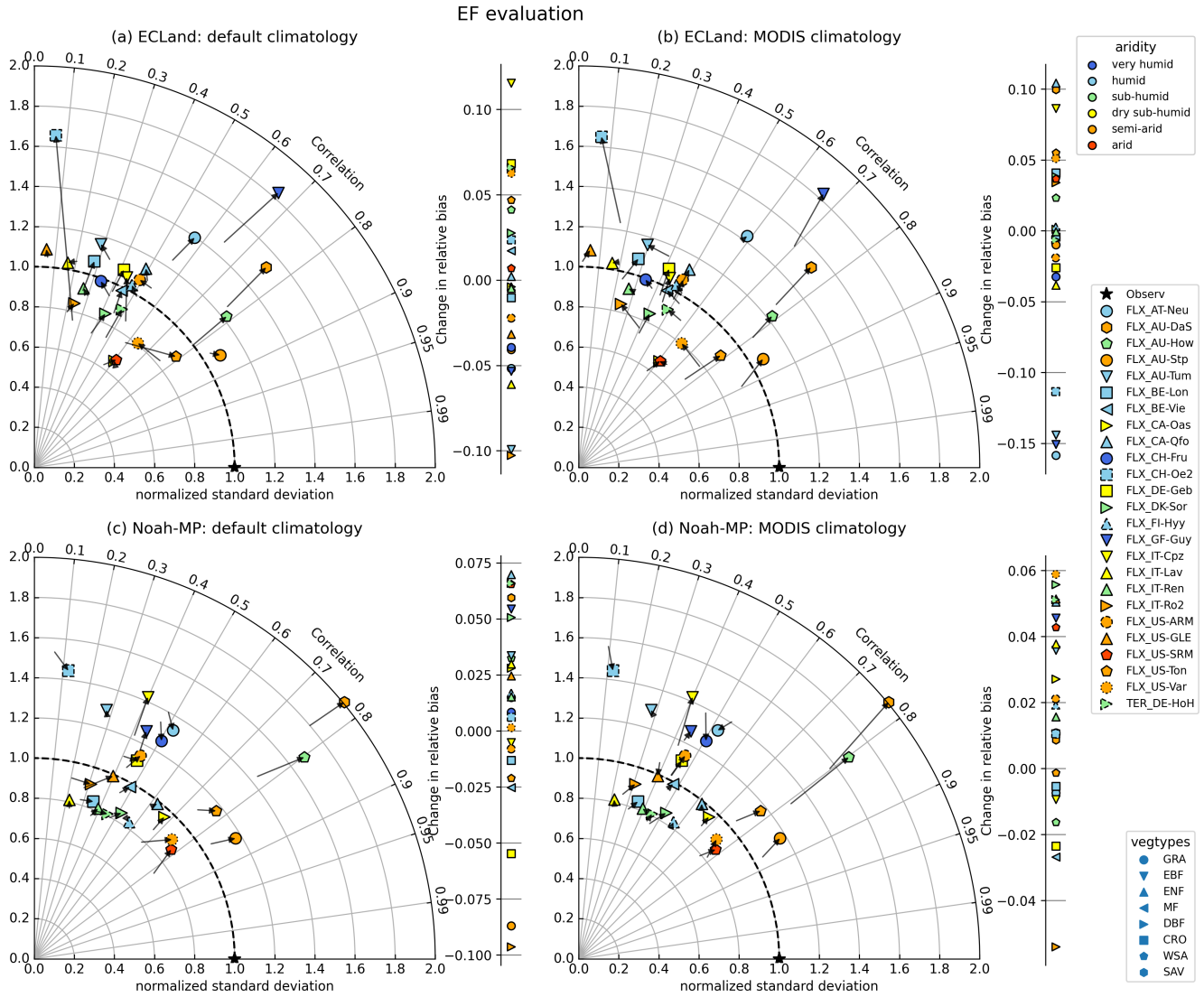

Figure 6. Same as before but for evaporative fraction which represents the turbulent flux partitioning.

3.3 Observed and simulated relationships between ecohydrological variables

One possible explanation for the small contribution of model quality of LAI to that of the turbulent fluxes could be a weak relation between LAI and carbon exchange in the model. However, this is not the case as illustrated in Figure 8. ~~On the contrary, the relationships between GPP and LAI is much more scattered in the observations (top row) compared to the models (other rows), and this is true for both models, across biomes and vegetation types. In general, ECLand shows a linear relationship with considerable less uncertainty compared to the observations. The slope and intercept of the linear regression is dependent on~~

~~the choice of static or dynamic vegetation. In contrast, Noah-MP shows a non-linear relationship with a pronounced hysteresis. This hysteresis is related to the partitioning of GPP to the carbon pools in the plants. Noah-MP uses a non-linear function for allocation of GPP to the leaves that limits the maximum LAI the model can grow. Figure 8 shows the~~ The figure shows the relation between GPP and LAI for four exemplary sites: *DE-HoH* is a deciduous broadleaf forest in a humid climate, *IT-Ren* is an evergreen needleleaf forest in a semi-arid climate, *GF-Guy* is an evergreen broadleaf forest in a tropical climate, and *US-Var* is a grassland in a semi-arid climate. In general, the relationships between GPP and LAI is much more scattered in the observations (top row) compared to the models (other rows), and this is true for both models, across biomes and vegetation types.

The two European sites (left columns, *De-HoH* and *IT-Ren*) reach maximum LAI and GPP in JJA and minimum values in DJF, leading to a correlation that is mainly governed by the seasonal cycle. Similarly, at the U.S. site, with an overall tighter relation, vegetation productivity and LAI peak together in spring (i.e., MAM). For these three sites, correlation coefficients range between 0.80 to 0.86 indicating a clear but not perfect relation between LAI and GPP. However, the scatter of the observed relation is considerable with the standard deviation of the residuals (σ_r) being between 58 and $102 \cdot 10^{-6}\ gCO_2 m^{-2} s^{-1}$. The variance is highest for the peak of the growing season, when GPP quickly responds to environmental conditions (e.g., cloudiness, precipitation, and soil moisture stress) that LAI responds much slower to. The tropical site in French Guiana (*GF-Guy*) shows, as expected, no seasonal cycle, leading to an extremely weak relation between LAI and GPP. The latter is comparatively high all year round (GPP between 250 and $600 \cdot 10^{-6}\ gCO_2 m^{-2} s^{-1}$) although LAI values from the MODIS dataset surprisingly varied between 1 and $7\ m^2 m^{-2}$. For this tropical site, GPP and LAI dynamics seem decoupled (Fig. 8 c). Noah-MP shows a ~~marked~~ non-linear relationship with a pronounced hysteresis effect at all sites except the tropical one (Fig. 8 ~~c-h), with GPP linearly increasing~~ m-p). Thereby, GPP increases linearly with LAI during biomass built-up up to a point where allocation to leaves becomes minimal (vegetation type specific), and ~~a substantial drop in GPP~~ drops considerably without any substantial reductions in LAI towards the end of the growing season (e.g., Fig. 8 ~~e~~m). When GPP values reduce below approximately $100 \cdot 10^{-6}\ gCO_2 m^{-2} s^{-1}$, then LAI reduces from values about three towards zero. This hysteresis is shifted in seasons due to local climate as for the site *US-Var* (Fig. 8 ~~h~~p). At the tropical site, Noah-MP shows some variability in GPP, but almost no change in LAI which is around a value of five.

ECLand, in general, shows a linear relationship with considerable less variability compared to the observations. The slope and intercept of the linear regression is dependent on the choice of static or dynamic vegetation. Dynamic ECLand shows a very tight linear relation between LAI and GPP with much lower scatter compared to the observations (Fig. 8 ~~fourth~~ third row) as R is larger than 0.99 and σ_r is between 10 and $14 \cdot 10^{-6}\ gCO_2 m^{-2} s^{-1}$ for all non-tropical sites. With slope values of 104 to $254 \cdot 10^{-6}\ gCO_2 m^{-2} s^{-1}$, that relationship is much steeper than in the observations. Even for the tropical site, the relationship between LAI and GPP is clearly and tightly linear (Fig. 8 ~~o~~k).

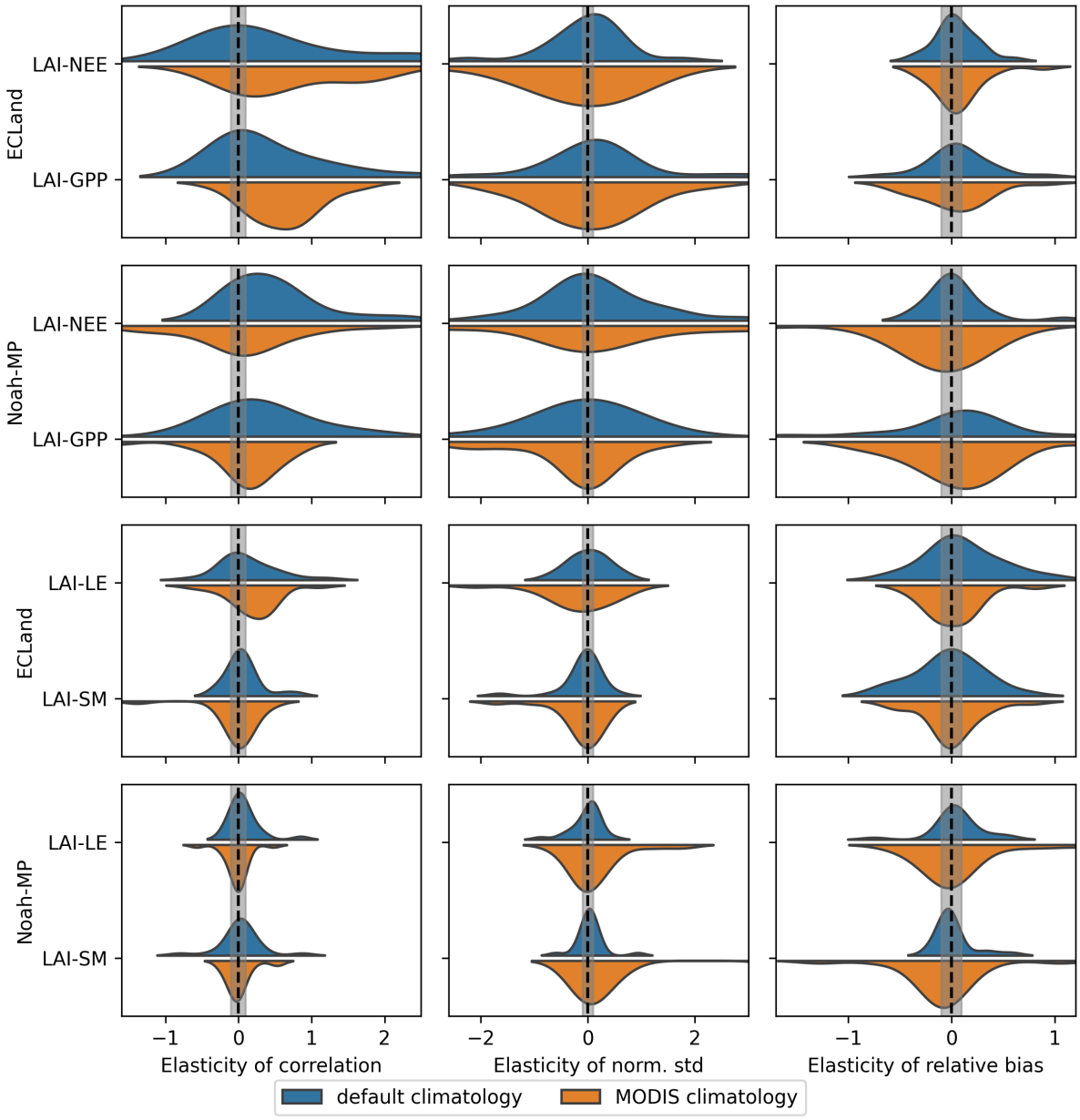

Figure 7. Density plots showing the elasticity of correlation (left column), normalized standard deviation (middle column) and relative bias (right column) for different variable relationships in both models when activating dynamic vegetation and using *default climatology* (blue) or *MODIS climatology* (orange) as forcing. For reasons of practicability, elasticity is used reciprocal. Accordingly, the explanatory variable is the first one of each relationship showed on the y-axis. The grey shaded area marks the range between the thresholds of independence.

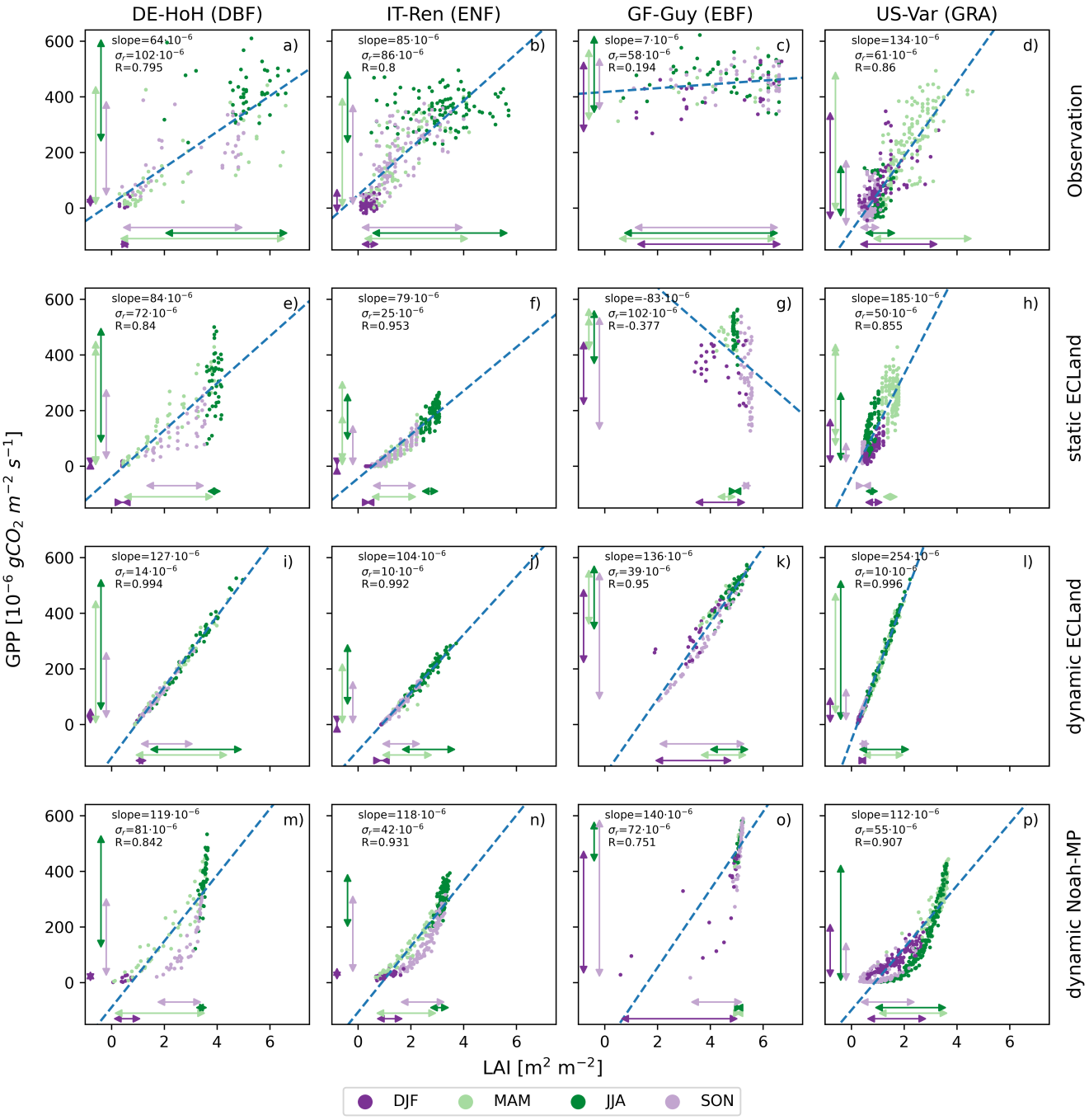

Figure 8. Scatter plots of the relationship between LAI on the x-axes and GPP on the y-axes as 8-day averages for four selected sites (columns). The rows from top to down show observations, static ECLand model output, dynamic ECLand model output, and dynamic Noah-MP model output. Seasons are represented by different dot colors. The arrows represent the range of GPP and LAI values for the individual seasons. A simple linear regression model was applied ~~as additional information~~ (blue dashed line) and its correlation coefficient (R), slope and standard deviation of the residuals (σ_r) are given for each relationship.

4 Discussion

4.1 Using LAI climatology for ECLand and Noah-MP runs is the best way to reproduce leaf area and carbon uptake

Comparison between model output and observational data of LAI, NEE or GPP on a daily basis is rarely done. The ability of the two models to reproduce these observed ecosystem variables was in line with previous results. For Noah-MP, model quality metrics were in the range of other studies (Brunsell et al., 2020; Li et al., 2022; Xu et al., 2021; Liang et al., 2020)~~,~~ ~~although LAI~~ . However, dynamic LAI modelled by Noah-MP in our assessment with a mean of $+70\,\%$ was more biased compared to a mean of $+20\,\%$ for annual LAI values reported by Li et al. (2022). Ma et al. (2017) reported a relative bias in GPP of ~~40%~~ 40 % on average which is higher than the relative bias found here. For ECLand, we could not find any comparable study reporting the performance of daily LAI or NEE/GPP specifically, neither for dynamic nor static simulations. However, for static ECLand, correlation coefficients between modeled and observed NEE and GPP were in line with those obtained by Boussetta et al. (2013) for 10-day averages at several FLUXNET sites. Also, for the mean annual cycles of NEE and GPP, Stevens et al. (2020) found a lower prediction error (RMSD) when using MODIS LAI forcing compared to default prescribed LAI, and, like in our study, a substantial bias in LAI.

For both models, using *MODIS climatology* in static simulations resulted in the best performances concerning LAI. This agreed with expectations. Since all our simulations were validated with MODIS data, a better performance using static runs using *MODIS climatology* itself would likely yield better results than the default values in either model. For Noah-MP, static simulations with *MODIS climatology* indeed yielded the best performance regarding LAI in some sites, but, interestingly, using the *default climatology* performed also well for others. LAI deviations with the *default climatology* occurred specifically in short vegetation, which was also true for the dynamic runs (see below). For ECLand, where the *default climatology* is already based on MODIS data (Boussetta et al., 2012), the performance of the static run was generally improved compared to the validation dataset, as the higher spatial resolution allowed for a better geographical mapping. Also, ECLand *default climatology* was created by disaggregating the total LAI in the MODIS data to the low and high vegetation type on the grid cell. Both points together can explain the better performance for LAI of static ECLand simulations with *MODIS climatology* compared to *default climatology*.

Dynamic vegetation yielded no better LAI results compared to using static runs with *MODIS climatology* for either model. Evergreen broadleaf forests showed the lowest correlation coefficients for dynamic LAI predictions which was also shown by Yang et al. (2011) for tropical regions simulated by Noah-MP. Additionally, Brunsell et al. (2020) reported overestimation of LAI with dynamic Noah-MP for the Eastern Amazonian Forest which we could not find here. ECland suffered from overall strong relative biases regarding LAI in dynamic simulations. The underestimation of prognostic LAI was already shown by Boussetta et al. (2021). Substantial biases also occurred in Noah-MP (also shown by Huang et al., 2022), but especially so for short or sparse vegetation types. The latter could be due to LAI overestimation in the early growing season as reported by Cai et al. (2014). Also, Liu et al. (2016) found that neither look-up table LAI nor predicted dynamic LAI annual cycles seemed to reproduce LAI observations for short vegetation. On the other hand, Pilotto et al. (2015) achieved satisfactory model predictions for crop sites without vegetation dynamics. Thus, for short vegetation such as grasslands, the Noah-MP Crop module maybe

better represents LAI dynamics (Liu et al., 2016), which should be tested in the future.

The performance of NEE and GPP in ECLand was not very sensitive to different vegetation dynamics. Generally, using static *MODIS climatology* yielded the best predictions of GPP and NEE, although the correlation between modeled and observed NEE was generally low (mean Pearson correlation coefficient was 0.44). In many sites, even static simulations with *default climatology* resulted in comparable performances. Interestingly, adding more detailed information by using *MODIS single-year* LAI forcing did not further improve model performance (not shown), as we would have expected if LAI dynamics contributed substantially to enhancing model performance for the carbon fluxes. However, other authors found improved model performance of turbulent fluxes, GPP and soil moisture for roughly 50% of their set of sites by updating the LAI forcing using near real-time data assimilation (Boussetta et al., 2015). In other words, a more frequent reset of LAI to the correct value can improve the ECLand performance in general, but did not have an effect for the annual resolution applied here.

Assimilation of LAI during model runs and instead of fixed forcing (as in a static case) also improved LAI and GPP model quality in a study by Xu et al. (2021) using dynamic Noah-MP. We, therefore, ~~expect~~ expected that LAI dynamics potentially improve model quality regarding carbon fluxes ~~, but we could not test this here, since carbon fluxes are not modeled for static vegetation~~which was predominantly not the case. However, dynamic Noah-MP is already known to overestimate GPP (Ma et al., 2017; Liang et al., 2020; Brunsell et al., 2020). Especially short and sparse vegetation types suffered from low predictive ~~efficiencies~~ power mainly in NEE correlation (Yang et al., 2021) and in GPP relative bias (Li et al., 2022) which could be also observed here. None of the parameter sets Yang et al. (2021) tested for simulations with dynamic Noah-MP resulted in well-fitting predictions of daily changes in NEE for three of the four sites with short vegetation within ChinaFLUX. Note, however, that LAI, NEE and GPP of short and sparse vegetation ~~was~~ were also not well-represented in static runs either. Also, Kumar et al. (2019) could only achieve marginal improvements in GPP representation by dynamic Noah-MP due to LAI assimilation for crops and grasslands which suggests that LAI dynamics had only a limited effect on simulated NEE there. One possible reason for lower predictive power of the models regarding the carbon fluxes of short or sparse vegetation could be that these vegetation types more quickly and dynamically respond to fluctuations in the environment (e.g. soil moisture limitations). Forest ecosystems might be able to compensate restrictions by a larger intrinsic carbon storage or deeper roots resulting in less variability of their productivity within and between the years. It seems that both models investigated here cannot mimic this differentiation. Nonetheless, it was shown here that correlation coefficients for GPP simulated with dynamic Noah-MP were high (also found by Liang et al., 2020; Li et al., 2022) and, at the same time, relative bias was small for all forests except the evergreen broadleaf forests (see section 3.1 and Fig. A1). Thus, although some previous studies found substantial uncertainties in modeled GPP for different vegetation types (Ma et al., 2017; Liang et al., 2020; Li et al., 2022), predicting ecosystem variables using dynamic Noah-MP could be useful at least for forests in studies when LAI climatology cannot be used such as climate change impact studies.

Considering the opposing biases in NEE (and GPP) indicates that the models differ in their estimates of ecosystem respiration. One important difference is the sequence of the calculation of GPP, NEE and respiration. ECLand estimates net assimilation and respiration first separately whereby respiration is set to be 11% of net assimilation and, then, both are used to calculate GPP. In Noah-MP, the first estimate is for GPP which is reduced by respiration to gain a values for NEE and, additionally,

respiration is scaled by GPP and available biomass ~~inclusively~~ inclusive of LAI. Including our findings, for dynamic ECLand, the underestimated LAI directly transfers into lower NEE values and, thus, also to GPP since respiration is a fixed fraction of NEE. Apart from the fraction of GPP that is directly needed for metabolism, the estimation of respiration in dynamic Noah-MP also considers leaf maintenance which is another difference compared to ECLand. As a result, respiration is slightly overestimated in ECLand, and slightly underestimated in Noah-MP.

4.2 Model performance of turbulent fluxes and soil moisture were almost unaffected by vegetation dynamics in both LSMs

The model performance of ECLand and Noah-MP regarding heat fluxes and soil moisture seems almost insensitive to vegetation dynamics. Correlation, variability and bias of turbulent fluxes in this study were comparable to other studies. While evaluating static ECLand with FLUXNET data, Stevens et al. (2020) found correlation coefficients of 0.79 and 0.77 for the annual cycle of latent and sensible heat, respectively, and Boussetta et al. (2013) showed a mean correlation coefficient of 0.81 for 10-day averages of latent heat. For Noah-MP, statistical measures for turbulent fluxes and soil moisture were mostly in line with other studies (Niu et al., 2011; Ma et al., 2017; Yang et al., 2018; Xu et al., 2021) although Pilotto et al. (2015) presented lower correlation coefficients between 0.20 and 0.43. Interestingly, Ma et al. (2017) showed opposing relative bias for evapotranspiration on annual time scale over the continental U.S. of 4% and 22% for static and dynamic simulations, respectively.

For ECLand, it had little impact on turbulent fluxes whether vegetation was simulated dynamically instead of statically. Model performance for LE and EF changed only for some sites and towards lower performance (see section 3.2). The predominant underestimation of LE agrees with the findings of Stevens et al. (2020). For dynamic ECLand, the underestimation of GPP and LAI (also in Boussetta et al., 2021) could also be the reason for the poor correlation of EF between modeled and observed values because the energy fraction that is used for transpiration is underestimated. Boussetta et al. (2021) found that dynamic vegetation in ECLand improved numerical weather predictions. There, the main improvements in model performance were achieved through updating land cover maps and the LAI in the look-up table or by including LAI seasonality which both is comparable with our experiment using *MODIS climatology* in static ECLand simulations. Here, we could not confirm theses findings being related to improved performance in heat fluxes since model performance of LE and EF were almost unaffected by the used LAI forcing, which was already experienced by others (Stevens et al., 2020; Nogueira et al., 2021). The reason might be that parameters are adapted to the prior vegetation information (Ruiz-Vásquez et al., 2023) and, thus, the model needs a re-calibration.

Also for Noah-MP, activating vegetation dynamics had mostly little impact on LE and EF predictions. A slight improvement in model performance was found for some sites with short vegetation types or semi-arid climates. Ma et al. (2017) found that using LAI climatology resulted in better model performances for LE than simulations with activated vegetation dynamics for Noah-MP using the monthly FLUXNET Multi-Tree Ensemble data over the U.S.. However, here, we did not find enhanced biases in LE predictions with dynamic Noah-MP compared to the static simulations as they did which could be due to the differing timescales for model evaluation. Both, overestimation and underestimation of LE predicted by dynamic Noah-MP is reported in the literature (Brunsell et al., 2020; Ma et al., 2017; Cai et al., 2014). Brunsell et al. (2020) showed a positive bias of

monthly evapotranspiration in the Eastern Amazonian Forest simulated with dynamic Noah-MP while we found a negative bias of LE for the FLUXNET site *GF-Guy*. For short vegetation types, using the Noah-MP Crop module with activated vegetation dynamics might be sufficient in predicting surface fluxes (Liu et al., 2016). Achieved improvement for LE might be not as large as for sensible heat flux (Liu et al., 2016) which could be a reason for poor performances in EF presented here.

Although vegetation and soil moisture state variables are directly coupled within land-surface models, we found almost no impact of different vegetation modeling on soil moisture predictions for both models. Activating vegetation dynamics or changing LAI forcing did not improve soil moisture representation on average. The reason might be due to the implemented interaction of carbon and water processes. First, the potential photosynthetic activity in dependence of leaf area and radiative conditions is calculated. Then, the limitation factor of extractable water is estimated according to available soil water and roots. Lastly, the photosynthetic activity is adapted to that restriction and transpiration rate adapted to conductivity and atmospheric conditions. As a result, the only included path is that soil moisture impacts photosynthetic activity and biomass build-up. But there is no feedback that more biomass needs/loses more water that will be taken from the soil because photosynthetic activity in the models relates only to the carbon fluxes but not to the water fluxes.

Additionally, modeled soil moisture suffers from substantial biases in both directions which was also found by Liang et al. (2020) for Noah-MP and by Garrigues et al. (2021) for ECLand although correlation between observed and modeled soil moisture can be satisfactory (Beck et al., 2021; Xu et al., 2021; Pilotto et al., 2015; Liang et al., 2019). The reason might be underlying default values for soil characteristics such as field capacity and permanent wilting point that possibly deviate from on-site soil conditions and optimal values for soil parameters are still uncertain (Li et al., 2020). Alternatively, it could be an effect of differing scales since the observation from FLUXNET refers to point measurements. The Multiscale parameter regionalization (MPR) might provide an improved way to estimate soil parameters by applying pedo-transfer function on local soil characteristics and, recently, has been applied to Noah-MP in a proof-of-concept (Schweppe et al., 2022).

Overall, the model performance of soil moisture and heat fluxes was barely affected by vegetation dynamics or applied LAI forcing. However, the sensitivity to LAI might be given since van den Hurk et al. (2003) found some effect of changed LAI values given into TESSEL, a predecessor of ECLand, as well as Ma et al. (2017) and Zhang et al. (2016) did for Noah-MP. Xu et al. (2021) showed improved LE and soil moisture simulations with more realistic LAI although, also there, the effect was not only site-dependent but also differed with season and year. But those authors also highlighted that transpiration is only partly determined by LAI and other factors controlling the canopy conductance to water vapor might play a larger role. Therefore, other compensating mechanisms may explain low elasticity between LAI and LE or soil moisture (see section 3.2). Yang et al. (2011) demonstrated that the applied runoff scheme more strongly determined model performance of soil moisture and evapotranspiration than the schemes for dynamic vegetation, stomatal resistance and soil moisture stress. Still, optimizing parameters can be effective in improving model predictions which could be shown by several studies (Bohm et al., 2020; Li et al., 2021, 2020). Even more, the sensitivity of soil moisture to vegetation parameters was shown to enlarge with dynamic vegetation representation (Arsenault et al., 2018). Yet, uncertainty about the optimal values for especially soil and vegetation parameters remains (Li et al., 2020).

Overall, the impact of vegetation dynamics and LAI on turbulent heat fluxes and soil moisture in this investigation was slim

across sites and seasons for both models. Thus, modelers who are mainly interested in the performance of carbon processes should be careful using performance metrics for hydrological variables as a proxy (e.g. LE) because the model formulation for the latter might have controlling processes other than LAI or NEE which dominate the result. Whether applying vegetation dynamics in model simulations is advantageous might depend on the target variables. While, for heat flux predictions, using *MODIS climatology* might be sufficient, activating vegetation dynamics could play a role for improve carbon flux predictions at seasonal or annual timescale (Jarlan et al., 2008).

4.3 Discrepancy between observed and simulated GPP-LAI relationship is caused by model structure

The substantial scatter in the observed relation between GPP and LAI is in close agreement with previous work, showing that GPP also depends on the short-term availability of resources (e.g., light, soil water) (Hu et al., 2022). Additionally, Zhang et al. (2021) found that in LSMs the relation between LAI and GPP was too tight. We therefore checked the underlying relations in the models causing this.

GPP-LAI relationship in Noah-MP showed a clear exponential hysteresis (see section 3.3). ~~The LAI dynamics in Noah-MP depend on several processes. Allocation of carbon to the leaves increases LAI , while~~ This hysteresis is related to the partitioning of GPP to the carbon pools in the plants and to LAI reducing processes as leaf turnover and leaf die-back~~reduce LAI~~ . ~~Leaf~~ Noah-MP uses a non-linear function for allocation of GPP to the leaves that limits the maximum LAI the model can grow resulting in the LAI saturation in summer that can be seen in Figure 8 m-p. On the other hand, leaf turnover due to leaf aging is implemented as a linear function of leaf mass ~~. Leaf~~ while leaf die-back due to environmental limitations follows exponential functions. Taken together, leaf die-back dominates in the later growing season which results in the hysteresis. The reduction of LAI (i.e., leaf die-back) is implemented to be dependent both on water and temperature stress, but temperature stress is the main driver. In the specific implementation used here, water stress only occurs at a very low soil saturation of $0.1\ vol\%$ for silt loam exemplarily which is even below the permanent wilting point of this soil texture type according to the look-up table value. These values are rarely reached and, thus, water stress is negligible most of the time. In contrast, temperature stress is implemented as an exponential function causing the late growing season non-linear decline of GPP observed throughout the non-tropical sites. Temperature stress is at maximum at $5\ ^{\circ}C$ for forest ecosystems resulting in no active biomass below this threshold. For this reason, LAI values are almost constant at the tropical forest site because temperature is never limiting there. ECLand with static vegetation shows a similar pattern of seasonal dynamics as Noah-MP with vegetation dynamics but with less pronounced exponential relationship. In contrast, dynamic ECLand simulates LAI that is strongly coupled to daily meteorological conditions, leading to higher daily fluctuations of LAI than expected, including strong drops of LAI in summer. Three processes govern these daily LAI dynamics: GPP, respiration and senescence. GPP is linearly related to LAI and varies with environmental and meteorological conditions causing the variability in static runs. In dynamic runs, losses in biomass due to high or low daily GPP linearly affect LAI. In other words, unfavourable GPP can reduce LAI almost immediately. The second process affecting LAI is senescence. ECLand distinguishes growing and senescence phases by comparing active biomass due to assimilation with the biomass from the previous time step. If active, then senescence is a linear function of active biomass and a folding-factor. The folding-factor reduces part of the senescent biomass, depending on photosynthesis (reduced in the

case of high assimilation) and LAI. Overall, the folding-factor changes only slightly with LAI. Additionally, a reduction of LAI and, thus, active biomass due to reduced GPP (as explained before) causes the model to trigger senescence because the active biomass of the previous time step was higher. The third process is respiration. About 11% of physiologically possible assimilation is used for dark respiration without considering actual light conditions. This might cause high values of dark respiration compared with possible assimilation based on meteorological conditions and, thus, reduce net primary production, even producing negative values. Notably, no aboveground biomass storage is built up and there is no turnover. Most locations show a linear relationship comparable to ECLand but with a higher variability (Fig. 8 first and ~~fourth~~ third row). This might be due to the fact that leaf growth and leaf fall, in particular for trees, happen on longer timescales than the daily one as implemented in ECLand which inhibits immediate effects of GPP on LAI.

Overall, the current implementations of leaf dynamics in both models use very different approaches to represent LAI dynamics. In Noah-MP it is mainly temperature-driven, and GPP depends little on LAI once the canopy is fully developed. In contrast, in ECLand, LAI and GPP are coupled very tightly and, thus, the LAI dynamics follow almost the same sensitivities to water limitation and radiation as turbulent fluxes, which is unrealistic. Realistic LAI is less dynamic and less sensitive to environmental conditions, as also indicated by the observations. Hence for very different reasons, in both models the performance regarding LAI and turbulent and carbon fluxes is disconnected.

4.4 Implications and limitations

For modeling LAI and carbon fluxes, using dynamic vegetation modules in their current implementation in either model is not yet efficient because they increase model complexity encompassing more dynamic processes and parameters without improving the predictive skill. As the dynamic vegetation components in ECLand are still under development, findings from this study can help better understand and represent the processes involved to improve its performance in modeling carbon and energy fluxes. But also for Noah-MP, we showed that the dynamic vegetation module has potential for improvement especially related to the relationship between GPP (and thus also NEE) and LAI. Underlying processes such as carbon allocation, root dynamics, plant hydraulics, feedbacks on photosynthesis and their parameterization can still be worked on (Ma et al., 2017; Li et al., 2021). Overall, we recommend using *MODIS climatology* forcing ~~or alternative remote sensing LAI products~~ for static simulations which yielded the best model performances for carbon and water fluxes. This might be valid for other remote sensing LAI products as well but would need to be tested beforehand.

The value of a model evaluation like in this study depends on the reliability of the included datasets. Uncertainty in the forcing data might have a larger impact on the model runs than processes within the models (Zhang et al., 2016), but Haughton et al. (2016) demonstrated that observational errors, in general, are unlikely to cause poor model performance. Nonetheless, model evaluations are also restricted by uncertainty in the reference data (Li et al., 2022) especially when considering flux measurements (Li et al., 2019). We tried to address by carefully inspecting the time series data from FLUXNET2015 before their usage. However, as in all measurements, there are still uncertainties, e.g. from instrumental errors or incomplete energy balance closure.

Also, the MODIS dataset harbors uncertainty originating from cloud coverage, especially in the tropics. We tried to minimize

this uncertainty by excluding all days from the dataset that were flagged with significant cloudiness. But saturation also limits the representativeness of the LAI measurements. Even when using only data with the highest possible quality flag, we found suspiciously low LAI values in summer for temperate forests and grasslands, and especially for tropical forests throughout the year (Fig. 8 c). ~~Thus, also the reference data are uncertain~~ Noisy and uncertain LAI data from MODIS for tropical forests was already reported among the literature (Weiss et al., 2007; Garrigues et al., 2008; Xiao et al., 2016; Zhang et al., 2024). As a result, reference data remains a source for uncertainty and a deviation ~~from them~~ in model outputs from it is expected. In any case, reference data is essential for model verification, calibration, and validation but should be treated carefully concerning its reliability and uncertainty.

5 Conclusions

Land-surface models often include modules for dynamic vegetation processes. Yet, an evaluation of the representativeness of key variables such as leaf area index or net ecosystem exchange is rarely done on high temporal resolution. The impact of different parameterization of vegetation processes on water and carbon flux estimates by land-surface models is still poorly understood. Therefore, we evaluated the change in model performance of ecohydrological target variables when dynamic vegetation processes are included for two land-surface models and further gained insight into critical process implementations that lead to the observed patterns.

Surprisingly, neither for ECLand nor for Noah-MP, including modules for dynamic vegetation in their implementation improved the model predictions of ecohydrological variables. We expected vegetation dynamics in these land-surface models to better capture the higher variability in ecosystem exchange, especially that of highly dynamic short or sparse vegetation types, but this was predominantly not the case. Using alternative input for leaf area index other than default climatology also had a negligible effect on the model performance but this needs to be evaluated in more detail since we were limited in data sources. Moreover, model performances of carbon and hydrological fluxes appeared to be weakly coupled. Therefore, the question arose whether exchange fluxes themselves in these land surface models are sensitive to changes in leaf area index estimates and not only to changing parameter sets. Indeed, different leaf area index estimates lead to different predictions in exchange fluxes but without affecting the overall model performance of these variables. This might be caused by the mismatch in the seasonal patterns between observations and models for the relationship of gross primary productivity and leaf area index. While this relationship in dynamic Noah-MP showed a logarithmic hysteresis, mainly driven by temperature, both variables are tightly linearly coupled in dynamic ECLand without allowing for the leaf area index to remain unchanged in suboptimal conditions for photosynthesis.

This deeper analysis of the model performance for ecohydrological fluxes that pinpoints to the reasons for model behavior was only possible with a reduced number of models. We used specific setups for the two land surface models evaluated here. Adapting or changing parameters and investigating the effect of other processes within the models were beyond the scope of this study. At this point, it remains unclear how representative our model selection is for the performance and process evaluation of other land surface models. Nonetheless, we highlighted some crucial relationships in the implementation of vegetation pro-

cesses that have the potential for further improvement. Additionally, they might be a good starting point for a similar intensive investigation with other land surface models or other alternative LAI climatology.

Code and data availability. Observational data from the FLUXNET2015 dataset were accessed via FLUXNET data portal (fluxnet.org, 2020). Observational data for TERENO observatory "Hohes Holz" can be found at PANGAEA (Rebmann and Pohl, 2023). IGBP Land Classification is published by National Center for Atmospheric Research (2022). Aridity index was taken from Trabucco and Zomer (2018). Gap-filling of meteorological data was done by using ERA5 re-analysis product (Hersbach et al., 2020), accessed by Climate Data Store API (Copernicus, 2018). USGS vegetation types can be found at University Corporation for Atmospheric Research (2023). Global gridded soil information (Hengl et al., 2014) is available at https://soilgrids.org. MODIS Leaf area index was retrieved via Earth Data Portal from NASA (Myneni et al., 2015).

Appendix

A.01 Dynamic ECLand processes

For more details, see the published model descriptions (Boussetta et al., 2012, 2013, 2021). Photosynthesis model is based on Calvet et al. (1998). Therein, potential net assimilation A_n is estimated from physiological constrains as

$$A_n = A_{max} \cdot (1 - e^{-\frac{g_{meso} \cdot (c_i - c_{comp})}{A_{max}}}) \tag{A.1}$$

where A_{max} is the leaf photosynthetic capacity, g_{meso} is the mesophyll conductance, c_i is the leaf-internal CO_2 concentration and c_{comp} is the CO_2 compensation point. Potential gross assimilation A_g, then, is calculated as

$$A_g = (A_n + R_d) \cdot \epsilon \tag{A.2}$$

where R_d is the dark respiration from

$$R_d = A_n \cdot f_R \tag{A.3}$$

with $f_R = \frac{1}{9}$ as dark respiration factor, and where ϵ is a quantum use efficiency factor, estimated as

$$\epsilon = 1 - e^{-\frac{\epsilon_0 \cdot E_{PAR}}{A_n + R_d}} \tag{A.4}$$

where ϵ_0 is the maximum quantum use efficiency and E_{PAR} is the absorbed photosynthetic active radiation. Actual gross assimilation GPP results from

$$GPP = A_g \cdot LAI \cdot \rho_a \tag{A.5}$$

where LAI is the leaf area index of the prior time step and ρ_a is the air density corrected for humidity.
A_n is used as the maximum leaf assimilation for the senescence model (Calvet and Soussana, 2001). To avoid immediate leaf die-back, a damping factor for senescence f_s is introduced as

$$f_s = \max(\frac{\tau_{lim} \cdot t_s}{100 \cdot N_{day}}, \max(10^{-8}, \frac{t_s}{N_{day}} \cdot \min(1, \frac{A_n}{A_{max}}) \cdot \frac{\max((r_{meso} \cdot 1000)^{0.321} \cdot LAI}{f_{LAI}}, 1))) \tag{A.6}$$

where τ_{lim} is a limiting factor for immediate biomass loss, t_s is the damping time for senescence, which basically is the amount of seconds per year, N_{day} is the amount of seconds per day, A_{max} is the maximum photosynthesis rate with optimal conditions and f_{LAI} is a LAI correction parameter that reduces mortality at high LAI values which would occur due to shadowing. The amount of biomass loss B_{loss} then is

$$B_{loss} = \min(B - LAI_{min} \cdot f_{LAI-B}, B \cdot (1 - e^{-\frac{1}{f_s}})) \tag{A.7}$$

where B is the biomass of the prior time step and f_{LAI-B} is a conversion factor between LAI and B. Then, biomass B is updated by subtracting B_{loss}. The change in biomass due to assimilation B_{gain} results from

$$B_{gain} = \max(LAI_{min} \cdot f_{LAI-B} - B, A_n \cdot f_{Cbiom}) \tag{A.8}$$

where $f_{Cbiom} \approx 0.68$ is a factor converting the amount of CO_2 uptake from assimilation to carbon in dry biomass. Biomass B is updated again by adding B_{gain}. In the end, this updated biomass is transferred into an updated LAI value by

$$LAI = \frac{B}{f_{LAI-B}} \tag{A.9}$$

LAI determines the interception reservoir W by

$$W = W_{max} \cdot (c_B + c_H \cdot LAI_H + c_L \cdot LAI_L) \tag{A.10}$$

where W_{max} is the maximum thickness of the water layer on leafs or bare ground, c_B, c_H and c_L are the fractions for bare soil, high vegetation and low vegetation on a grid cell and LAI_H and LAI_L are the LAI values for high and low vegetation, respectively (Boussetta et al., 2012). Additionally, canopy resistance r_c depends on LAI via

$$r_c = f_1 f_2 f_3 \cdot \frac{r_{s,min}}{LAI} \tag{A.11}$$

where $r_{s,min}$ is the minimum stomatal resistance and f_n are the restriction factors for low input in shortwave radiation, soil moisture stress and saturated atmospheric conditions (Boussetta et al., 2012).

A.02 Dynamic Noah-MP processes

For more details, see the published model descriptions (Niu et al., 2011; Ma et al., 2017; Oleson et al., 2012). The model for leaf dynamics within Noah-MP is based on Dickinson et al. (1998). Leaf biomass C_{leaf} is balanced over time with

$$\frac{\delta C_{leaf}}{\delta t} = f_{leaf} \cdot A_{tot} - (d_{stress} + d_{turnover} + R_{leaf}) \cdot C_{leaf} \tag{A.12}$$

where A_{tot} is the total carbon assimilation rate, f_{leaf} is the fraction of allocation to the leaves, d_{stress} is the dying rate caused by cold and drought stress, $d_{turnover}$ is the turnover rate due to senescence, herbivory or mechanical loss as a vegetation-type dependent parameter and R_{leaf} is the respiration rate of the leaf biomass. f_{leaf} is determined by LAI via

$$f_{leaf} = e^{0.01 \cdot LAI(1-e^{\chi \cdot LAI})} \tag{A.13}$$

where $\chi = 0.75$ is a parameter defining the partitioning of carbon allocation between leaves and stem. A_{tot} is split up to photosynthesis rates from sunlit and shaded leaves, respectively:

$$A_{tot} = 12 \cdot 10^{-6} \cdot (A_{sunlit} \cdot LAI_{sunlit} + A_{shaded} \cdot LAI_{shaded}) \tag{A.14}$$

where the first factor is for unit conversion. The partitioning of sunlit and shaded LAI results from a two-stream radiation transfer scheme (Niu et al., 2011). Assimilation rate for sunlit and shaded leaves, respectively, is estimated with a bottle-neck

principle as

$$A = I_g \min(A_L, A_C, A_S) \tag{A.15}$$

where I_g is a growing season index according to leaf temperature and A_L, A_C, A_S are the photosynthesis rates limited by light, Rubisco and export, respectively (Bonan, 1996). A_L results from

$$A_L = \frac{4.6 \cdot \epsilon \cdot E_{PAR}(c_i - c_{comp})}{c_i + 2c_{comp}} \tag{A.16}$$

with c_i being the leaf-internal CO_2 concentration, c_{comp} being the CO_2 compensation point, ϵ being the quantum use efficiency and E_{PAR} being the absorbed photosynthetic active radiation. Additionally, $A_S = 0.5 \cdot V_{max}$ and

$$A_C = \frac{V_{max}(c_i - c_{comp})}{c_i + K_c(1 + \frac{c_o}{K_o})} \tag{A.17}$$

where c_o is the atmospheric O_2 concentration, K_c and K_o are the Michaelis-Menton constants for CO_2 and O_2 (Collatz et al., 1991), respectively, and V_{max} is the maximum carboxylation rate, defined by

$$V_{max} = V_{max,25} \cdot \alpha_{max}^{\frac{T_v - 25}{10}} \cdot f_N f_{T_v} \beta \tag{A.18}$$

where $V_{max,25}$ is the maximum carboxylation rate at 25 $°C$, α_{max} is a temperature conversion factor, T_v is the vegetation temperature, f_N is a factor for nitrogen limitation of the leaves, f_{T_v} is a factor for temperature limitation (Collatz et al., 1991) and β represents the limitation by available soil moisture.

d_{stress} for the leaf mass balance is estimated from

$$d_{stress} = d_{cold} \cdot e^{-0.3 \cdot \max(0, T_v - T_{min})} \frac{C_{leaf}}{120} + d_{dry} \cdot e^{-100\beta} \tag{A.19}$$

where T_{min} is a vegetation type dependent threshold temperature for leaf survival, β is the soil moisture limitation factor and d_{cold} and d_{dry} are vegetation type dependent dying rates (prescribed parameter) for temperature and dryness stress, respectively. Leaf respiration R_{leaf} is calculated with

$$R_{leaf} = f_{res}((f_{leaf} - \frac{LAI}{\chi \cdot f_{leaf}}) \cdot A_{tot} - R_l \tag{A.20}$$

where f_{res} is a factor defining the fraction of assimilation that is used for respiration and R_l is the respiration for leaf maintenance from

$$R_l = \min(\frac{C_{leaf} - C_{leaf,min}}{\Delta t}, 0.5 \cdot 12 \cdot 10^{-6} \cdot r_l(T_v) \cdot LAI \cdot \beta \cdot \frac{c_N}{c_{N,max}}) \tag{A.21}$$

where $C_{leaf,min}$ is the minimum leaf biomass, Δt is the time step duration, 0.5 is a reduction factor for respiration during non-growing season, $r_l(T_v)$ is the vegetation type dependent respiration rate for leaf maintenance at T_v and $\frac{c_N}{c_{N,max}}$ is the nitrogen saturation within the leaves. Afterwards, net primary production NPP is estimated as

$$NPP = (f_{leaf} - \frac{LAI}{\chi \cdot f_{leaf}}) \cdot A_{tot} - R_{leaf} - R_l \tag{A.22}$$

GPP is set to A_{tot} and LAI is updated with

$$LAI = C_{leaf} \cdot f_{LAI-B} \tag{A.23}$$

where f_{LAI-B} is the leaf area per biomass.

Assimilation rate A determines the stomatal resistance r_s by

$$\frac{1}{r_s} = g_{min} + \frac{m \cdot p_{air} \cdot A}{c_{air}} \frac{e_{air}}{e_{sat}(T_v)} \tag{A.24}$$

where g_{min} is the minimum stomatal conductance, m is an empirical parameter for the relationship between transpiration and CO_2 flux, p_{air} is the surface air pressure, c_{air} is the CO_2 concentration at leaf surface, e_{air} is the vapor pressure at leaf surface and $e_{sat}(T_v)$ is the saturation vapor pressure inside the leaves (Ball et al., 1987; Bonan, 1996). r_s then is used to estimate latent heat flux and, thus, evapotranspiration.

A.03 Additional figures

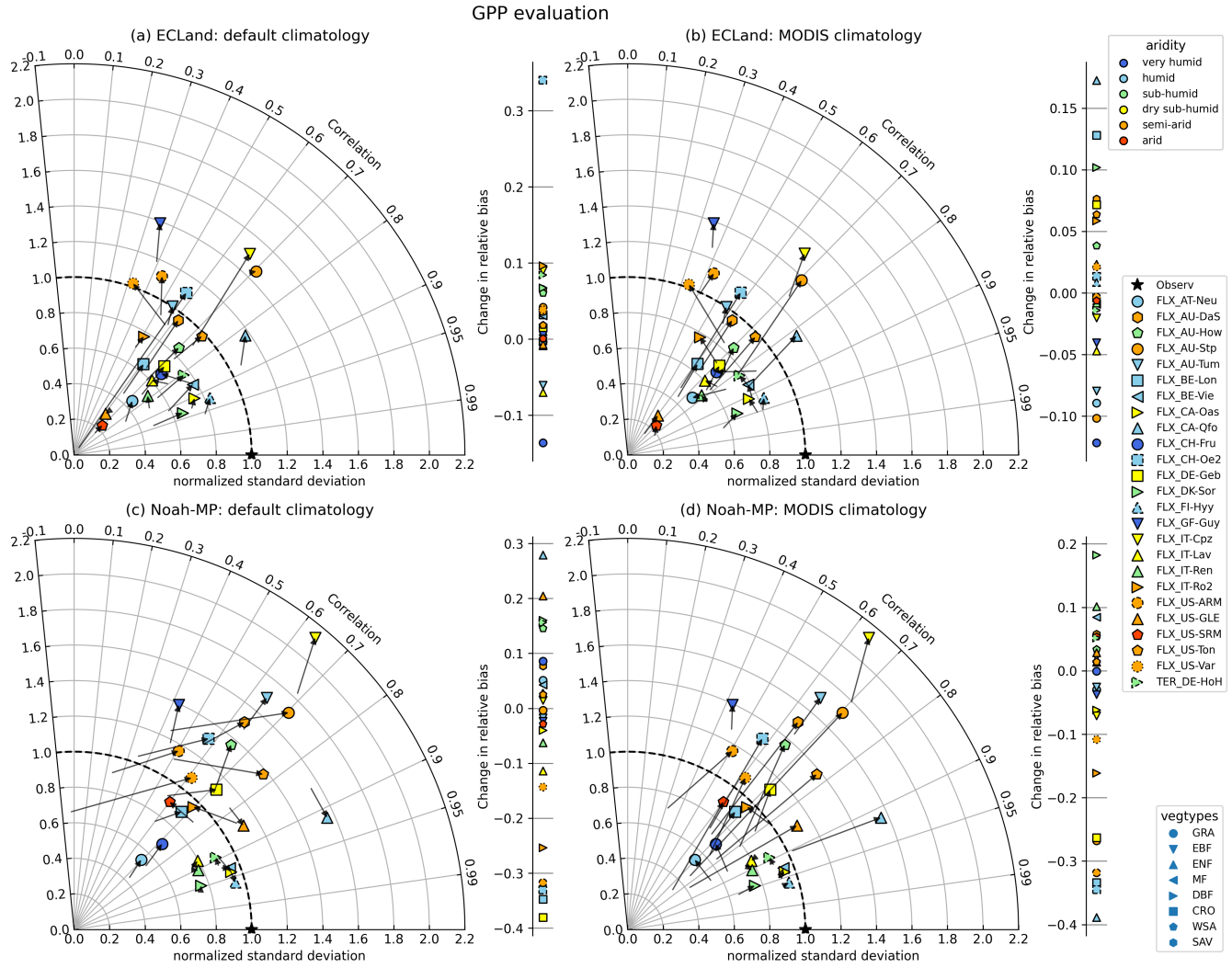

Figure A1. Change of model quality metrics for GPP prediction when switching on dynamic vegetation for all included sites and by using *default climatology* (left) or MODIS climatology (right). The star ("Observ") marks the location of the perfect correlation between observation and model and perfect agreement between observed and modelled variance. The model performance of the static runs can be read from the start of each arrow. The point colors indicate the site aridity (top right legend). Vegetation types are symbolized by different marker types (bottom right legend).~~Since GPP is not generated as variable from Noah-MP when running the model without dynamics, no change in statistical measures can be presented.~~

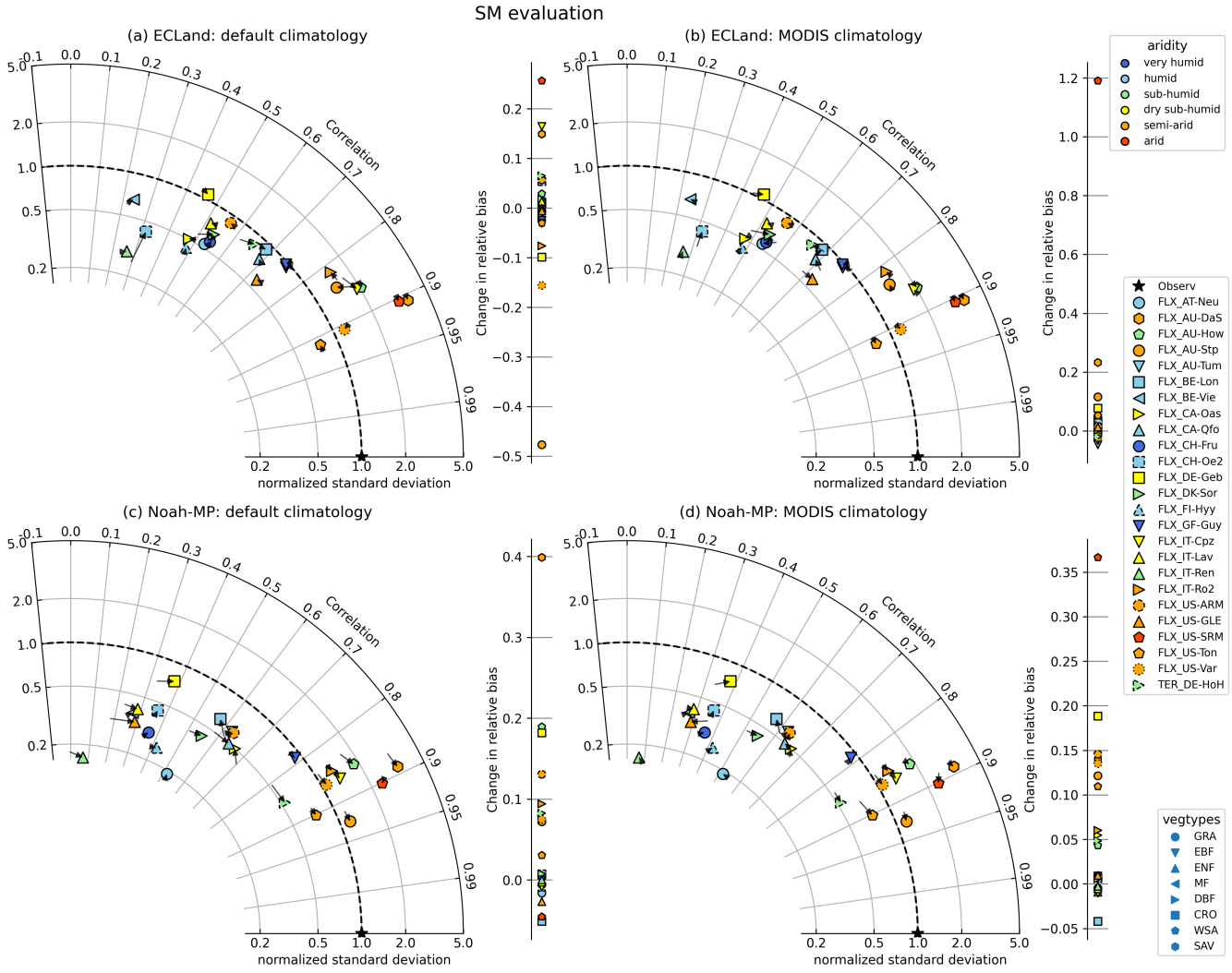

Figure A2. Same as before but for soil moisture.

A.04 Performance metrics tables

Table A1. Relative bias for LAI. The word climatology is shortened with clim.. MODIS single refers to the MODIS single-year setup.

ECLand						Location	Noah-MP					
default clim.		MODIS clim.		MODIS single			default clim.		MODIS clim.		MODIS single	
static	dynamic	static	dynamic	static	dynamic		static	dynamic	static	dynamic	static	dynamic
-68%	-77%	-28%	-73%	-31%	-73%	AT-Neu	-54%	-14%	5%	-14%	0%	-14%
0%	22%	-24%	20%	-42%	19%	AU-DaS	-54%	~~21~~51%	-9%	~~21~~51%	-3%	~~21~~51%
-7%	0%	-17%	-1%	-17%	-1%	AU-How	-75%	~~91~~27%	-3%	~~91~~27%	-1%	~~91~~27%
153%	-24%	-51%	-36%	-50%	-36%	AU-Stp	176%	~~214~~231%	-4%	~~214~~231%	-5%	~~214~~231%
-31%	-74%	-1%	-72%	0%	-71%	AU-Tum	0%	-5%	0%	-5%	1%	-5%
29%	51%	-7%	48%	-10%	47%	BE-Lon	-28%	110%	3%	110%	0%	110%
-26%	-19%	-16%	-18%	-15%	-18%	BE-Vie	3%	9%	-6%	9%	-6%	9%
-4%	-10%	-12%	-11%	-14%	-11%	CA-Oas	-3%	-7%	-3%	-7%	-5%	-10%
51%	52%	-17%	47%	-17%	47%	CA-Qfo	200%	92%	-7%	92%	-7%	92%
-19%	-67%	-35%	-67%	-34%	-67%	CH-Fru	-44%	-3%	-5%	-3%	-4%	-3%
-95%	141%	-10%	148%	-10%	148%	CH-Oe2	6%	146%	0%	146%	0%	146%
56%	30%	-8%	26%	-11%	26%	DE-Geb	-20%	99%	3%	99%	-1%	99%
-52%	-32%	-20%	-30%	-10%	-29%	DE-HoH	-45%	-16%	-9%	-16%	0%	-16%
21%	44%	-11%	42%	-11%	42%	DK-Sor	13%	62%	-1%	62%	-1%	61%
-8%	-9%	-16%	-10%	-15%	-10%	FI-Hyy	62%	-11%	-6%	-11%	-5%	-10%
-5%	-16%	4%	-16%	1%	-16%	GF-Guy	-7%	4%	5%	4%	3%	4%
-32%	-9%	5%	-7%	-1%	-7%	IT-Cpz	57%	21%	5%	21%	0%	20%
32%	-22%	0%	-24%	-3%	-24%	IT-Lav	109%	14%	12%	14%	8%	14%
2%	-9%	-15%	-9%	-14%	-9%	IT-Ren	129%	29%	-5%	29%	-4%	29%
78%	-1%	-13%	-7%	-14%	-8%	IT-Ro2	-38%	22%	0%	22%	-2%	22%
-9%	-51%	-36%	-53%	-36%	-53%	US-ARM	12%	144%	1%	144%	-3%	144%
266%	152%	-14%	135%	-16%	135%	US-GLE	872%	348%	-3%	348%	-5%	348%
182%	231%	-13%	221%	-14%	220%	US-SRM	365%	186%	-6%	186%	-1%	186%
149%	87%	-15%	77%	-14%	77%	US-Ton	38%	93%	-3%	93%	0%	93%
18%	-57%	-40%	-61%	-40%	-61%	US-Var	-2%	100%	-2%	100%	-1%	100%

Table A2. Relative bias for NEE. Note that a positive bias in NEE means an underestimation of carbon uptake by the ecosystem. Abbreviations in the headings are as before. ~~Note that for static Noah-MP no NEE output is created.~~

ECLand						Location	Noah-MP					
default clim.		MODIS clim.		MODIS single			default clim.		MODIS clim.		MODIS single	
static	dynamic	static	dynamic	static	dynamic		static	dynamic	static	dynamic	static	dynamic
-21%	-20%	-34%	-22%	-33%	-22%	AT-Neu	~~-~~19%	-23%	~~-~~25%	-23%	~~-~~24%	-23%
67%	62%	69%	62%	72%	62%	AU-DaS	~~-~~9%	~~-4-~~6%	~~-~~11%	~~-4-~~6%	~~-~~11%	~~-4-~~6%
70%	65%	68%	65%	68%	65%	AU-How	~~-~~8%	~~7~~14%	~~-~~0%	~~7~~14%	~~-~~1%	~~7~~14%
57%	59%	65%	60%	65%	60%	AU-Stp	~~-~~22%	2%	~~-~~22%	2%	~~-~~22%	2%
-2%	2%	-3%	2%	-3%	2%	AU-Tum	~~-~~34%	-32%	~~-~~34%	-32%	~~-~~33%	-32%
-6%	-6%	-3%	-6%	-3%	-6%	BE-Lon	~~-~~12%	-17%	~~-~~16%	-17%	~~-~~16%	-17%
18%	16%	15%	16%	15%	16%	BE-Vie	~~-~~6%	-6%	~~-~~5%	-6%	~~-~~5%	-7%
-6%	-6%	-5%	-5%	-5%	-5%	CA-Oas	~~-~~23%	-9%	~~-~~22%	-9%	~~-~~21%	-10%
-1%	-2%	10%	-1%	11%	-1%	CA-Qfo	~~-~~32%	-31%	~~-~~22%	-31%	~~-~~22%	-31%
-17%	-6%	-15%	-6%	-15%	-6%	CH-Fru	~~-~~2%	-6%	~~-~~6%	-6%	~~-~~6%	-6%
5%	-20%	-9%	-20%	-9%	-20%	CH-Oe2	~~-~~20%	-26%	~~-~~21%	-26%	~~-~~21%	-26%
-7%	-7%	-4%	-7%	-4%	-7%	DE-Geb	~~-~~15%	-18%	~~-~~19%	-18%	~~-~~18%	-18%
7%	3%	3%	3%	2%	3%	DE-HoH	~~-~~16%	-6%	~~-~~21%	-6%	~~-~~21%	-6%
-1%	-4%	0%	-4%	0%	-4%	DK-Sor	~~-~~20%	-7%	~~-~~19%	-7%	~~-~~19%	-9%
5%	6%	6%	6%	6%	6%	FI-Hyy	~~-~~3%	-4%	~~-~~6%	-4%	~~-~~6%	-6%
13%	14%	13%	14%	14%	14%	GF-Guy	~~-~~62%	-54%	~~-~~62%	-54%	~~-~~61%	-54%
15%	10%	7%	9%	8%	9%	IT-Cpz	~~-~~40%	-30%	~~-~~36%	-30%	~~-~~34%	-33%
45%	49%	46%	49%	47%	49%	IT-Lav	~~-~~30%	32%	~~-~~32%	32%	~~-~~33%	32%
20%	20%	20%	20%	20%	20%	IT-Ren	~~-~~0%	5%	~~-~~7%	5%	~~-~~7%	5%
14%	19%	22%	19%	22%	20%	IT-Ro2	~~-~~9%	3%	~~-~~18%	3%	~~-~~17%	3%
-3%	-1%	-1%	-1%	-2%	-1%	US-ARM	~~-~~2%	-9%	~~-~~2%	-9%	~~-~~3%	-9%
-1%	0%	2%	0%	2%	0%	US-GLE	~~-~~27%	-19%	~~-~~7%	-19%	~~-~~7%	-19%
60%	59%	59%	59%	59%	59%	US-SRM	~~-~~8%	-6%	~~-~~3%	-6%	~~-~~4%	-6%
10%	8%	15%	9%	15%	9%	US-Ton	~~-~~7%	-9%	~~-~~8%	-9%	~~-~~9%	-9%
-11%	-7%	-9%	-7%	-9%	-7%	US-Var	~~-~~4%	-13%	~~-~~9%	-13%	~~-~~9%	-13%

Table A3. Relative bias for GPP. Abbreviations in the headings are as before.~~Note that for static Noah-MP no GPP output is produced.~~

ECLand						Location	Noah-MP					
default clim.		MODIS clim.		MODIS single			default clim.		MODIS clim.		MODIS single	
static	dynamic	static	dynamic	static	dynamic		static	dynamic	static	dynamic	static	dynamic
-25%	-25%	-15%	-23%	-15%	-24%	AT-Neu	~~-~~-25%	-20%	~~-~~-17%	-20%	~~-~~-17%	-20%
-38%	-31%	-39%	-31%	-42%	-31%	AU-DaS	~~-~~-24%	~~-21~~-16%	~~-~~-22%	~~-21~~-16%	~~-~~-21%	-16%
-44%	-38%	-41%	-38%	-42%	-38%	AU-How	~~-~~-33%	~~-1~~-18%	~~-~~-22%	~~-1~~-18%	~~-~~-22%	~~-1~~-18%
16%	12%	0%	10%	0%	10%	AU-Stp	~~-~~-30%	30%	~~-~~-3%	30%	~~-~~-4%	30%
-8%	-14%	-6%	-14%	-6%	-14%	AU-Tum	~~-~~-21%	23%	~~-~~-21%	23%	~~-~~-20%	23%
-8%	-5%	-18%	-6%	-19%	-6%	BE-Lon	~~-~~-7%	42%	~~-~~-9%	42%	~~-~~-7%	42%
-27%	-24%	-23%	-24%	-24%	-24%	BE-Vie	~~-~~-7%	-3%	~~-~~-11%	-3%	~~-~~-11%	-3%
-13%	-14%	-13%	-14%	-15%	-14%	CA-Oas	~~-~~-4%	8%	~~-~~-2%	8%	~~-~~-0%	5%
-4%	-3%	-21%	-4%	-22%	-4%	CA-Qfo	~~-~~-69%	41%	~~-~~-2%	41%	~~-~~-1%	41%
-15%	-29%	-17%	-29%	-17%	-29%	CH-Fru	~~-~~-32%	-23%	~~-~~-23%	-23%	~~-~~-23%	-23%
-49%	15%	-17%	16%	-17%	16%	CH-Oe2	~~-~~-2%	35%	~~-~~-1%	35%	~~-~~-1%	35%
-6%	-5%	-12%	-5%	-13%	-5%	DE-Geb	~~-~~-4%	42%	~~-~~-16%	42%	~~-~~-13%	42%
-25%	-17%	-15%	-16%	-13%	-16%	DE-HoH	~~-~~-16%	0%	~~-~~-5%	0%	~~-~~-4%	0%
-34%	-27%	-38%	-27%	-38%	-27%	DK-Sor	~~-~~-27%	-11%	~~-~~-29%	-11%	~~-~~-29%	-11%
-25%	-25%	-26%	-25%	-27%	-25%	FI-Hyy	~~-~~-10%	-8%	~~-~~-10%	-8%	~~-~~-10%	-8%
-12%	-12%	-8%	-12%	-10%	-12%	GF-Guy	~~-~~-2%	4%	~~-~~-0%	4%	~~-~~-1%	4%
-22%	-13%	-10%	-12%	-12%	-12%	IT-Cpz	~~-~~-16%	14%	~~-~~-7%	14%	~~-~~-5%	13%
-51%	-58%	-53%	-58%	-54%	-58%	IT-Lav	~~-~~-17%	-29%	~~-~~-30%	-29%	~~-~~-32%	-29%
-39%	-40%	-39%	-40%	-39%	-40%	IT-Ren	~~-~~-4%	-11%	~~-~~-21%	-11%	~~-~~-21%	-11%
11%	-1%	-9%	-3%	-9%	-3%	IT-Ro2	~~-~~-5%	30%	~~-~~-14%	30%	~~-~~-14%	30%
12%	9%	8%	8%	10%	8%	US-ARM	~~-~~-7%	38%	~~-~~-7%	38%	~~-~~-7%	38%
-22%	-23%	-25%	-23%	-25%	-23%	US-GLE	~~-~~-33%	13%	~~-~~-15%	13%	~~-~~-16%	13%
-23%	-23%	-22%	-23%	-22%	-23%	US-SRM	~~-~~-2%	5%	~~-~~-11%	5%	~~-~~-10%	5%
-7%	-5%	-11%	-5%	-11%	-5%	US-Ton	~~-~~-6%	3%	~~-~~-5%	3%	~~-~~-5%	3%
12%	8%	9%	7%	9%	7%	US-Var	~~-~~-1%	16%	~~-~~-5%	16%	~~-~~-5%	16%

Table A4. Relative bias for latent heat flux. Abbreviations in the headings are as before.

ECLand						Location	Noah-MP					
default clim.		MODIS clim.		MODIS single			default clim.		MODIS clim.		MODIS single	
static	dynamic	static	dynamic	static	dynamic		static	dynamic	static	dynamic	static	dynamic
-27%	-31%	-13%	-28%	-13%	-28%	AT-Neu	-25%	-19%	-21%	-19%	-22%	-19%
-27%	-18%	-30%	-18%	-37%	-19%	AU-DaS	~~-24~~-14%	~~-23~~-13%	~~-21~~-12%	~~-23~~-13%	~~-21~~-12%	~~-23~~-13%
-53%	-49%	-51%	-48%	-51%	-48%	AU-How	~~-31~~-43%	~~-29~~-43%	~~-29~~-40%	~~-29~~-43%	~~-29~~-40%	~~-29~~-43%
2%	-1%	-3%	-1%	-3%	-1%	AU-Stp	8%	~~1~~-1%	-3%	~~1~~-1%	-4%	~~1~~-1%
-11%	-17%	-7%	-17%	-7%	-17%	AU-Tum	5%	7%	4%	7%	~~5~~4%	7%
-16%	-14%	-22%	-14%	-24%	-14%	BE-Lon	-3%	0%	-3%	0%	-4%	0%
-27%	-20%	-19%	-20%	-20%	-20%	BE-Vie	-5%	1%	-4%	1%	-4%	1%
-9%	-9%	-9%	-9%	-10%	-10%	CA-Oas	3%	8%	4%	8%	3%	7%
-22%	-21%	-35%	-22%	-36%	-22%	CA-Qfo	-36%	-36%	-38%	-36%	-38%	-36%
-21%	-28%	-22%	-29%	-22%	-29%	CH-Fru	-30%	-25%	-29%	-25%	-29%	-25%
-65%	-1%	-25%	0%	-25%	0%	CH-Oe2	3%	9%	2%	9%	2%	9%
8%	3%	-5%	2%	-8%	2%	DE-Geb	-2%	5%	-1%	5%	-1%	5%
-41%	-33%	-30%	-32%	-29%	-32%	DE-HoH	-12%	-8%	-11%	-8%	-10%	-8%
-37%	-29%	-36%	-29%	-37%	-29%	DK-Sor	-19%	-12%	-21%	-12%	-21%	-12%
-22%	-21%	-22%	-21%	-22%	-21%	FI-Hyy	-34%	-32%	-35%	-32%	-35%	-32%
-31%	-36%	-26%	-35%	-30%	-36%	GF-Guy	-17%	-15%	-17%	-15%	-16%	-15%
-21%	-8%	-1%	-7%	-3%	-7%	IT-Cpz	17%	16%	16%	16%	14%	14%
-40%	-46%	-42%	-47%	-43%	-47%	IT-Lav	-50%	-47%	-50%	-47%	-50%	-47%
-41%	-41%	-41%	-41%	-41%	-41%	IT-Ren	-43%	-41%	-43%	-41%	-43%	-41%
-30%	-38%	-39%	-39%	-39%	-39%	IT-Ro2	-9%	-6%	-8%	-6%	-8%	-6%
6%	4%	7%	4%	6%	4%	US-ARM	6%	11%	7%	11%	6%	11%
-62%	-64%	-68%	-64%	-68%	-64%	US-GLE	-54%	-63%	-73%	-63%	-73%	-63%
-22%	-21%	-27%	-21%	-26%	-22%	US-SRM	-20%	-19%	-21%	-19%	-21%	-19%
-5%	-12%	-19%	-13%	-19%	-13%	US-Ton	-8%	-7%	-10%	-7%	-10%	-7%
29%	28%	29%	27%	28%	27%	US-Var	21%	23%	17%	23%	17%	22%

Table A5. Relative bias for evaporative fraction. Abbreviations in the headings are as before.

ECLand						Location	Noah-MP					
default clim.		MODIS clim.		MODIS single			default clim.		MODIS clim.		MODIS single	
static	dynamic	static	dynamic	static	dynamic		static	dynamic	static	dynamic	static	dynamic
-34%	-39%	-21%	-37%	-22%	-37%	AT-Neu	-12%	-10%	-9%	-10%	-9%	-10%
-43%	-36%	-47%	-37%	-53%	-37%	AU-DaS	~~-51~~-40%	~~-43~~-34%	~~-44~~-35%	~~-43~~-34%	~~-43~~-35%	~~-43~~-34%
-49%	-45%	-47%	-45%	-47%	-45%	AU-How	~~-29~~-43%	~~-22~~-40%	~~-25~~-38%	~~-22~~-40%	~~-25~~-38%	~~-22~~-40%
-14%	-18%	-16%	-17%	-17%	-17%	AU-Stp	-1%	~~-9~~-10%	~~-11~~-10%	~~-9~~-10%	-11%	~~-9~~-10%
-50%	-60%	-45%	-60%	-45%	-60%	AU-Tum	-26%	-23%	-27%	-23%	-27%	-23%
-4%	-5%	-10%	-6%	-11%	-6%	BE-Lon	8%	10%	9%	10%	9%	10%
-12%	-10%	-10%	-10%	-10%	-10%	BE-Vie	0%	3%	0%	3%	0%	3%
-4%	-5%	-5%	-5%	-5%	-5%	CA-Oas	-4%	-1%	-4%	-1%	-4%	-1%
-21%	-21%	-32%	-22%	-33%	-22%	CA-Qfo	-33%	-26%	-31%	-26%	-31%	-26%
-8%	-12%	-9%	-12%	-9%	-12%	CH-Fru	-10%	-9%	-10%	-9%	-10%	-9%
-32%	-30%	-18%	-29%	-18%	-29%	CH-Oe2	-4%	-4%	-5%	-4%	-5%	-4%
10%	4%	0%	3%	-2%	3%	DE-Geb	8%	13%	11%	13%	10%	13%
-52%	-46%	-45%	-45%	-43%	-45%	DE-HoH	-27%	-21%	-26%	-21%	-25%	-21%
-14%	-11%	-15%	-11%	-15%	-11%	DK-Sor	-9%	-4%	-10%	-4%	-10%	-4%
-5%	-6%	-6%	-6%	-6%	-6%	FI-Hyy	-11%	-10%	-12%	-10%	-12%	-10%
-73%	-78%	-63%	-78%	-67%	-78%	GF-Guy	-48%	-42%	-47%	-42%	-47%	-42%
-12%	0%	9%	1%	7%	1%	IT-Cpz	34%	34%	33%	34%	32%	33%
-25%	-31%	-28%	-32%	-29%	-32%	IT-Lav	-33%	-30%	-34%	-30%	-34%	-30%
-7%	-8%	-8%	-8%	-8%	-8%	IT-Ren	-13%	-12%	-13%	-12%	-13%	-12%
-7%	-17%	-22%	-18%	-22%	-18%	IT-Ro2	6%	16%	11%	16%	11%	16%
-7%	-9%	-7%	-9%	-8%	-9%	US-ARM	1%	2%	4%	2%	4%	2%
-41%	-44%	-50%	-45%	-50%	-45%	US-GLE	-29%	-26%	-31%	-26%	-31%	-26%
-8%	-7%	-11%	-7%	-11%	-7%	US-SRM	-15%	-9%	-13%	-9%	-13%	-9%
5%	0%	-6%	0%	-6%	0%	US-Ton	1%	3%	3%	3%	3%	3%
8%	2%	7%	2%	6%	2%	US-Var	9%	9%	15%	9%	15%	9%

Table A6. Relative bias of soil moisture. Abbreviations in the headings are as before.

ECLand						Location	Noah-MP					
default clim.		MODIS clim.		MODIS single			default clim.		MODIS clim.		MODIS single	
static	dynamic	static	dynamic	static	dynamic		static	dynamic	static	dynamic	static	dynamic
1%	2%	-5%	1%	-4%	1%	AT-Neu	-10%	-11%	-11%	-11%	-10%	-11%
695%	680%	704%	681%	711%	681%	AU-DaS	~~371~~481%	~~353~~441%	~~357~~455%	~~353~~441%	~~356~~456%	~~353~~441%
196%	193%	198%	193%	198%	193%	AU-How	~~192~~129%	~~146~~110%	~~170~~114%	~~146~~110%	~~169~~114%	~~146~~110%
116%	163%	180%	169%	179%	169%	AU-Stp	62%	54%	66%	54%	66%	54%
54%	57%	52%	57%	52%	57%	AU-Tum	29%	28%	29%	28%	29%	28%
10%	9%	13%	9%	14%	9%	BE-Lon	-8%	-13%	-8%	-13%	-8%	-13%
37%	36%	36%	36%	36%	36%	BE-Vie	7%	7%	7%	7%	7%	6%
131%	133%	133%	133%	133%	134%	CA-Oas	73%	65%	71%	65%	71%	66%
84%	83%	86%	83%	86%	83%	CA-Qfo	97%	96%	95%	96%	95%	96%
-33%	-32%	-33%	-32%	-33%	-32%	CH-Fru	-44%	-44%	-44%	-44%	-44%	-44%
53%	47%	50%	47%	50%	47%	CH-Oe2	29%	28%	29%	28%	29%	28%
82%	92%	101%	93%	102%	93%	DE-Geb	45%	27%	45%	27%	46%	27%
161%	154%	152%	154%	150%	153%	DE-HoH	109%	101%	106%	101%	105%	101%
80%	78%	80%	78%	80%	78%	DK-Sor	12%	11%	11%	11%	11%	11%
51%	50%	51%	50%	50%	50%	FI-Hyy	-3%	-4%	-3%	-4%	-4%	-5%
251%	253%	250%	253%	251%	253%	GF-Guy	159%	159%	160%	159%	160%	159%
246%	230%	228%	229%	230%	239%	IT-Cpz	124%	125%	124%	125%	123%	124%
-87%	-85%	-86%	-85%	-86%	-85%	IT-Lav	-25%	-25%	-25%	-25%	-25%	-25%
-42%	-42%	-42%	-42%	-42%	-42%	IT-Ren	-11%	-11%	-11%	-11%	-11%	-12%
75%	83%	84%	83%	83%	83%	IT-Ro2	25%	16%	22%	16%	22%	16%
-7%	-1%	-2%	0%	-2%	0%	US-ARM	14%	1%	16%	1%	16%	1%
48%	48%	50%	49%	50%	49%	US-GLE	36%	38%	39%	38%	39%	38%
455%	429%	552%	433%	552%	433%	US-SRM	298%	303%	339%	303%	338%	303%
36%	39%	45%	40%	45%	40%	US-Ton	6%	3%	14%	3%	14%	3%
58%	74%	72%	74%	72%	74%	US-Var	60%	53%	66%	53%	66%	53%

Author contributions. SW prepared model setups for the selected sites and prepared input data from available datasets in consultation with ST and AH. Model source code was provided by ST. SB supported setup of ECLand model runs. Simulations, analysis and plotting were done by SW with the involvement of AH and ST. SW took the lead in writing the manuscript with contributions from all authors.

Competing interests. The authors declare that they have no conflict of interest.

Acknowledgements. This work used eddy covariance data acquired and shared by the FLUXNET community and by the TERENO network. On-site LAI data from site "Hohes Holz" was acquired, analyzed, and shared by the working group Model Driven Monitoring led by site PI Corinna Rebmann at Helmholtz-Centre for Environmental Research - UFZ. We thank all station PIs, scientists, and technicians for their efforts in collecting, processing, and sharing their data.

References

Arsenault, K. R., Nearing, G. S., Wang, S., Yatheendradas, S., and Peters-Lidard, C. D.: Parameter Sensitivity of the Noah-MP Land Surface Model with Dynamic Vegetation, Journal of Hydrometeorology, 19, 815 –830, https://doi.org/10.1175/jhm-d-17-0205.1, 2018.

Ashaolu, E. D. and Iroye, K. A.: Rainfall and potential evapotranspiration patterns and their effects on climatic water balance in the Western Lithoral Hydrological Zone of Nigeria, Ruhuna Journal of Science, 9, https://doi.org/10.4038/rjs.v9i2.45, 2018.

Ball, J. T., Woodrow, I. E., and Berry, J. A.: A Model Predicting Stomatal Conductance and its Contribution to the Control of Photosynthesis under Different Environmental Conditions, pp. 221–224, Springer Netherlands, Dordrecht, https://doi.org/10.1007/978-94-017-0519-6_48, 1987.

Balsamo, G., Viterbo, P., Beljaars, A., van den Hurk, B., Hirschi, M., Betts, A. K., and Scipal, K.: A Revised Hydrology for the ECMWF Model: Verification from Field Site to Terrestrial Water Storage and Impact in the Integrated Forecast System, Journal of Hydrometeorology, 10, 623–643, https://doi.org/10.1175/2008jhm1068.1, 2009.

Beck, H. E., Pan, M., Miralles, D. G., Reichle, R. H., Dorigo, W. A., Hahn, S., Sheffield, J., Karthikeyan, L., Balsamo, G., Parinussa, R. M., van Dijk, A. I. J. M., Du, J., Kimball, J. S., Vergopolan, N., and Wood, E. F.: Evaluation of 18 satellite- and model-based soil moisture products using in situ measurements from 826 sensors, Hydrology and Earth System Sciences, 25, 17–40, https://doi.org/10.5194/hess-25-17-2021, 2021.

Benesty, J., Chen, J., Huang, Y., and Cohen, I.: Pearson correlation coefficient, in: Noise reduction in speech processing, pp. 37–40, Springer, 2009.

Best, M. J., Abramowitz, G., Johnson, H. R., Pitman, A. J., Balsamo, G., Boone, A., Cuntz, M., Decharme, B., Dirmeyer, P. A., Dong, J., Ek, M., Guo, Z., Haverd, V., van den Hurk, B. J. J., Nearing, G. S., Pak, B., Peters-Lidard, C., Santanello, J. A., Stevens, L., and Vuichard, N.: The Plumbing of Land Surface Models: Benchmarking Model Performance, Journal of Hydrometeorology, 16, 1425–1442, https://doi.org/10.1175/jhm-d-14-0158.1, 2015.

Blyth, E. M., Arora, V. K., Clark, D. B., Dadson, S. J., De Kauwe, M. G., Lawrence, D. M., Melton, J. R., Pongratz, J., Turton, R. H., Yoshimura, K., and Yuan, H.: Advances in Land Surface Modelling, Current Climate Change Reports, 7, 45–71, https://doi.org/10.1007/s40641-021-00171-5, 2021.

Bohm, K., Ingwersen, J., Milovac, J., and Streck, T.: Distinguishing between early- and late-covering crops in the land surface model Noah-MP: impact on simulated surface energy fluxes and temperature, Biogeosciences, 17, 2791–2805, https://doi.org/10.5194/bg-17-2791-2020, 2020.

Bonan, G. B.: Land surface model (LSM version 1.0) for ecological, hydrological, and atmospheric studies: Technical description and user's guide., Technical Note PB-97-131494/XAB; NCAR/TN-417-STR; TRN: 70341497, U.S. Department of Energy, Office of Scientific and Technical Information, https://www.osti.gov/biblio/442360, 1996.

Boussetta, S., Balsamo, G., Beljaars, A., Kral, T., and Jarlan, L.: Impact of a satellite-derived leaf area index monthly climatology in a global numerical weather prediction model, International Journal of Remote Sensing, 34, 3520–3542, https://doi.org/10.1080/01431161.2012.716543, 2012.

Boussetta, S., Balsamo, G., Beljaars, A., Panareda, A.-A., Calvet, J.-C., Jacobs, C., van den Hurk, B., Viterbo, P., Lafont, S., Dutra, E., Jarlan, L., Balzarolo, M., Papale, D., and van der Werf, G.: Natural land carbon dioxide exchanges in the ECMWF integrated forecasting system: Implementation and offline validation, Journal of Geophysical Research: Atmospheres, 118, 5923–5946, https://doi.org/https://doi.org/10.1002/jgrd.50488, 2013.

Boussetta, S., Balsamo, G., Dutra, E., Beljaars, A., and Albergel, C.: Assimilation of surface albedo and vegetation states from satellite observations and their impact on numerical weather prediction, Remote Sensing of Environment, 163, 111–126, https://doi.org/10.1016/j.rse.2015.03.009, 2015.

Boussetta, S., Balsamo, G., Arduini, G., Dutra, E., McNorton, J., Choulga, M., Agustí-Panareda, A., Beljaars, A., Wedi, N., Munõz-Sabater, J., de Rosnay, P., Sandu, I., Hadade, I., Carver, G., Mazzetti, C., Prudhomme, C., Yamazaki, D., and Zsoter, E.: ECLand: The ECMWF Land Surface Modelling System, Atmosphere, 12, https://doi.org/10.3390/atmos12060723, 2021.

Brunsell, N. A., de Oliveira, G., Barlage, M., Shimabukuro, Y., Moraes, E., and Aragão, L.: Examination of seasonal water and carbon dynamics in eastern Amazonia: a comparison of Noah-MP and MODIS, Theoretical and Applied Climatology, 143, 571–586, https://doi.org/10.1007/s00704-020-03435-6, 2020.

Budyko, M. I.: Climate and Life: English Ed. edited by David H. Miller, Academic Press, New York, 1974.

Cai, X., Yang, Z.-L., Xia, Y., Huang, M., Wei, H., Leung, L. R., and Ek, M. B.: Assessment of simulated water balance from Noah, Noah-MP, CLM, and VIC over CONUS using the NLDAS test bed, Journal of Geophysical Research: Atmospheres, 119, 13,751–13,770, https://doi.org/10.1002/2014jd022113, 2014.

Calvet, J. C. and Soussana, J. F.: Modelling CO2-enrichment effects using an interactive vegetation SVAT scheme, Agricultural and Forest Meteorology, 108, 129–152, https://doi.org/Doi 10.1016/S0168-1923(01)00235-0, 2001.

Calvet, J. C., Noilhan, J., Roujean, J. L., Bessemoulin, P., Cabelguenne, M., Olioso, A., and Wigneron, J. P.: An interactive vegetation SVAT model tested against data from six contrasting sites, Agricultural and Forest Meteorology, 92, 73–95, https://doi.org/Doi 10.1016/S0168-1923(98)00091-4, 1998.

Chen, F. and Dudhia, J.: Coupling an advanced land surface-hydrology model with the Penn State-NCAR MM5 modeling system. Part I: Model implementation and sensitivity, Monthly Weather Review, 129, 569–585, https://doi.org/Doi 10.1175/1520-0493(2001)129<0569:Caalsh>2.0.Co;2, 2001.

Copernicus: Climate Data Store, https://cds.climate.copernicus.eu/, accessed via: CDS API, last access: 2024-04-23, 2018.

Copin, Y.: Taylor diagram for python/matplotlib, https://doi.org/10.5281/zenodo.5548061, 2021.

De Kauwe, M. G., Zhou, S. X., Medlyn, B. E., Pitman, A. J., Wang, Y. P., Duursma, R. A., and Prentice, I. C.: Do land surface models need to include differential plant species responses to drought? Examining model predictions across a mesic-xeric gradient in Europe, Biogeosciences, 12, 7503–7518, https://doi.org/10.5194/bg-12-7503-2015, 2015.

Dickinson, R. E., Shaikh, M., Bryant, R., and Graumlich, L.: Interactive canopies for a climate model, Journal of Climate, 11, 2823–2836, https://doi.org/Doi 10.1175/1520-0442(1998)011<2823:Icfacm>2.0.Co;2, 1998.

Dirmeyer, P. A., Chen, L., Wu, J., Shin, C. S., Huang, B., Cash, B. A., Bosilovich, M. G., Mahanama, S., Koster, R. D., Santanello, J. A., Ek, M. B., Balsamo, G., Dutra, E., and Lawrence, D. M.: Verification of land-atmosphere coupling in forecast models, reanalyses and land surface models using flux site observations, J Hydrometeorol, 19, 375–392, https://doi.org/10.1175/JHM-D-17-0152.1, 2018.

Dirmeyer, P. A., Balsamo, G., Blyth, E. M., Morrison, R., and Cooper, H. M.: Land-Atmosphere Interactions Exacerbated the Drought and Heatwave Over Northern Europe During Summer 2018, AGU Advances, 2, https://doi.org/10.1029/2020av000283, 2021.

Dutra, E., Balsamo, G., Viterbo, P., Miranda, P. M. A., Beljaars, A., Schär, C., and Elder, K.: An Improved Snow Scheme for the ECMWF Land Surface Model: Description and Offline Validation, Journal of Hydrometeorology, 11, 899–916, https://doi.org/10.1175/2010jhm1249.1, 2010.

Ek, M. B., Mitchell, K. E., Lin, Y., Rogers, E., Grunmann, P., Koren, V., Gayno, G., and Tarpley, J. D.: Implementation of Noah land surface model advances in the National Centers for Environmental Prediction operational mesoscale Eta model, Journal of Geophysical Research: Atmospheres, 108, https://doi.org/10.1029/2002jd003296, 2003.

Fang, H., Wei, S., and Liang, S.: Validation of MODIS and CYCLOPES LAI products using global field measurement data, Remote Sensing of Environment, 119, 43–54, https://doi.org/10.1016/j.rse.2011.12.006, 2012.

Fisher, J. B., Huntzinger, D. N., Schwalm, C. R., and Sitch, S.: Modeling the Terrestrial Biosphere, Annual Review of Environment and Resources, 39, 91–123, https://doi.org/10.1146/annurev-environ-012913-093456, 2014.

fluxnet.org: FLUXNET2015 Dataset, https://fluxnet.org/data/fluxnet2015-dataset/, last access: 2024-04-23, 2020.

Forzieri, G., Miralles, D. G., Ciais, P., Alkama, R., Ryu, Y., Duveiller, G., Zhang, K., Robertson, E., Kautz, M., Martens, B., Jiang, C. Y., Arneth, A., Georgievski, G., Li, W., Ceccherini, G., Anthoni, P., Lawrence, P., Wiltshire, A., Pongratz, J., Piao, S. L., Sitch, S., Goll, D. S., Arora, V. K., Lienert, S., Lombardozzi, D., Kato, E., Nabel, J. E. M. S., Tian, H. Q., Friedlingstein, P., and Cescatti, A.: Increased control of vegetation on global terrestrial energy fluxes, Nature Climate Change, 10, 356–+, https://doi.org/10.1038/s41558-020-0717-0, 2020.

Garrigues, S., Lacaze, R., Baret, F., Morisette, J. T., Weiss, M., Nickeson, J. E., Fernandes, R., Plummer, S., Shabanov, N. V., Myneni, R. B., Knyazikhin, Y., and Yang, W.: Validation and intercomparison of global Leaf Area Index products derived from remote sensing data, Journal of Geophysical Research: Biogeosciences, 113, https://doi.org/10.1029/2007jg000635, 2008.

Garrigues, S., Verhoef, A., Blyth, E., Wright, A., Balan-Sarojini, B., Robinson, E. L., Dadson, S., Boone, A., Boussetta, S., and Balsamo, G.: Capability of the variogram to quantify the spatial patterns of surface fluxes and soil moisture simulated by land surface models, Progress in Physical Geography: Earth and Environment, 45, 279–293, https://doi.org/10.1177/0309133320986147, 2021.

Harrigan, S., Zoster, E., Cloke, H., Salamon, P., and Prudhomme, C.: Daily ensemble river discharge reforecasts and real-time forecasts from the operational Global Flood Awareness System, Hydrology and Earth System Sciences Discussions, pp. 1–22, https://doi.org/10.5194/hess-2020-532, publisher: Copernicus GmbH, 2020.

Haughton, N., Abramowitz, G., Pitman, A. J., Or, D., Best, M. J., Johnson, H. R., Balsamo, G., Boone, A., Cuntz, M., Decharme, B., Dirmeyer, P. A., Dong, J., Ek, M., Guo, Z., Haverd, V., van den Hurk, B. J. J., Nearing, G. S., Pak, B., Santanello, J. A., J., Stevens, L. E., and Vuichard, N.: The plumbing of land surface models: is poor performance a result of methodology or data quality?, J Hydrometeorol, 17, 1705–1723, https://doi.org/10.1175/JHM-D-15-0171.1, 2016.

Haughton, N., Abramowitz, G., De Kauwe, M. G., and Pitman, A. J.: Does predictability of fluxes vary between FLUXNET sites?, Biogeosciences, 15, 4495–4513, https://doi.org/10.5194/bg-15-4495-2018, 2018a.

Haughton, N., Abramowitz, G., and Pitman, A. J.: On the predictability of land surface fluxes from meteorological variables, Geoscientific Model Development, 11, 195–212, https://doi.org/10.5194/gmd-11-195-2018, 2018b.

Haverd, V., Smith, B., Nieradzik, L., Briggs, P. R., Woodgate, W., Trudinger, C. M., Canadell, J. G., and Cuntz, M.: A new version of the CABLE land surface model (Subversion revision r4601) incorporating land use and land cover change, woody vegetation demography, and a novel optimisation-based approach to plant coordination of photosynthesis, Geoscientific Model Development, 11, 2995–3026, https://doi.org/10.5194/gmd-11-2995-2018, 2018.

Hengl, T., de Jesus, J. M., MacMillan, R. A., Batjes, N. H., Heuvelink, G. B., Ribeiro, E., Samuel-Rosa, A., Kempen, B., Leenaars, J. G., Walsh, M. G., and Gonzalez, M. R.: SoilGrids1km–global soil information based on automated mapping, PLoS One, 9, e105 992, https://doi.org/10.1371/journal.pone.0105992, 2014.

Hersbach, H., Bell, B., Berrisford, P., Hirahara, S., Horányi, A., Muñoz-Sabater, J., Nicolas, J., Peubey, C., Radu, R., Schepers, D., Simmons, A., Soci, C., Abdalla, S., Abellan, X., Balsamo, G., Bechtold, P., Biavati, G., Bidlot, J., Bonavita, M., De Chiara, G., Dahlgren, P., Dee,

D., Diamantakis, M., Dragani, R., Flemming, J., Forbes, R., Fuentes, M., Geer, A., Haimberger, L., Healy, S., Hogan, R. J., Hólm, E., Janisková, M., Keeley, S., Laloyaux, P., Lopez, P., Lupu, C., Radnoti, G., de Rosnay, P., Rozum, I., Vamborg, F., Villaume, S., and Thépaut, J.-N.: The ERA5 global reanalysis, Q. J. Roy. Meteor. Soc., n/a, https://doi.org/10.1002/qj.3803, 2020.

Hu, Z., Piao, S., Knapp, A. K., Wang, X., Peng, S., Yuan, W., Running, S., Mao, J., Shi, X., Ciais, P., Huntzinger, D. N., Yang, J., and Yu, G.: Decoupling of greenness and gross primary productivity as aridity decreases, Remote Sensing of Environment, 279, 113 120, https://doi.org/10.1016/j.rse.2022.113120, 2022.

Huang, A., Shen, R., Di, W., and Han, H.: A methodology to reconstruct LAI time series data based on generative adversarial network and improved Savitzky-Golay filter, International Journal of Applied Earth Observation and Geoinformation, 105, https://doi.org/10.1016/j.jag.2021.102633, 2021.

Huang, A., Shen, R., Shi, C., and Sun, S.: Effects of satellite LAI data on modelling land surface temperature and related energy budget in the Noah-MP land surface model, Journal of Hydrology, 613, https://doi.org/10.1016/j.jhydrol.2022.128351, 2022.

Jarlan, L., Balsamo, G., Lafont, S., Beljaars, A., Calvet, J. C., and Mougin, E.: Analysis of leaf area index in the ECMWF land surface model and impact on latent heat and carbon fluxes: Application to West Africa, Journal of Geophysical Research: Atmospheres, 113, https://doi.org/10.1029/2007jd009370, 2008.

Jung, M., Koirala, S., Weber, U., Ichii, K., Gans, F., Camps-Valls, G., Papale, D., Schwalm, C., Tramontana, G., and Reichstein, M.: The FLUXCOM ensemble of global land-atmosphere energy fluxes, Scientific Data, 6, 74, https://doi.org/10.1038/s41597-019-0076-8, 2019.

Krinner, G., Derksen, C., Essery, R., Flanner, M., Hagemann, S., Clark, M., Hall, A., Rott, H., Brutel-Vuilmet, C., Kim, H., Ménard, C. B., Mudryk, L., Thackeray, C., Wang, L., Arduini, G., Balsamo, G., Bartlett, P., Boike, J., Boone, A., Chéruy, F., Colin, J., Cuntz, M., Dai, Y., Decharme, B., Derry, J., Ducharne, A., Dutra, E., Fang, X., Fierz, C., Ghattas, J., Gusev, Y., Haverd, V., Kontu, A., Lafaysse, M., Law, R., Lawrence, D., Li, W., Marke, T., Marks, D., Ménégoz, M., Nasonova, O., Nitta, T., Niwano, M., Pomeroy, J., Raleigh, M. S., Schaedler, G., Semenov, V., Smirnova, T. G., Stacke, T., Strasser, U., Svenson, S., Turkov, D., Wang, T., Wever, N., Yuan, H., Zhou, W., and Zhu, D.: ESM-SnowMIP: assessing snow models and quantifying snow-related climate feedbacks, Geoscientific Model Development, 11, 5027–5049, https://doi.org/10.5194/gmd-11-5027-2018, 2018.

Kumar, S. V., M. Mocko, D., Wang, S., Peters-Lidard, C. D., and Borak, J.: Assimilation of Remotely Sensed Leaf Area Index into the Noah-MP Land Surface Model: Impacts on Water and Carbon Fluxes and States over the Continental United States, Journal of Hydrometeorology, 20, 1359–1377, https://doi.org/10.1175/jhm-d-18-0237.1, 2019.

Lawrence, D. M., Fisher, R. A., Koven, C. D., Oleson, K. W., Swenson, S. C., Bonan, G., Collier, N., Ghimire, B., van Kampenhout, L., Kennedy, D., Kluzek, E., Lawrence, P. J., Li, F., Li, H., Lombardozzi, D., Riley, W. J., Sacks, W. J., Shi, M., Vertenstein, M., Wieder, W. R., Xu, C., Ali, A. A., Badger, A. M., Bisht, G., van den Broeke, M., Brunke, M. A., Burns, S. P., Buzan, J., Clark, M., Craig, A., Dahlin, K., Drewniak, B., Fisher, J. B., Flanner, M., Fox, A. M., Gentine, P., Hoffman, F., Keppel-Aleks, G., Knox, R., Kumar, S., Lenaerts, J., Leung, L. R., Lipscomb, W. H., Lu, Y., Pandey, A., Pelletier, J. D., Perket, J., Randerson, J. T., Ricciuto, D. M., Sanderson, B. M., Slater, A., Subin, Z. M., Tang, J., Thomas, R. Q., Val Martin, M., and Zeng, X.: The Community Land Model Version 5: Description of New Features, Benchmarking, and Impact of Forcing Uncertainty, Journal of Advances in Modeling Earth Systems, 11, 4245–4287, https://doi.org/10.1029/2018MS001583, _eprint: https://onlinelibrary.wiley.com/doi/pdf/10.1029/2018MS001583, 2019.

Lawrence, P. J., Lawrence, D. M., and Hurtt, G. C.: Attributing the Carbon Cycle Impacts of CMIP5 Historical and Future Land Use and Land Cover Change in the Community Earth System Model (CESM1), Journal of Geophysical Research: Biogeosciences, 123, 1732–1755, https://doi.org/10.1029/2017jg004348, 2018.

Li, J., Zhang, G., Chen, F., Peng, X., and Gan, Y.: Evaluation of Land Surface Subprocesses and Their Impacts on Model Performance With Global Flux Data, Journal of Advances in Modeling Earth Systems, 11, 1329–1348, https://doi.org/10.1029/2018ms001606, 2019.

Li, J., Chen, F., Lu, X., Gong, W., Zhang, G., and Gan, Y.: Quantifying Contributions of Uncertainties in Physical Parameterization Schemes and Model Parameters to Overall Errors in Noah-MP Dynamic Vegetation Modeling, Journal of Advances in Modeling Earth Systems, 12, https://doi.org/10.1029/2019ms001914, 2020.

Li, J., Miao, C., Zhang, G., Fang, Y., Shangguan, W., and Niu, G.: Global Evaluation of the Noah-MP Land Surface Model and Suggestions for Selecting Parameterization Schemes, Journal of Geophysical Research: Atmospheres, 127, https://doi.org/10.1029/2021jd035753, 2022.

Li, L., Yang, Z., Matheny, A. M., Zheng, H., Swenson, S. C., Lawrence, D. M., Barlage, M., Yan, B., McDowell, N. G., and Leung, L. R.: Representation of Plant Hydraulics in the Noah-MP Land Surface Model: Model Development and Multiscale Evaluation, Journal of Advances in Modeling Earth Systems, 13, https://doi.org/10.1029/2020ms002214, 2021.

Liang, J., Yang, Z., and Lin, P.: Systematic Hydrological Evaluation of the Noah-MP Land Surface Model over China, Advances in Atmospheric Sciences, 36, 1171–1187, https://doi.org/10.1007/s00376-019-9016-y, 2019.

Liang, J., Yang, Z.-L., Cai, X., Lin, P., Zheng, H., and Bian, Q.: Modeling the Impacts of Nitrogen Dynamics on Regional Terrestrial Carbon and Water Cycles over China with Noah-MP-CN, Advances in Atmospheric Sciences, 37, 679–695, https://doi.org/10.1007/s00376-020-9231-6, 2020.

Liu, X., Chen, F., Barlage, M., Zhou, G., and Niyogi, D.: Noah-MP-Crop: Introducing dynamic crop growth in the Noah-MP land surface model, Journal of Geophysical Research: Atmospheres, 121, 13,953–13,972, https://doi.org/10.1002/2016jd025597, 2016.

Luo, J., Ying, K., and Bai, J.: Savitzky-Golay smoothing and differentiation filter for even number data, Signal Processing, 85, 1429–1434, https://doi.org/10.1016/j.sigpro.2005.02.002, 2005.

Ma, N., Niu, G.-Y., Xia, Y., Cai, X., Zhang, Y., Ma, Y., and Fang, Y.: A Systematic Evaluation of Noah-MP in Simulating Land-Atmosphere Energy, Water, and Carbon Exchanges Over the Continental United States, Journal of Geophysical Research: Atmospheres, 122, 12,245–12,268, https://doi.org/10.1002/2017jd027597, 2017.

Menard, C. B., Essery, R., Krinner, G., Arduini, G., Bartlett, P., Boone, A., Brutel-Vuilmet, C., Burke, E., Cuntz, M., Dai, Y., Decharme, B., Dutra, E., Fang, X., Fierz, C., Gusev, Y., Hagemann, S., Haverd, V., Kim, H., Lafaysse, M., Marke, T., Nasonova, O., Nitta, T., Niwano, M., Pomeroy, J., Schädler, G., Semenov, V. A., Smirnova, T., Strasser, U., Swenson, S., Turkov, D., Wever, N., and Yuan, H.: Scientific and Human Erros in a Snow Model Intercomparison, https://doi.org/https://doi.org/10.1175/BAMS-D-19-0329.1, 2021.

Myneni, R., Knyazikhin, Y., and Park, T.: MOD15A2H MODIS/Terra Leaf Area Index/FPAR 8-Day L4 Global 500m SIN Grid V006, https://doi.org/https://doi.org/10.5067/MODIS/MOD15A2H.006, 2015.

National Center for Atmospheric Research: The Climate Data Guide: CERES: IGBP Land Classification., https://climatedataguide.ucar.edu/climate-data/ceres-igbp-land-classification, accessed: 2024-06-03, 2022.

Niu, G.-Y., Yang, Z.-L., Dickinson, R. E., Gulden, L. E., and Su, H.: Development of a simple groundwater model for use in climate models and evaluation with Gravity Recovery and Climate Experiment data, Journal of Geophysical Research, 112, https://doi.org/10.1029/2006jd007522, 2007.

Niu, G.-Y., Yang, Z.-L., Mitchell, K. E., Chen, F., Ek, M. B., Barlage, M., Kumar, A., Manning, K., Niyogi, D., Rosero, E., Tewari, M., and Xia, Y.: The community Noah land surface model with multiparameterization options (Noah-MP): 1. Model description and evaluation with local-scale measurements, Journal of Geophysical Research, 116, https://doi.org/10.1029/2010jd015139, 2011.

Nogueira, M., Boussetta, S., Balsamo, G., Albergel, C., Trigo, I. F., Johannsen, F., Miralles, D. G., and Dutra, E.: Upgrading Land-Cover and Vegetation Seasonality in the ECMWF Coupled System: Verification With FLUXNET Sites, METEOSAT Satellite Land Surface Temperatures, and ERA5 Atmospheric Reanalysis, J Geophys Res Atmos, 126, e2020JD034 163, https://doi.org/10.1029/2020JD034163, 2021.

Oleson, K. W., Lawrence, D. M., Bonan, G. B., Flanner, M. G., Kluzek, E., Lawrence, P. J., Levis, S., Swenson, S. C., and Thornton, P. E.: Technical Description of version 4.0 of the Community Land Model (CLM), NCAR Technical Note, 2010.

Pastorello, G., Trotta, C., Canfora, E., Chu, H., Christianson, D., Cheah, Y. W., Poindexter, C., Chen, J., Elbashandy, A., Humphrey, M., Isaac, P., Polidori, D., Reichstein, M., Ribeca, A., van Ingen, C., Vuichard, N., Zhang, L., Amiro, B., Ammann, C., Arain, M. A., Ardo, J., Arkebauer, T., Arndt, S. K., Arriga, N., Aubinet, M., Aurela, M., Baldocchi, D., Barr, A., Beamesderfer, E., Marchesini, L. B., Bergeron, O., Beringer, J., Bernhofer, C., Berveiller, D., Billesbach, D., Black, T. A., Blanken, P. D., Bohrer, G., Boike, J., Bolstad, P. V., Bonal, D., Bonnefond, J. M., Bowling, D. R., Bracho, R., Brodeur, J., Brummer, C., Buchmann, N., Burban, B., Burns, S. P., Buysse, P., Cale, P., Cavagna, M., Cellier, P., Chen, S., Chini, I., Christensen, T. R., Cleverly, J., Collalti, A., Consalvo, C., Cook, B. D., Cook, D., Coursolle, C., Cremonese, E., Curtis, P. S., D'Andrea, E., da Rocha, H., Dai, X., Davis, K. J., Cinti, B., Grandcourt, A., Ligne, A., De Oliveira, R. C., Delpierre, N., Desai, A. R., Di Bella, C. M., Tommasi, P. D., Dolman, H., Domingo, F., Dong, G., Dore, S., Duce, P., Dufrene, E., Dunn, A., Dusek, J., Eamus, D., Eichelmann, U., ElKhidir, H. A. M., Eugster, W., Ewenz, C. M., Ewers, B., Famulari, D., Fares, S., Feigenwinter, I., Feitz, A., Fensholt, R., Filippa, G., Fischer, M., Frank, J., Galvagno, M., Gharun, M., et al.: The FLUXNET2015 dataset and the ONEFlux processing pipeline for eddy covariance data, Sci Data, 7, 225, https://doi.org/10.1038/s41597-020-0534-3, 2020.

Piayda, A., Dubbert, M., Werner, C., Vaz Correia, A., Pereira, J. S., and Cuntz, M.: Influence of woody tissue and leaf clumping on vertically resolved leaf area index and angular gap probability estimates, Forest Ecology and Management, 340, 103–113, https://doi.org/https://doi.org/10.1016/j.foreco.2014.12.026, 2015.

Pilotto, I. L., Rodríguez, D. A., Tomasella, J., Sampaio, G., and Chou, S. C.: Comparisons of the Noah-MP land surface model simulations with measurements of forest and crop sites in Amazonia, Meteorology and Atmospheric Physics, 127, 711–723, https://doi.org/10.1007/s00703-015-0399-8, 2015.

Rebmann, C. and Pohl, F.: Carbon, water and energy fluxes at the TERENO/ICOS ecosystem station Hohes Holz in Central Germany since 2015, https://doi.org/10.1594/PANGAEA.940760, 2023.

Ruiz-Vásquez, M., O, S., Arduini, G., Boussetta, S., Brenning, A., Bastos, A., Koirala, S., Balsamo, G., Reichstein, M., and Orth, R.: Impact of Updating Vegetation Information on Land Surface Model Performance, Journal of Geophysical Research: Atmospheres, 128, https://doi.org/10.1029/2023jd039076, 2023.

Sakaguchi, K. and Zeng, X.: Effects of soil wetness, plant litter, and under-canopy atmospheric stability on ground evaporation in the Community Land Model (CLM3.5), Journal of Geophysical Research: Atmospheres, 114, https://doi.org/10.1029/2008jd010834, 2009.

Savitzky, A. and Golay, M. J. E.: Smoothing + Differentiation of Data by Simplified Least Squares Procedures, Analytical Chemistry, 36, 1627–, https://doi.org/DOI 10.1021/ac60214a047, 1964.

Sayed, A. H.: Fundamentals of adaptive filtering, John Wiley & Sons, 2003.

Schweppe, R., Thober, S., Müller, S., Kelbling, M., Kumar, R., Attinger, S., and Samaniego, L.: MPR 1.0: a stand-alone multiscale parameter regionalization tool for improved parameter estimation of land surface models, Geoscientific Model Development, 15, 859–882, https://doi.org/10.5194/gmd-15-859-2022, 2022.

Stevens, D., Miranda, P. M. A., Orth, R., Boussetta, S., Balsamo, G., and Dutra, E.: Sensitivity of Surface Fluxes in the ECMWF Land Surface Model to the Remotely Sensed Leaf Area Index and Root Distribution: Evaluation with Tower Flux Data, Atmosphere, 11, https://doi.org/10.3390/atmos11121362, 2020.

Trabucco, A. and Zomer, R. J.: Global Aridity Index and Potential Evapo-Transpiration (ET0) Climate Database v2, CGIAR-CSI GeoPortal, 2018.

Ukkola, A. M., De Kauwe, M. G., Pitman, A. J., Best, M. J., Abramowitz, G., Haverd, V., Decker, M., and Haughton, N.: Land surface models systematically overestimate the intensity, duration and magnitude of seasonal-scale evaporative droughts, Environmental Research Letters, 11, https://doi.org/10.1088/1748-9326/11/10/104012, 2016.

University Corporation for Atmospheric Research: Noah-Multiparameterization Land Surface Model (Noah-MP®LSM), https://ral.ucar.edu/model/noah-multiparameterization-land-surface-model-noah-mp-lsm, accessed: 2024-06-04, 2023.

van den Hurk, B. J. J. M., Viterbo, P., and Los, S. O.: Impact of leaf area index seasonality on the annual land surface evaporation in a global circulation model, Journal of Geophysical Research: Atmospheres, 108, https://doi.org/10.1029/2002jd002846, 2003.

van Genuchten, M. T.: A Closed-form Equation for Predicting the Hydraulic Conductivity of Unsaturated Soils, Soil Science Society of America Journal, 44, 892–898, https://doi.org/10.2136/sssaj1980.03615995004400050002x, 1980.

Weiss, M., Baret, F., Garrigues, S., and Lacaze, R.: LAI and fAPAR CYCLOPES global products derived from VEGETATION. Part 2: validation and comparison with MODIS collection 4 products, Remote Sensing of Environment, 110, 317–331, https://doi.org/10.1016/j.rse.2007.03.001, 2007.

Wollschläger, U., Attinger, S., Borchardt, D., Brauns, M., Cuntz, M., Dietrich, P., Fleckenstein, J. H., Friese, K., Friesen, J., Harpke, A., Hildebrandt, A., Jäckel, G., Kamjunke, N., Knöller, K., Kögler, S., Kolditz, O., Krieg, R., Kumar, R., Lausch, A., Liess, M., Marx, A., Merz, R., Mueller, C., Musolff, A., Norf, H., Oswald, S. E., Rebmann, C., Reinstorf, F., Rode, M., Rink, K., Rinke, K., Samaniego, L., Vieweg, M., Vogel, H.-J., Weitere, M., Werban, U., Zink, M., and Zacharias, S.: The Bode hydrological observatory: a platform for integrated, interdisciplinary hydro-ecological research within the TERENO Harz/Central German Lowland Observatory, Environmental Earth Sciences, 76, https://doi.org/10.1007/s12665-016-6327-5, 2016.

Xiao, Z., Liang, S., Wang, J., Jiang, B., and Li, X.: Real-time retrieval of Leaf Area Index from MODIS time series data, Remote Sensing of Environment, 115, 97–106, https://doi.org/10.1016/j.rse.2010.08.009, 2011.

Xiao, Z., Liang, S., Wang, J., Xiang, Y., Zhao, X., and Song, J.: Long-Time-Series Global Land Surface Satellite Leaf Area Index Product Derived From MODIS and AVHRR Surface Reflectance, IEEE Transactions on Geoscience and Remote Sensing, 54, 5301–5318, https://doi.org/10.1109/tgrs.2016.2560522, 2016.

Xu, T., Chen, F., He, X., Barlage, M., Zhang, Z., Liu, S., and He, X.: Improve the Performance of the Noah-MP-Crop Model by Jointly Assimilating Soil Moisture and Vegetation Phenology Data, Journal of Advances in Modeling Earth Systems, 13, https://doi.org/10.1029/2020ms002394, 2021.

Yang, F., Dan, L., Peng, J., Yang, X., Li, Y., and Gao, D.: Subdaily to Seasonal Change of Surface Energy and Water Flux of the Haihe River Basin in China: Noah and Noah-MP Assessment, Advances in Atmospheric Sciences, 36, 79–92, https://doi.org/10.1007/s00376-018-8035-4, 2018.

Yang, Q., Dan, L., Lv, M., Wu, J., Li, W., and Dong, W.: Quantitative assessment of the parameterization sensitivity of the Noah-MP land surface model with dynamic vegetation using ChinaFLUX data, Agricultural and Forest Meteorology, 307, https://doi.org/10.1016/j.agrformet.2021.108542, 2021.

Yang, Z.-L. and Niu, G.-Y.: Effects of Frozen Soil on Snowmelt Runoff and Soil Water Storage at a Continental Scale, Journal of Hydrometeorology, 7, 937–952, https://doi.org/10.1175/jhm538.1, 2006.

Yang, Z.-L., Niu, G.-Y., Mitchell, K. E., Chen, F., Ek, M. B., Barlage, M., Longuevergne, L., Manning, K., Niyogi, D., Tewari, M., and Xia, Y.: The community Noah land surface model with multiparameterization options (Noah-MP): 2. Evaluation over global river basins, Journal of Geophysical Research, 116, https://doi.org/10.1029/2010jd015140, 2011.

Zhang, G., Chen, F., and Gan, Y.: Assessing uncertainties in the Noah-MP ensemble simulations of a cropland site during the Tibet Joint International Cooperation program field campaign, Journal of Geophysical Research: Atmospheres, 121, 9576–9596, https://doi.org/10.1002/2016jd024928, 2016.

Zhang, X., Yan, K., Liu, J., Yang, K., Pu, J., Yan, G., Heiskanen, J., Zhu, P., Knyazikhin, Y., and Myneni, R. B.: An Insight Into the Internal Consistency of MODIS Global Leaf Area Index Products, IEEE Transactions on Geoscience and Remote Sensing, 62, 1–16, https://doi.org/10.1109/tgrs.2024.3434366, 2024.

Zhang, Z., Xin, Q., and Li, W.: Machine Learning-Based Modeling of Vegetation Leaf Area Index and Gross Primary Productivity Across North America and Comparison With a Process-Based Model, Journal of Advances in Modeling Earth Systems, p. 25, https://doi.org/10.1029/2021MS002802, 2021.

Does dynamically ~~modelled~~ modeled leaf area improve predictions of land surface water and carbon fluxes? - Insights into dynamic vegetation modules

Sven A. Westermann[1], Anke Hildebrandt[1,2], Souhail Bousetta[3], and Stephan Thober[1]

[1]Helmholtz Centre for Environmental Research GmbH - UFZ, Computational Hydrosystems, Leipzig, Germany
[2]Friedrich Schiller University Jena, Institute for Geosciences, Jena, Germany
[3]European Centre for Medium-Range Weather Forecasts, Reading, UK

Correspondence: Sven Westermann (sven.westermann@ufz.de)

Abstract. Land-surface models represent exchange processes between soil and atmosphere via the land surface by coupling water, energy and carbon fluxes. As ~~it strongly mediates the link~~ a strong mediator between these cycles~~and~~, vegetation is an important component of ~~land-surface models. In doing so, some of these~~ land surface models. Some land surface models include modules for vegetation dynamics~~which allow adaptation~~, which allow the adjustment of vegetation biomass, especially leaf area index, to environmental conditions. Here, we conducted a model-data comparison to investigate whether and how vegetation dynamics in the models ~~improves~~ improve the representation of vegetation processes and related surface fluxes in two specific models, ECLand and Noah-MP, in contrast to using prescribed values from look-up tables or satellite-based products. We ~~compare~~ compared model results with ~~stations from the FLUXNET 2015 dataset covering a range in~~ observations across a range of climate and vegetation types ~~, the~~ from the FLUXNET2015 dataset and the MODIS leaf area product, and ~~use more detailed information from the TERENO site"Hohes Holz". With the current implementation, switching vegetation dynamics on~~ used on-site measured leaf area from an additional site. Yet, switching on the dynamic vegetation did not enhance representativeness of ~~e.g.~~ leaf area index and net ecosystem exchange in ECLand, while it improved performance in Noah-MP ~~improved it~~ only for some sites. The representation of energy fluxes and soil moisture was almost unaffected for both models. Interestingly, ~~for both models,~~ the performance regarding ~~vegetation- and hydrology-related variables was unrelated~~variables of the carbon and water cycle was unrelated for both models, such that the weak performance ~~regarding~~ of e.g. leaf area index did not ~~detoriate the performance regarding~~ deteriorate the performance of e.g. latent heat flux. ~~One reason , we showed here, might be that~~ We show that one potential reason for this could be that the implemented ecosystem processes diverge from the observations in their seasonal patterns and variability. Noah-MP includes a seasonal hysteresis ~~of~~ in the relationship between leaf area index and gross primary production that ~~cannot be~~ is not found in observations. The same relationship is represented by a strong linear response in ECLand, which substantially underestimates the ~~variability seen in observations~~observed variability. For both ~~,~~ water and carbon fluxes, the ~~current implemented modules for vegetation dynamics~~ currently implemented dynamic vegetation modules in these two models ~~yielded no~~ did not result in better model performance compared to runs with static vegetation and prescribed ~~leaf-area~~ leaf area climatology.

Copyright statement.

1 Introduction

Land-surface models (LSMs) represent the energy, water and biogeochemical cycles at the land surface. ~~The~~ Traditionally, their main purpose has been to provide a surface component in coupled atmosphere-land models~~, but~~ . LSMs are applied in meteorological models, reanalysis products or in the Coupled Model Intercomparison Project (CMIP). However, their scope is widening and new fields of application like historical land cover change simulations (Lawrence et al., 2018) or flood alert services (Harrigan et al., 2020) are arising. ~~Active~~ There is active development within the ~~land-surface modelling communityis ongoing, adding~~ land surface modeling community, with more and more features being added to existing models to make them more realistic (Blyth et al., 2021).

Given the wide use of these models and the implications of their results~~as they are used in the Coupled Model Intercomparison Project (CMIP)~~, extensive model validation has been done already. Model validation covers a wide range of water, energy and carbon fluxes at global~~and point scale (a.o. Niu et al., 2011; Haverd et al., 2018; Lawrence et al., 2019; Boussetta et al., 2021)~~ , regional and site scale (e.g. Niu et al., 2011; Haverd et al., 2018; Lawrence et al., 2019; Boussetta et al., 2021). Such works that introduce individual evaluation schemes are often accompanied by studies that perform comparisons between ~~them like Best et al. (2015) or Krinner et al. (2018)~~models (e.g. Best et al., 2015; Krinner et al., 2018). Comparisons like those are conducted for different reasons. For example, one aim is to create a ranking between models that allows the assessment against alternative schemes. Using this method, Best et al. (2015) reported that simple statistical methods achieve a higher performance in energy partitioning at eddy-covariance sites than ~~an ensemble of LSMs~~any single LSM tested. One limitation of that study is that they did not report metrics of individual model performance, but only normalized ones. This procedure does not allow to judge whether the investigated methods have achieved a (dis-)satisfactory performance, since all methods might have a poor individual model performance. Other challenges in these activities are to maintain a standard protocol for model comparison, while not creating a superficial performance contest among them, and to minimize human errors (Menard et al., 2021).

Haughton et al. (2016) ~~had a closer look on~~ more closely explored the cause of poor model performance of LSMs shown in the PLUMBER study by Best et al. (2015), which they presented as the bias for the evaporative fraction (EF) ~~across~~ derived from various tower sites exemplarily. From all ~~different~~ investigated aspects they concluded that mismatches between ~~modelled~~ modeled and observed heat fluxes are most likely caused by calculations within the models and not related to errors in the observations. Yet, ~~the~~ specific reasons for this mismatch, for example over-parameterization, missing processes, calibration issues etc., cannot be identified by benchmarking studies or model rankings alone, but requires further investigation of individual model performance. At the same time, the causes of poor model performance can be multifaceted, rendering their identification challenging (Haughton et al., 2018b). Nonetheless, ~~there is no way around further understanding~~ further LSM development needs understanding of how individual process implementation and parameterization affect model performances~~, if LSMs are expected to be further evolved~~.

A wealth of studies evaluated different LSMs with respect to radiation, heat fluxes or surface temperature, and carbon fluxes.

Carbon fluxes like gross primary production (GPP) ~~, thereby,~~ are often validated by using global gridded fluxes like ~~FLUXNET Multi-Tree Ensembles~~ FLUXCOM (Ma et al., 2017; Jung et al., 2019; Lawrence et al., 2019). The correct implementation of ecosystem processes and related variables is crucial ~~to make use of LSMs in an assessment of~~ for using LSMs in assessing impacts due to climate change for example in drought evaluation (Ukkola et al., 2016; Dirmeyer et al., 2021) because plant transpiration directly links the terrestrial carbon and water cycle. ~~Over the past decades, vegetation dynamics became more strongly determined by soil moisture (Li et al., 2022b) and the sensitivity of heat flux partitioning to vegetation enlarged in turn (Forzieri et al., 2020), in particular in water-limited regions. At the same time, Li et al. (2022b) reported that LSMs do misrepresent water-sensitive regions. Especially during drought events, predictions by LSMs appear to deviate from the observations.~~ For example, a substantial underestimation of evapotranspiration ~~(ET)~~ by eight LSMs during drought conditions was shown across different plant communities (Ukkola et al., 2016). De Kauwe et al. (2015) concluded from their simulations of drought responses for the European FLUXNET sites with the Community Atmosphere Biosphere Land Exchange (CABLE) model that accounting for differing drought sensitivity of plant communities into LSMs may be required to correctly capture drought impacts. Currently, most LSMs are not able to represent ~~a~~ direct vegetation control on surface exchange, ~~amongst others because~~ in part because they under-represent biophysical responses to changing water availability ~~are underrepresented and vegetation, more specifically~~ and oversimplify vegetation dynamics, in particular leaf area index (LAI) ~~, dynamics are simplified~~ (Forzieri et al., 2020). LSMs typically work with climatological LAI, e.g. seasonality read from look-up table ~~(LUT) files~~files, or calculate LAI as a prognostic variable internally. At the same time, LAI has a large impact on both water and carbon fluxes (e.g. Fisher et al., 2014), and an understanding of how its parameterization impacts flux estimates by LSMs ~~helps~~ would help to shed light on the known discrepancies in representing vegetation.

Here, we investigate model ~~performances~~ performance for water and carbon fluxes ~~especially with~~ with a focus on vegetation processes. We additionally check the reasons for model-data mismatch, by analysis of the underlying computer source code of the models (as stated by Dirmeyer et al. (2018)), ~~that~~ which can only be ~~executed~~ done for a limited set of models due to the large effort that is needed. For this scope, we chose ECLand and Noah-MP as frequently used and continuously developing LSMs with available ~~vegetation dynamics modules~~modules for vegetation dynamics. In this manuscript, we aim to answer the following research questions: (1) Does the representation of net ecosystem exchange (NEE) and ~~leaf area index (LAI)~~ LAI improve, if ~~LSMs~~ ECLand or Noah-MP represent vegetation dynamically? (2) How does dynamic vegetation in ~~those LSMs~~ ECLand or Noah-MP impact other variables like heat fluxes and soil moisture? ~~Does improving one variable , compromise performance in the other or improves it along with it~~Do improvements in model performance for one variable compromise performance for other variables? (3) What are the mechanics behind ~~different~~ modeled temporal patterns in vegetation dynamics and ~~possible misrepresentations of~~ occurring misfits to the observations?

2 Methods

2.1 Data basis

~~For this study, observational data is required for two purposes: first, as model input and, second, for performance evaluation. We used readily available data products.~~

Site selection

The ~~FLUXNET 2015~~ FLUXNET2015 dataset (Pastorello et al., 2020) provides measurements from globally distributed eddy covariance sites. We selected a subset from all ~~the~~ available FLUXNET sites, focusing on sites with long observation periods, covering different vegetation types and a gradient in aridity within each vegetation type. Vegetation types within FLUXNET rely on the IGBP Land Classification (National Center for Atmospheric Research, 2022). The aridity index of all sites was retrieved from the ~~closest grid cell on a global map~~ CGIAR-CSI Global-Aridity and Global-PET Database (Trabucco and Zomer, 2018) and inverted afterwards~~.~~, bringing it back to the definition as the ratio of the long-term mean annual potential evapotranspiration to the long-term mean annual precipitation by Budyko (1974). We excluded sites with observation periods less than ~~5~~ six years because they might not represent the local ~~climatology (Haughton et al., 2018a) .~~ climate (Haughton et al., 2018a) and extreme years could create a systematic bias. Due to the small number of sites per vegetation type with long observation periods, the vegetation types savanna (SAV), woody savanna (WSA) and open shrubland (OSH) were merged into one savanna group before continuing with the selection procedure. For each vegetation type ~~(or groupe.g. for savannas)~~or group, first, we ~~selected~~ chose the site with the longest observation record. Next, other sites with similar aridity (± 0.1 logarithmic aridity index) were dropped to avoid ~~including more than one representative site for each combination of aridity and vegetation type~~an overrepresentation of some vegetation type-aridity combinations due to heterogeneous site distribution within FLUXNET. We used logarithmic values to create a linear scale of the aridity index so that a selection of too many dry sites was prevented. Afterwards, we repeated these steps for the remaining sites and continued until no more sites were available for selection in this vegetation type or group. For the selected sites, we double-checked data availability and quality and replaced with an alternative site if necessary. The most common reasons for discarding sites were missing or poor quality soil moisture data or low-quality gap-filling, which reduced the length of the observation record below the threshold of six years. By doing so, only two sites with mixed forests (MF) were left which is critically few. Thus, we included all MF sites into the deciduous broadleaf forest (DBF) vegetation type and repeated the selection for this group. We were left with ~~22~~ 24 sites, covering a ~~range of aridity and vegetation types with varying observation periods , as shown in~~ wide range of site characteristics as recommended by Haughton et al. (2018a) including aridity, vegetation types and observation periods (Fig. 1~~, and thus, we assumed them to be neither very predictable nor very unpredictable in total, as recommended by Haughton et al. (2018a).~~). Additionally, we also used data of the eddy covariance site "Hohes Holz" (Rebmann and Pohl, 2023) which is part of the TERENO Harz/Central German Lowland Observatory (Wollschläger et al., 2016) and is included in the ICOS network since 2019, because on-site measured LAI data was available for that ~~site.~~ DBF site.

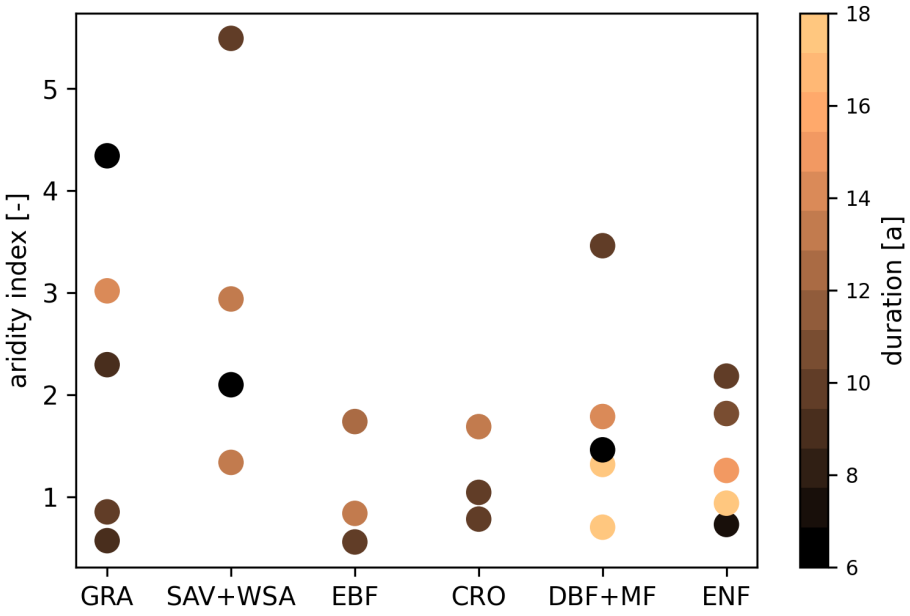

Figure 1. Selected FLUXNET sites grouped by their vegetation type. For each group, sites were chosen to cover a gradient in aridity (y-axis) if available. The vegetation types are: GRA - grassland, SAV - savanna, WSA - woody savanna, EBF - evergreen broadleaf forest, CRO - cropland, MF - mixed forest, DBF - deciduous broadleaf forest, ENF - evergreen needleleaf forest. The color scale represents the duration of the available time series in years.

Variables used and data pre-processing

From the FLUXNET (Pastorello et al., 2020) and Hohes Holz (Rebmann and Pohl, 2023) datasets, air temperature, downward short- and long-wave radiation, wind speed, relative humidity, air pressure and precipitation were used for model forcing. Turbulent fluxes, ~~e.g.~~ i.e. latent heat flux (LE) and sensible heat flux (H), as well as net ecosystem exchange (NEE), gross primary production (GPP) and volumetric soil water content in ~~10 cm~~ 10 cm depth were used for model evaluation. All data were provided and used at half-hourly resolution. FLUXNET data was retrieved from their website (fluxnet.org, 2020).

LE and H in FLUXNET2015 are available in two different variables: One is a product that corrects the turbulent fluxes for energy balance closure, while the other one provides a continuous time series filled by Marginal Distribution Sampling. We decided to use the first one as long as they were available in the dataset since LSMs also consider for energy balance. Missing data in the ~~Hohes Holz~~ "Hohes Holz" meteorological dataset was filled using a Kalman filter (Sayed, 2003) for short gaps up to ~~3 h~~3 h, except for precipitation which was set to 0. For longer gaps, ~~filling data~~ the Kalman procedure tends to overestimate the observations which resulted in offsets at the end of the filling periods. Thus, filling data for these gaps was retrieved from the ERA5 (Hersbach et al., 2020) data product ~~(via Climate Data Store API from Copernicus, ©2018 ECMWF)~~(Copernicus, 2018) with 0.1° spatial and 1 h temporal resolution.

For calculation of the evaporative fraction $\frac{LE}{LE+H}$, all time steps with $H \leq 0$ were excluded. ~~We adopted the same procedure~~

to the LE values to focus The same time steps were left out for LE to focus the comparison of turbulent fluxes on periods with evaporative demand. For performance evaluationestimation of model performance, we excluded longer gap filled periods that were longer than one month.

2.2 Model description

We investigated how dynamic vegetation affects model outputs in two land-surface models capable of representing both static and dynamic vegetation: ECLand (Balsamo et al., 2009; Dutra et al., 2010; Boussetta et al., 2021) and Noah-MP (Chen and Dudhia, 2001; Dutra et al., 2010; Niu et al., 2007, 2011)(Chen and Dudhia, 2001; Ek et al., 2003; Niu et al., 2007, 2011) .

ECLand

The European Centre for Medium-range Weather Forecasts (ECMWF) developed a Carbon-Hydrology Tiled Scheme for Surface Exchanges over Land (CHTESSEL) (Balsamo et al., 2009; Dutra et al., 2010; Boussetta et al., 2013) which reprents represents the land component of the Integrated Forecasting System (IFS). As part of the IFS, CHTESSEL has evolved into a more flexible system ECLand (Boussetta et al., 2021), which also allows for several modular extensions. Among these, an under-development vegetation dynamic a dynamic vegetation module simulates the temporal evolution of vegetation. Therein, LAI, vegetation biomass and vegetation coverage are calculated from the daily carbon budget, instead of taking them from the climatological LAI. However, climatological values LAI climatology can still be used for fully static or in partly dynamic simulations.

In ECLand (IFS cycle version "CY46R1"), each of the 19 vegetation types receives its own parameter values (e.g. for roughness lengths, stomata resistanceto water and carbon flux, root distribution) from LUTs look-up tables (Boussetta et al., 2012, 2021). These vegetation types are categorized into high or low vegetation. Each grid-cell has one dominant high and one dominant low vegetation type, together forming the vegetation of a grid-cell (Balsamo et al., 2009). Surface fluxes are computed for the high and low vegetation tiles separately then merged for the whole grid-cell according to their respective coverto be used for the vertical exchange with the atmospherefractional cover. The vegetation coverage is calculated from a prescribed climatological vegetation fraction (part of input) and a vegetation type dependent density (from LUTlook-up table) and corrected by current LAI (Boussetta et al., 2021). Leaf biomass growth Net assimilation results from carbon accumulation uptake of atmospheric CO_2 by the available leaf area current leaf area (defines absorbed radiation) and is restricted by environmental factors such as soil moisture and nitrogen availability . (important equations can be found in section A.01). Together with the dark respiration and after scaling with a quantum use efficiency factor, potential gross assimilation is calculated. This value, then, is linearly linked to LAI and the humidity-corrected air density, resulting in gross primary productivity (GPP). With activated vegetation dynamics, LAI depends on the built up green biomass and a LUT value of a potential net assimilation, together with LAI, forms a damping factor for biomass senescence. Biomass senescence is determined from current biomass, linearly linked to current LAI, and the damping factor. The change in biomass results from this updated biomass and the net assimilation. Then, biomass is updated again and linearly transferred into updated LAI by using specific leaf area from a look-up table

(Boussetta et al., 2021). For static ECLand, the prescribed climatological LAI is used. LAI in ECLand determines the canopy resistance for water vapour transport and thus, the evapotranspiration as well as the interception ~~(Boussetta et al., 2012, 2021)~~ (Boussetta et al., 2012, 2013, 2021).

Noah-MP

Noah-MP is the widely used community Noah land-surface model ~~(Chen and Dudhia, 2001; Dutra et al., 2010)~~ (Chen and Dudhia, 2001; E with multi-parameterization options (Niu et al., 2007, 2011). Predicted LAI in Noah-MP is calculated based on leaf carbon allocation and specific leaf-area per vegetation type (Ma et al., 2017). In contrast to ECLand, Noah-MP can either use ~~LAI values from LUT~~ prescribed LAI values per vegetation type or depend solely on dynamic LAI estimates, without the option to mix between the two.

In Noah-MP (version "HRLDAS 3.9"), ~~parameterization~~ parameter values (e.g. value range of stomatal resistance, number of rooted soil layers, specific leaf area) of the 27 vegetation types ~~is taken from LUT~~are taken from look-up tables. The vegetated sub-grid area of each grid cell is dominated by one vegetation type forming a one-layer canopy. Calculation of canopy interception and transpiration consider aerodynamic and stomatal resistances for the water vapour and carbon fluxes within the canopy and between the canopy and the atmosphere (Ma et al., 2017). ~~Thereby~~Among others, stomatal resistance is predominantly controlled by photosynthesis (Niu et al., 2011) which depends on leaf area, and is limited by light and root zone soil moisture ~~. Assimilated carbon, afterwards,~~ (important equations can be found in section A.02). Assimilation depends on LAI and is constrained by physiology and light availability. Assimilated carbon is allocated to different plant tissues (leaf, stem, wood, root), forming GPP, and reduced by respiration, dying and turnover processes such as drought stress and senescence representing leaf dynamics (Dickinson et al., 1998). Respiration rate is determined by LAI, GPP, temperature and soil moisture stress. Carbon that is allocated to leaves together with biomass losses forming an updated leaf biomass which converts into the LAI by using specific leaf area (Ma et al., 2017). Carbon assimilation and allocation and, thus, also GPP and NEE estimation are usually deactivated for the static Noah-MP since a prescribed LAI is given. We adapted the model code in a way that GPP and NEE for the static simulations are calculated anyways, but resetting all variables that would be dynamically predicted within the same function.

2.3 Model setup and simulations

Simulations with activated modules that predict LAI time series will be *activated vegetation dynamics* or *dynamic ECLand* and *dynamic Noah-MP* hereafter. For both models, the reference height (level of the forcing input) was set to the flux tower height of the sites which depends on the vegetation type. The models were set up as closely as possible to the available site information but there are some technical differences in the structure of the model input, i.e. in the initial files. Forcing and model calculation were done in 30 minutes resolution if available, otherwise, hourly resolution was applied. We used four layered soil representation and used the uppermost layer for evaluation of soil moisture which is 7 cm and 10 cm deep for ECLand and Noah-MP, respectively. Every simulation started with a ten year spin-up phase by recalculating the first year.

ECLand

We used ERA5-based (Hersbach et al., 2020) global initial data for ECLand and selected the grid cells where the flux towers are located. These initial files contain information on albedo, orography, soil type, surface roughness and monthly LAI which is not available in the FLUXNET metadata. For the simulations that use alternative LAI ~~forcings~~forcing, monthly LAI in the initial files was replaced by the scenario specific alternative values ~~,~~(see section 2.3). We defined the vegetation on that grid-cell to be either high or low vegetation (and not a mixture) depending on the site information. Forests and savannas were treated as high vegetation types while grasslands ~~, crops and shrublands~~ and croplands were allocated to low vegetation types. The vegetation type that fits most to the FLUXNET characterization was selected (see Tab. 1). The coverage of that vegetation type was set to 100 %. Meteorological forcing was taken from the FLUXNET/TERENO data sets mentioned above (section 2.1). The ECLand simulations were done with van Genuchten soil hydrologic parameters (van Genuchten, 1980), activated sub-grid surface runoff and activated snow parameterization.

Table 1. Assignment of vegetation types used in ECLand and in Noah-MP and referred initial LAI. The values in brackets for Noah-MP initial LAI refer to sites on the Southern Hemisphere due to shifted seasons.

Fluxnet vegetation type	ECLand vegetation type	ECLand vegetation class	Noah-MP USGS	Noah-MP vegetation class	Noah-MP initial LAI
ENF	Evergreen Needleleaf Trees	3 (high)	Evergreen Needleleaf Forest	14	4.0
MF	Mixed Forest/Woodland	18 (high)	Mixed Forest	15	2.0 (4.3)
DBF	Deciduous Broadlead Trees	5 (high)	Deciduous Broadleaf Forest	11	0.0 (4.5)
EBF	Evergreen Broadleaf Trees	6 (high)	Evergreen Broadleaf Forest	13	4.5
SAV	Interrupted Forest	19 (high)	Savanna	10	0.3 (3.8)
WSA	Interrupted Forest	19 (high)	Savanna	10	0.3 (3.8)
CRO	Crops, Mixed Farming	1 (low)	Mixed Dryland/Irrigated Cropland and Pasture	4	0.0 (3.0)
GRA	Tall Grass	7 (low)	Grassland	7	0.4 (3.5)

Noah-MP

Soil type for ~~the~~ Noah-MP was taken from ~~the~~ a global soil grid ~~by PLOS ONE (Hengl et al., 2014) . The soil types of the grid-cell itself and its surrounding four neighbors were averaged~~(Hengl et al., 2014) by selecting the grid cell including the flux tower location. Initial values for temperatures and soil moisture were taken as the FLUXNET/TERENO observations at January 1st 00:~~30~~00 h in the first year of the simulation period. Vegetation types were chosen to match as closely as possible the USGS vegetation types ~~(©2023 UCAR)~~[1] (University Corporation for Atmospheric Research, 2023) and the initial LAI values were set according to the defaults in the parameter file (~~Table~~see Tab. 1). Vegetation cover fraction was set to ~~100%~~ 100 % so that the entire grid-cell represents the vegetation type of the observation site. ~~Green~~ Minimum green vegetation fraction was set to ~~1 because otherwise~~ 1 % to ensure that not the whole vegetation cover dies during winter which would hinder temperate short vegetation ~~did not re-grow~~ from growing in spring. For the simulations with alternative LAI forcing, the monthly LAI in the ~~LUT~~ look-up table was replaced by the scenario specific alternative values ~~,~~ (see section 2.3). The Noah-MP simulations were done with ~~LUT soil parameterization~~ soil parameterization from look-up tables, Ball-Berry stomatal resistance approach ~~and~~ (Ball et al., 1987; Bonan, 1996) with using matric potential ~~therefor and fully implicit temperature time schemes. Other options were used as their defaults~~limitation. All other selected options can be found in Table 2.

Leaf area index data and scenarios

~~Leaf area index (LAI) values were~~ Monthly LAI values are part of the initial input of both models via look-up tables. These tables contain annual cycles of LAI for each vegetation type separately. This *default climatology* is already based on values from MODIS. For ECLand, the gridded values of LAI were disaggregated to the high and low vegetation type of the grid cell for the time span 2000-2008 (Boussetta et al., 2013). For alternative LAI inputs, these values in the look-up tables were replaced manually.

LAI values were taken from the MOD15A2H data product from NASA's EarthData portal (Myneni et al., 2015). One grid cell of 500 m x 500 m was selected per eddy covariance tower according to the site coordinates and LAI values ~~were extracted. We used LAI values with respective quality flags of 0, 32, 48 and 65 (see MODIS documentation for more details) as~~ with temporal resolution of eight days were extracted for the years 2000 to 2014. To assure reliability of the values, the "MODIS15A2H" data product comes with numeric quality flags. Although Fang et al. (2012) recommend using all values with quality flags less than 64, we excluded data with quality flag 8 because many of these LAI values were extremely low during the vegetation period which is unrealistic. Then again, due to lacking LAI values during winter or wet seasons, values with quality flags of 73 (empirically filled with clouds present), 81 (empirically filled with mixed cloudiness) and 97 (empirically filled for other reasons) were included as a trade-off between excluding as much bad-flagged data as possible and keeping roughly the same amount of data values for each month (see MODIS documentation for more details). Afterwards, we smoothed the remaining values by using a Savgol filter (window length: 11, polyorder: 2) (similarly done by e.g. Xiao et al., 2011; Huang et al., 2021) from the scipy-package (Savitzky and Golay, 1964; Luo et al., 2005) and prepared a mean annual LAI cycle for all available

[1] ~~data can be found here:~~

Table 2. ~~Assignment of vegetation types used in~~ Options chosen for Noah-MP ~~according to USGS classification and referred initial LAI~~parameterization.

~~Fluxnet vegetation type~~	Physical process	Noah-MP ~~USGS Noah-MP vegetation class Noah-MP initial LAI~~Option
	~~ENF~~ Runoff and groundwater	~~Evergreen Needleleaf Forest 14 4.0~~TOPMODEL with groundwater (Niu et al., 2007)
	~~MF~~ Surface layer roughness	~~Mixed Forest 15 2.0~~Monin-Obukhov
	~~DBF~~ Supercooled water	~~Deciduous Broadleaf Forest 11 0.0~~no iteration (Yang and Niu, 2006)
	~~EBF~~ Radiative transfer	~~Evergreen Broadleaf Forest 13 4.5~~two-stream (vegetated vs. vegetation-free)
	~~SAV~~ Snow albedo	~~Savanna 10 0.3~~fresh snow with aging effects
	~~WSA~~ Rain/snow partitioning	~~Savanna 10 0.3~~threshold temperature at 2.2 $^{\circ}C$
	~~OSH~~ Lower boundary for soil temperature	~~Mixed Shrubland 9 0.2~~temperature at 8 m depth (part of input)
	~~CRO Mixed Dryland~~Snow/~~Irrigated Cropland and Pasture~~ soil temperature time scheme	~~4~~ fully implicit (original Noah)
	Surface resistance for evaporation	~~0.0~~Sakaguchi and Zeng (2009)
	~~GRA~~ Glacier treatment	~~Grassland 7 0.4~~ phase change of ice included

years with monthly resolution, further ~~name~~ named *MODIS climatology*. For an additional experiment, the monthly LAI ~~of the first year of~~ from MODIS of each year within the simulation period ~~was used~~separately was used as input, called *MODIS single-year* from this point on. ~~Each following year was then forced by the monthly MODIS LAI for that specific year. In case the LAI value for a month in that year was missing, we set it to be the mean~~ Missing LAI values for a month were filled by the average value of the adjacent months. If LAI values for ~~more than one month~~ at least two consecutive months were not available, the ~~LUT LAI values~~ LAI values from the default look-up table were used for those months.~~For the Hohes Holz site, also~~

For the "Hohes Holz" site, on-site measured LAI data ~~from Digital Hemispheric Photography was available~~was available from

Digital Cover Photography (DCP), which was shown to yield comparable results to established methods (Piayda et al., 2015). For each measurement date, we averaged the values from the whole plot area and, afterwards, calculated monthly means over time span 2014-2019. This alternative LAI forcing will be called *on-site LAI* hereafter. The nomenclature of all LAI scenarios can be found in Table 3.

Table 3. Nomenclature of all model scenarios using LAI data sources.

Term	LAI source
default ~~climatological LAI~~ climatology	~~global gridded initial files~~ default monthly LAI for the dominant high and low vegetation type on respective grid cell (ECLand) or ~~look-up table~~ default monthly values per vegetation type from look-up table (Noah-MP)
MODIS ~~climatological LAI~~ climatology	mean annual cycle of monthly LAI values derived from MODIS dataset from 2000 to 2014
MODIS single-year	same as before but without averaging, resulting in an annual cycle for each year separately within the observation period
on-site LAI	mean annual cycle of ~~distinct years of~~ monthly LAI values ~~derived from MODIS dataset~~based on on-site measured LAI ~~on-site measured LAI values~~

The MODIS LAI was also applied for model evaluation but in high temporal resolution of eight days. Due to the usage of single day values, we solely used data with ~~good quality flags (~~quality flags 0 (no issues) and 32 ~~) and~~ (saturated) to lower the uncertainty. Additionally, we refrained from smoothing ~~. Gaps were left~~ to avoid an offset of the LAI values and left gaps as they were. For the static runs, comparison with MODIS LAI on daily basis provides the information how well a LAI climatology represents the local LAI evolution and whether an incorporation of more site-specific climatology can improve the representativeness. For the dynamic simulations, comparing modeled LAI with daily MODIS values is used to examine whether the models are able to capture inter- and intra-annual LAI dynamics.

2.4 Performance evaluation

~~We transferred model~~ Model outputs and observational data from the flux towers ~~into~~ were averaged/summed to daily values for direct comparison. For LAI, we calculated the eight-day mean of the LAI model output ~~,~~ to correspond to the temporal resolution of the MODIS LAI estimates. As performance criteria we used the Pearson's correlation coefficient, the normalized standard deviation and a modified relative bias for the model-observation relationship. Pearson's correlation coefficient R describes the fit between model and observation values (Benesty et al., 2009) and is calculated from the numpy-package~~as~~

$$R_{xy} = \frac{Cov_{xy}}{\sqrt{Cov_{xx} \cdot Cov_{yy}}}$$

~~where Cov refers to the covariance of the observations x and the model predictions y~~. The normalized standard deviation $s_{\mathcal{D}}$ is the ratio of the standard deviation of the model predictions and the standard deviation of the observations. It is used to

describe the models' ability to reproduce the variability of the observations. The relative bias b applied here was adapted to the ~~co-domain~~ domain of the variable to avoid division by zero or by values very close to zero (especially important for NEE). ~~Therefor, the basis of the relative bias~~ For this purpose, the distribution of the observed values was shifted by ~~the minimumof the observations~~their minimum, resulting in only positive values with a minimum of zero:

$$b = \frac{\overline{y - x}}{\overline{x} - \check{x}} \tag{1}$$

whereby y represents the model predictions, x the ~~observational data~~observations, $\overline{x}$ the mean and $\check{x}$ the minimum of the observed values. To compare the model performance of simulations with static and dynamic ~~simulations~~vegetation, we determined the ~~shift~~ change in relative bias as follows:

$$\Delta b = |b_{static}| - |b_{dynamic}| \tag{2}$$

Negative values mean that the relative bias of the dynamic simulation was greater than that of the static simulation and, thus, that the performance was reduced by activating vegetation dynamics.~~To account for the dependence of~~

To investigate the sensitivity of dynamically modelled vegetation on the model performance~~of~~ , we checked how strongly the quality of the model simulation of one target variable ~~to that~~ (e.g. LE) depends on the model quality of another one (e.g LAI). For this, we used the ~~slope of their correlation, called~~ *elasticity* ~~in the following. This allows an evaluation of the impact of, for example, changing LAI representation on the GPP model performance.~~ as a metric. Elasticity is calculated as ratio of the ~~shift~~ change in one statistical measure (analogous to equation 2) for two different target variables:

$$E = \frac{\Delta m_i}{\Delta m_j} \tag{3}$$

where m is one of the statistical measures mentioned above, ~~e.g.~~ i.e. R, ~~normalized standard deviation~~ s_n or b, while i and j denote different target variables, e.g. GPP or ~~latent heat flux~~LE. For variables that are strongly related, like LAI and GPP, we expect ~~elasticitiy~~ elasticity to be positive. Two variables ~~were considered as~~ are considered independent if $-0.1 \leq E \leq 0.1$ because the change in m_j then would need to be larger than one order of magnitude to cause a change in m_i. ~~We plotted the shifts~~ Changes in model performances of the target variables were plotted in Taylor diagrams ~~. The class design for drawing the Taylor diagrams in Python was adapted from Yannick Copin~~[2]~~. (Copin, 2021).~~

3 Results

3.1 ~~Using LAI climatology for ECLand and Noah-MP runs is the best way to reproduce~~ Effect of dynamic or prescribed leaf area index on leaf area and carbon uptake prediction

Figure ~~??~~ ~~shows the model~~ 2 shows the quality metrics for the ~~LAI model performance~~ model performance regarding LAI in a Taylor diagram. The ~~point of optimal model performance~~ location an optimal model simulation would occupy is indicated with

[2] ~~, 2023-02-14~~

a star. The model performance of the dynamic run is shown with the ~~symbol~~symbols, while the static runs can be read from the start of each arrow. The direction and length of each arrow highlights the difference in the performance metrics between static and dynamic runs. Shown are simulations started (dynamic) or run (static) with ~~default vs. MODIS climatological LAI~~*default vs. MODIS climatology*.

While in the Noah-MP simulations with static vegetation ~~in Noah-MP~~ the model performance depended on the ~~applied LAI forcing ,~~ LAI forcing applied, the simulation results were unaffected by the type of LAI forcing with vegetation dynamics switched on ~~(Fig. ?? c +d). This~~ since the symbols in Figure 2 c and d have the same positions. For ECLand, this was also the case for ~~ECLand, as for the TERENO site "Hohes Holz", but not necessarily for allsites~~ many sites but not all, e.g. *AT-Neu* and *AU-How* (Fig. ??2 a+b). Initializing ECLand with ~~default climatological LAI forcing~~ *default climatology* (Fig. ??2 a) and activating vegetation dynamics generally increased the variance of simulated LAI compared to static simulations but it also decreased model performance, e.g., mean Pearson correlation decreased from 0.72 to 0.62. At the same time, whether the predicted LAI fit better to MODIS observations than ~~default climatological LAI was random~~*default climatology* was ambiguous, as can be seen by the shift in relative bias which ranged between -0.5 and ~~1.9~~1.3. On the contrary, the results for Noah-MP showed a different pattern (Fig. ??2 c) ~~,~~ because there was no clear shift to higher variances or worse correlation when activating vegetation dynamics. Especially short ~~or sparse~~ (GRA+CRO) or sparse (SAV+WSA) vegetation types had the highest changes towards decreased but also enhanced model performance for LAI. For other sites (mostly forests), modelled dynamic LAI correlated well with the observations.

For both models, using ~~MODIS-based forcings~~ *MODIS climatology* instead of *default climatology* in static simulations resulted in the best performances with regard to LAI of all simulations (start of the arrows in Fig. ??2 b+d), e.g., the mean correlation coefficient increased to 0.83 and 0.84 and mean relative bias (Tab. A1) improved to -16% and -2% for ECLand and Noah-MP, respectively. This can be expected because MODIS was also used as reference dataset for LAI evaluation. With activated vegetation dynamics, the performance of both models decreased, as all quality metrics shift away from the point indicating best performance in the Taylor diagram ~~.~~(Fig. 2 b+d). The same applied to the relative biases of LAI since their shift was predominantly negative. In other words, switching on vegetation dynamics did not ~~contribute to improve~~ result in improved LAI representation compared to just using ~~MODIS climatology.~~*MODIS climatology*.

Forest ecosystems, in general, were better represented by model predictions with vegetation dynamics than short or sparse vegetation. Figure ~~?? shows in more detail~~ 3 shows the results of the forest site "Hohes Holz" in more detail. Although the representation of LAI variability detoriated when simulating dynamic vegetation with Noah-MP, those runs resulted in LAI predictions that closely match MODIS observations (Fig. ??3 d-f), represented by ~~the~~ a relative bias of ~~-16%~~-18% and a correlation coefficient of 0.78. ECLand more generally suffered from ~~large~~ larger relative biases in LAI, especially when simulating with vegetation dynamics (-30% on average, Fig. ??3 c). ~~Change of model quality metrics for LAI modeling when switching on vegetation dynamics for all included sites and by using default climatological LAI forcing (left) or MODIS climatological LAI (right). The star ("Observ") marks the location of the perfect correlation between observation and model and perfect agreement between observed and modelled variance. The model performance of the static runs can be read from the start of each arrow. When no arrow appears, either no correlation could be calculated (e.g. for evergreen forests where~~

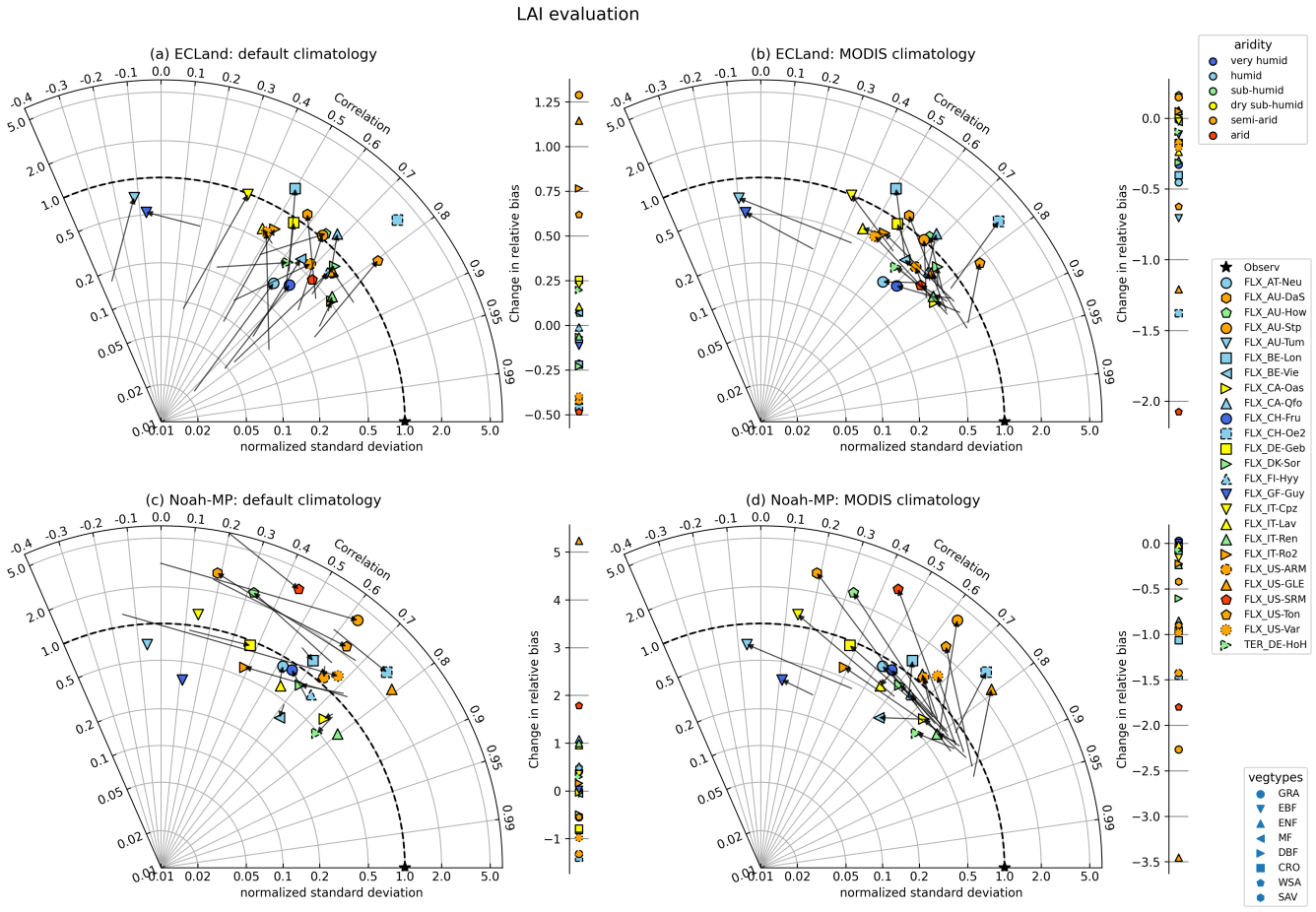

Figure 2. Change of model quality metrics for LAI when switching on vegetation dynamics for all included sites and by using *default climatology* (left) or *MODIS climatology* (right). The star ("Observ") marks the location of the perfect correlation between observation and model and perfect agreement between observed and modelled variance. The model performance of the static runs can be read from the start of each arrow. When no arrow appears, either no correlation could be calculated (e.g. for evergreen forests where default climatological LAI is constant) or values could not be placed on the logarithmic axis. The symbol colors indicate the site aridity (top right legend) as following: very humid - aridity index (AI) < 0.6, humid - $AI < 1.25$, sub-humid - $AI < 1.54$, dry sub-humid - $AI < 2$, semi-arid - $AI < 5$, arid - $AI \geq 5$ (Ashaolu and Iroye, 2018). Vegetation types are symbolized by different marker types (bottom right legend).

~~default climatological LAI is constant) or values could not be placed on the logarithmic axis. The point colors indicate the site aridity (top right legend). Vegetation types are symbolized by different marker types (bottom right legend). Statistical measures for die variables LAI, NEE and GPP of the model runs for Hohes Holz. The categories on the y-axis mark the different LAI forcings. Statistical measure of the static and dynamic simulations of the same variable are connected by a horizontal line. The red dotted vertical line marks the optimum of each measure.~~ The only scenario where model performance generally increased

for ECLand, was through switching on vegetation dynamics compared to static runs with *default climatology*.

In contrast to LAI, the model performance of ecosystem exchange variables in ECLand was less affected by activating vegetation dynamics. A common feature is ~~, however,~~ that the variance predominantly increased when using dynamic vegetation (Fig. ~~??~~4 a+b). Mostly, sites with short or sparse vegetation reacted more sensitively to dynamic vegetation modeling in their NEE and GPP representation especially when forcing with ~~MODIS climatology~~*MODIS climatology*, which is indicated by the longer arrows in ~~Fig. ??~~ Figure 4 a and b (for GPP see Fig. A1 in Appendix). For forest ecosystems in general, the changes in the model performance of NEE and GPP were small, as also shown for the ~~TERENO~~ site "Hohes Holz" (Fig. ~~??~~3 a-c). Nevertheless, the performance of NEE ~~and GPP~~ (and GPP) decreased when activating vegetation dynamics, mainly driven by lowered correlation coefficients, on average from 0.41 to 0.37 (0.72 to 0.68). Only three sites showed improvements in NEE representation when predicting with dynamic ECLand and just one did so for GPP. Relative bias changed in both directions, towards lower and higher model performance. Dynamic ECLand mainly overestimated NEE by 11% on average, indicating that ecosystems were predicted to be a smaller carbon sink than observed ~~.~~ (Tab. A2). Instead, dynamic Noah-MP estimated on average 10% lower NEE compared to the observations for the most sites (Fig. ~~??~~4 c+d, Fig. ~~??~~3 c+f).~~Overall,~~

Activating the dynamic vegetation affected the model performance of NEE and GPP for Noah-MP heterogeneously. Some sites showed very small changes (e.g. *IT-Lav* and *IT-Ren*, Fig 4 c+d) while model performance of NEE was largely impacted by vegetation dynamics for other sites (e.g *US-Var* and *AU-DaS*). In contrast to ECLand, no evidence could be found that certain vegetation types or aridity classes were more sensitive to activated vegetation dynamics in Noah-MP and even forests showed larger changes in model performance (Fig. 3 e). While, for GPP, the variance predominantly enlarged by activating vegetation dynamics in Noah-MP (Fig. A1 c+d), the normalized standard deviation of NEE changed in opposing directions which is another difference compared to ECLand. Despite the higher sensitivity of NEE model performance to Noah-MP vegetation dynamics, the overall model performance was barely affected since relative bias shifted from $-12\,\%$ to $-11\,\%$ and correlation coefficient from 0.50 to 0.53 on average. Changes of statistical measures can be in opposing directions as can be seen for normalized standard deviation and relative bias of the forest site "Hohes Holz" (Fig. 3 e+f) which eliminated trends towards improved or reduced model performance. Only the site *AU-Stp* clearly improved regarding NEE representation by activating vegetation dynamics in Noah-MP by initializing with either *default* or *MODIS climatology*. The GPP performance showed small improvements by activating vegetation dynamics in Noah-MP as the mean correlation coefficient shifted from 0.68 to 0.74 and the range of the relative bias was lowered from $-32\,\% - +69\,\%$ to $-28\,\% - +42\,\%$.

In general, Noah-MP seemed to capture NEE representations better as the ~~values scattered more closely to~~ mean deviance from a normalized standard deviation of ~~1 in the Taylor diagram~~ 1 was 0.33 (ECLand: 0.39) and showed with 0.51 a higher correlation coefficient on average than ECLand (Fig. ~~??~~4 c). Remarkably, the ~~seven~~ four and the nine best sites regarding NEE ~~representation in both models were forests~~ correlation and variance were forests for ECLand and Noah-MP, respectively. At the same time, ~~both tropical~~ all evergreen broadleaf forests suffered from low performance in both models. GPP representation in both models was better than for NEE (Fig. A1~~). Considering the opposing biases in NEE indicates that the models differ in their estimates of ecosystem respiration.Same as Taylor diagram before but with NEE evaluation. Since NEE is not generated as variable from Noah-MP when running the model without dynamics, no change in statistical measures can be presented.~~

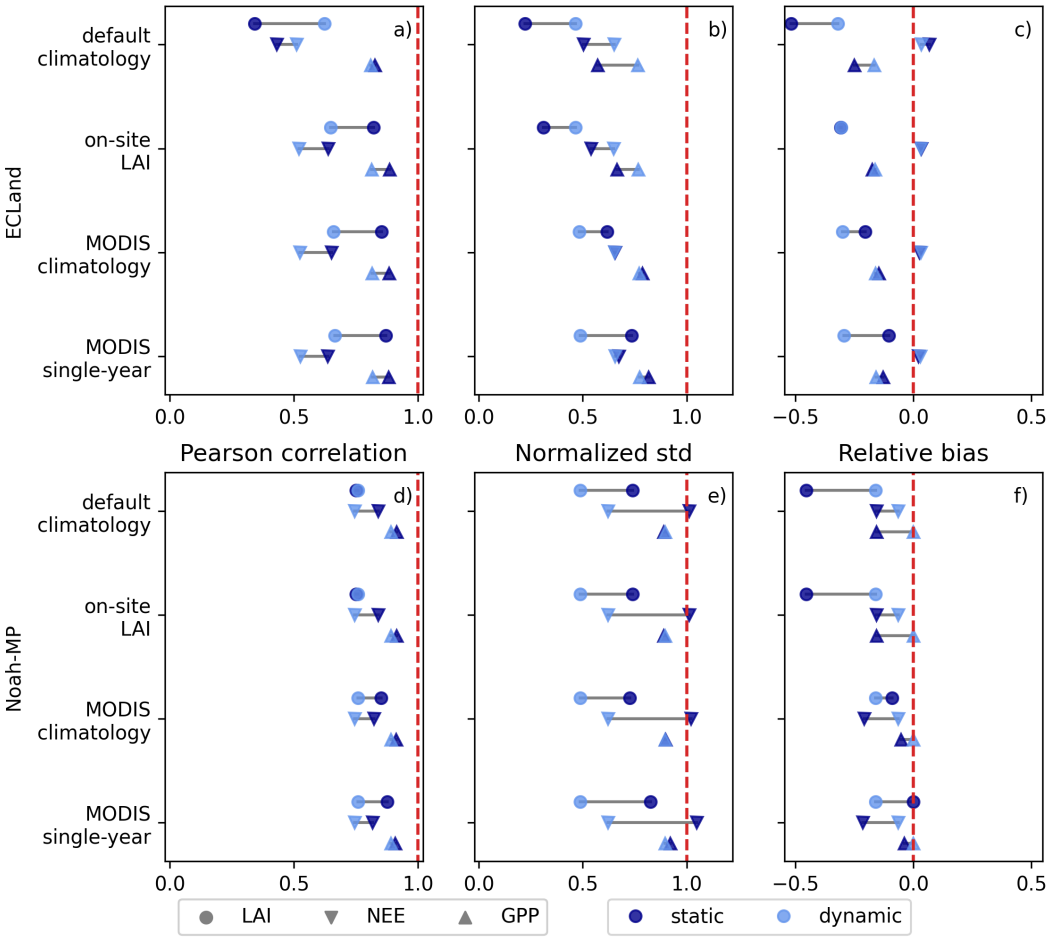

Figure 3. Statistical measures for the variables LAI, NEE and GPP of the model runs for the site "Hohes Holz". The categories on the y-axis mark the different LAI forcings. Statistical measure of the static and dynamic simulations of the same variable are connected by a horizontal line. The red dotted vertical line marks the optimum of each measure.

~~Additionally, because all the simulations with dynamic vegetation created the same output for Noah-MP, only one Taylor diagram is shown.~~ , Tab. A3). Overall, static and dynamic Noah-MP performed well in representing NEE and GPP for most forest sites apart the evergreen broadleaf forests.

~~Consistent with~~ In line with the finding that model performances of dynamic Noah-MP ~~being~~ were independent of the prescribed LAI forcing, the availability of ~~on-site LAI data~~ *on-site LAI* data for the site "Hohes Holz" yielded no improvement in the representation of NEE or GPP ~~. Interestingly, forcing ECLandwith on-site LAI data even decreased model performances for~~ compared to other LAI climatology (Fig. 3). The same appeared for dynamic ECLand. Forcing static ECLand with *on-site LAI* data resulted in NEE and GPP ~~regardless of the choice in vegetation dynamics for the TERENO site "Hohes Holz", where~~

~~on-site LAI data was available to us (Fig. ??).~~ correlation and relative bias comparable to the forcing with *MODIS climatology*, only variability was lower.

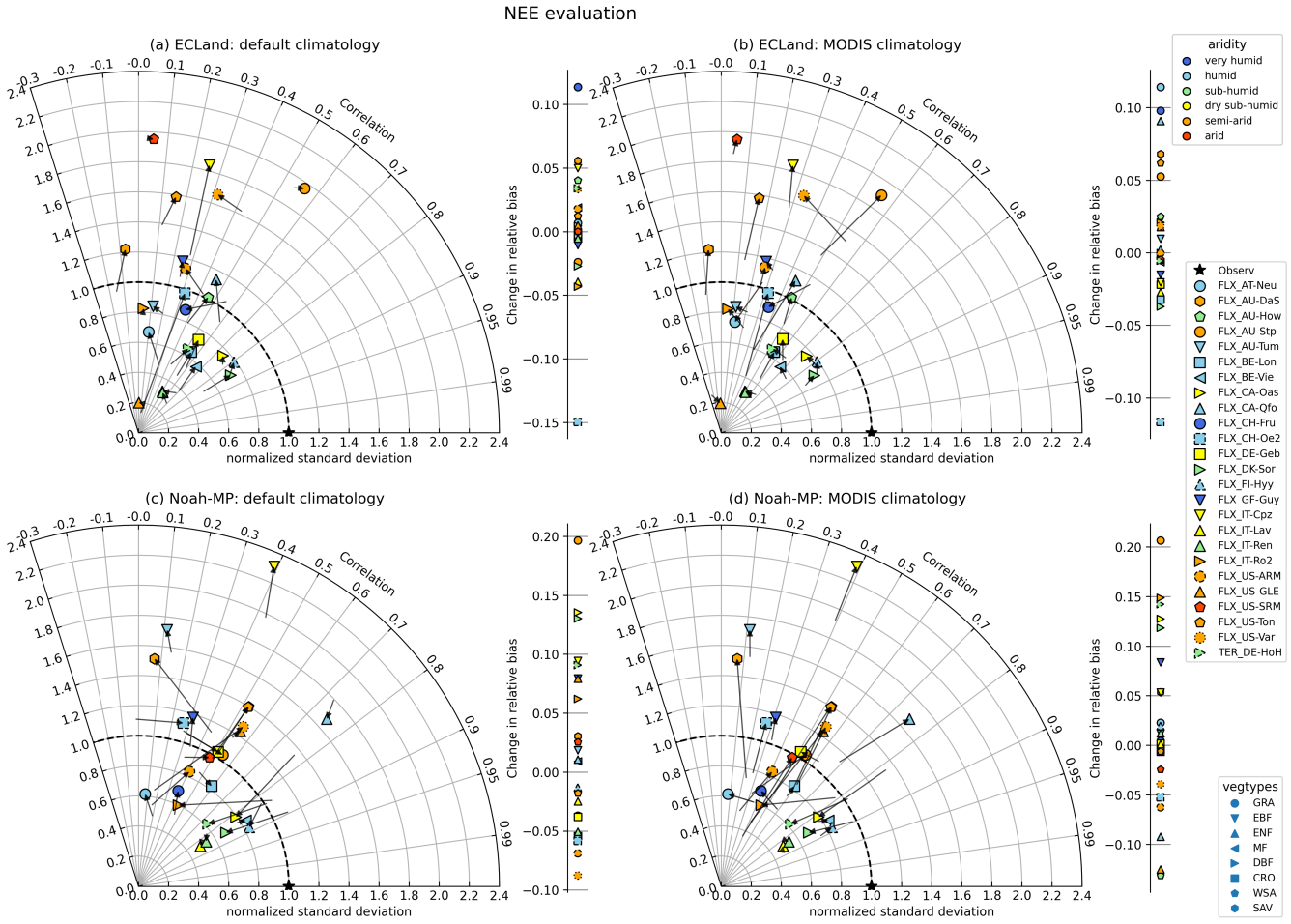

Figure 4. Same as Taylor diagram before but with NEE evaluation.

3.2 ~~Modelled turbulent~~ On the sensitivity of heat fluxes and soil moisture ~~were almost unaffected by vegetation dynamics~~ in ~~both~~ LSMs to vegetation dynamics

385 For both models, activating vegetation dynamics had a ~~negligible~~ small impact on the representation of turbulent fluxes and soil moisture. The strongest changes occurred for short or sparse vegetation types or for drier climates ~~as these points appeared to have~~ which had the largest arrows in the Taylor diagrams (Fig. ??5, Fig. ??6). In ECLand, activating vegetation dynamics enhanced the variance of latent heat flux for the most sites ~~,~~ (from 0.80 and 0.84 to 0.94 on average for *default* and *MODIS climatology*, respectively), but correlation between simulated and observed values remained unaffected or even diminished

(mean change smaller than -0.03). For several sites, ~~latent heat~~ LE estimates from dynamic ECLand better represented the observations as shown by the positive shift in relative bias (reduction from -32% to -21%) (Fig. ~~??~~ ~~a~~5 a, Tab. A4), but no ~~trend~~ relationship regarding vegetation type or site aridity can be seen and changes are small in general. The big exception appeared for *CH-Oe2* which was caused by its default LAI climatology that did not fit the vegetation type.

Activating vegetation dynamics in Noah-MP hardly affected model performance of ~~latent heat flux. Only sites with short or sparse vegetation types~~ LE (mean change in correlation was 0.02, in standard deviation 0.00 and in relative bias 0.02). Sites that showed some sensitivity predominantly have drier climate (e.g ~~AU-Stp, US-Var~~*AU-Stp*, *US-Var*, see Fig. ~~??~~5 c). Several sites showed ~~slightly enhanced fit of latent heat predictions to the observations due to vegetation dynamics~~ less bias in LE predictions when using dynamics vegetation predictions in Noah-MP~~as can be seen by the positive shift in relative bias~~. When using ~~MODIS climatology~~ *MODIS climatology* as LAI forcing, activating vegetation dynamics could be advantageous for some sites regarding ~~latent heat flux representation~~ LE representation (*AU-Stp*, *CH-Fru*, *US-GLE*), but mostly it would not lead to higher model performance.

Model performance regarding the evaporative fraction ~~appeared to be~~ (EF) was lower compared to ~~latent heat flux~~ LE as points are further away from the point of optimal model performance (Fig. ~~??~~). ~~Forest ecosystems thereby showed the lowest performance which is interesting since their prediction in NEE was the best.~~ 6). Running ECLand with activated vegetation dynamics lowered the representation of the evaporative fraction which is demonstrated by many points in the Taylor diagram drifting away from the star indicating best performance. Thereby, the mean standard deviation changed from 0.95 to 1.08 and correlation coefficient was reduced slightly from 0.48 to 0.46 on average (Fig. 6 a+b). Exceptions were *BE-Lon*, *US-SRM* and *US-Ton* where model performance slightly improved regarding correlation and variability. Again, relative bias of EF changed in both directions without any trend regarding vegetation type or aridity for both models (see also Tab. A5). For Noah-MP, ~~some~~ eight sites showed an improved representation of the evaporative fraction when running the model with vegetation dynamics~~even~~ . This amount was reduced to six when the model was initialized with ~~MODIS climatological LAI.~~ *MODIS climatology*. But changes were very small on average.

Regarding soil moisture, the model performance was almost insensitive to the used vegetation dynamics option or the type of LAI forcing for both models (~~results not shown).~~ Fig. A2). Some sites showed improvement of soil moisture prediction by activating vegetation dynamics for both models although the improvement was very weak. Interestingly, no humid site was among them. However, the simulation of soil moisture resulted in a broad range of model performances starting with very well-fitting predictions (~~correlation coefficient > 0.9, relative bias $\approx 0\%$~~$R > 0.9$, $b \approx 0\%$) up to very poor-fitting predictions (~~correlation coefficient < 0.2, relative bias $< -40\%$ or $> 100\%$~~$R < 0.2$, $b < -40\%$ or $b > 100\%$, see Tab. A6).~~Change of statistical measures for latent heat modeling when switching on dynamic vegetation for all included sites and by using default climatological LAI forcing (left) or MODIS climatological LAI forcing (right). Same as before but for evaporative fraction which represents the turbulent flux partitioning.~~

To investigate the sensitivity of dynamically ~~modelled~~ modeled vegetation on the model performance, we checked how strongly the quality ~~of the model simulation of latent heat flux~~ metrics of NEE, GPP, LE and soil moisture ~~depends on the model quality of LAI and NEE~~change with the quality metrics of LAI. For this, we used the elasticity (defined in ~~section 2.4) as~~ equation 3) as

a metric which is summarized for all sites in ~~the bar plots of Fig. ??~~Figure 7. Surprisingly, the ~~model quality of those actually~~ quality metrics of those closely related variables ~~was independent~~ were independent from each other, i.e. the elasticity was very low (within grey band) or randomly distributed around zero. The strongest ~~connections~~ connection of all pairs tested ~~are between NEE and latent heat flux and GPP and latent heat flux in ECLand~~ could be found for the correlation coefficient between LAI and GPP in ECLand when using *MODIS climatology* but without affecting normalized standard deviation or relative bias. Here, the mean elasticity of correlation and normalized standard deviation is positive, meaning that, as expected, an increased model performance in ~~LE~~ LAI co-occurs with enhanced performance for ~~NEE and GPP , respectively. For the GPP-LE relation, even the elasticity of the relative bias is positive which underlines the co-relation of GPP and LE performances in ECLand. The fact that this is not the case for NEE might be caused by uncertainties in the predictions of respiration in the model. But~~ GPP in the same order of magnitude. In a similar manner, NEE and LAI performance were positively related regarding correlation coefficient in Noah-MP. Other elasticity values that include LAI were small predominantly. ~~Only the correlation coefficient as model performance metric of LAI and LE in ECLand seems to be coupled but without affecting normalized standard deviation of relative bias.~~ In other words, changes in the model quality for LAI~~do~~ , for most of the sites, do not affect the model performance of ~~latent heat flux~~ LE or soil moisture and even not that of carbon fluxes.

3.3 Observed and simulated relationships between ecohydrological variables

One possible explanation for the small contribution of model quality of LAI to that of the turbulent fluxes could be a weak relation between LAI and carbon exchange in the model. However, this is not the case as illustrated in ~~Fig. ??. On the contrary, the relationships between GPP and LAI is much more scattered in the observations (top row) compared to the models (other rows), and this is true for both models, across biomes and vegetation types. In general, ECLand shows a linear relationship with considerable less uncertainty compared to the observations. The slope and intercept of the linear regression is dependent on the choice of static or dynamic vegetation. In contrast, Noah-MP shows a non-linear relationship with a pronounced hysteresis. This hysteresis is related to the partitioning of GPP to the carbon pools in the plants. Noah-MP uses a non-linear function for allocation of GPP to the leaves that limits the maximum LAI the model can grow. Scatter plots of the relationship between LAI on the x-axes and GPP on the y-axes as 8-day averages for four selected sites (columns). The rows from top to down show observations, static ECLand, dynamic ECLand, and dynamic Noah-MP. Seasons are represented by different dot colors. A simple linear regression model was applied as additional information (blue dashed line) and its correlation coefficient (R), slope and standard deviation of the residuals (σ_r) are given for each relationship. Figure ?? shows the~~ Figure 8. The figure shows the relation between GPP and LAI for four exemplary sites: ~~DE-HoH~~ *DE-HoH* is a deciduous broadleaf forest in a humid climate, ~~IT-Ren is a~~ *IT-Ren* is an evergreen needleleaf forest in a semi-arid climate, ~~GF-Guy is a~~ *GF-Guy* is an evergreen broadleaf forest in a tropical climate, and ~~US-Var~~ *US-Var* is a grassland in a semi-arid climate. In general, the relationships between GPP and LAI is much more scattered in the observations (top row) compared to the models (other rows), and this is true for both models, across biomes and vegetation types.

The two European sites (left columns, ~~De-HoH and IT-Ren~~*De-HoH* and *IT-Ren*) reach maximum LAI and GPP in JJA and minimum values in DJF, leading to a correlation that is mainly governed by the seasonal cycle. Similarly, at the U.S. site,

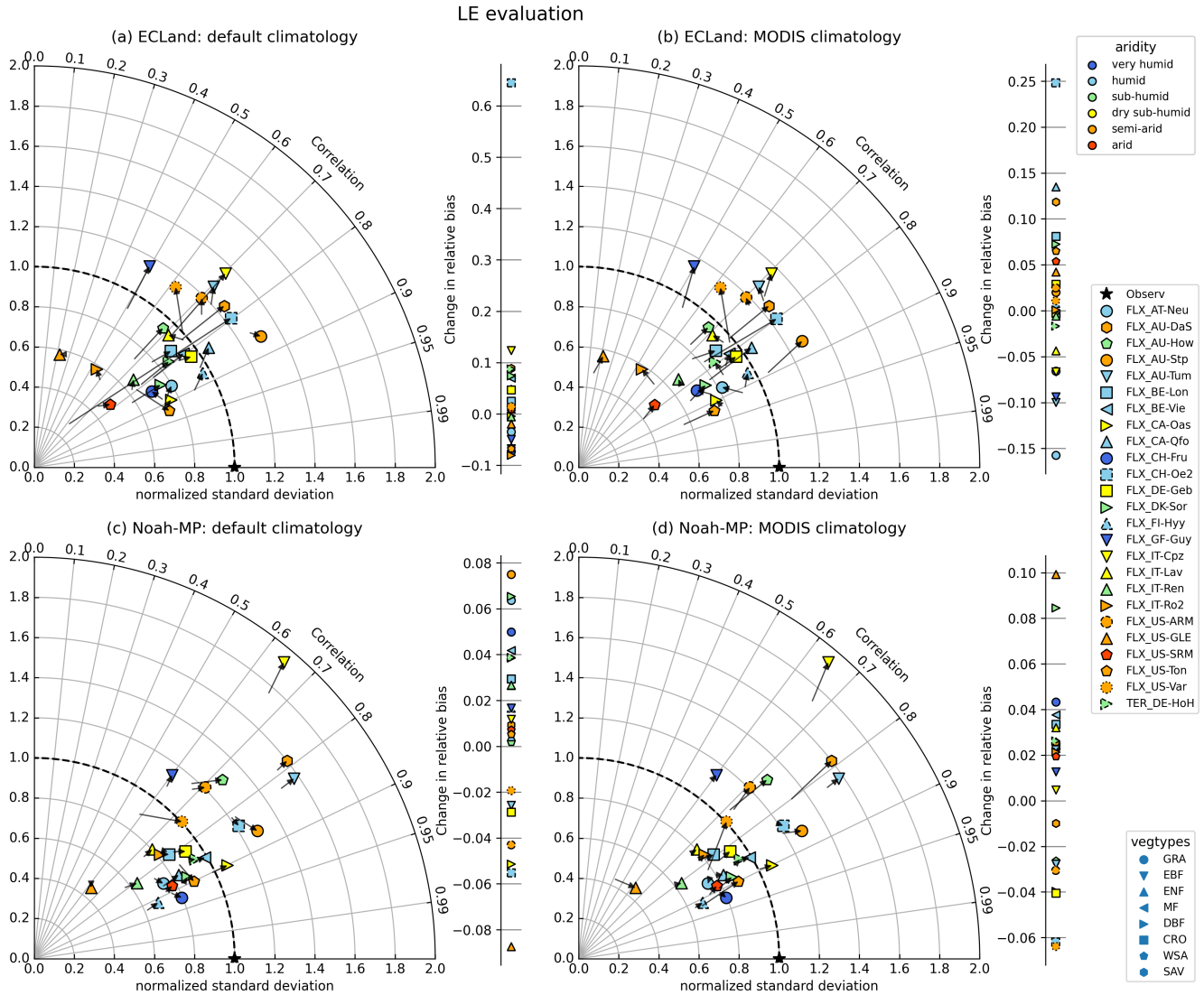

Figure 5. ~~Box plots showing the elasticity~~ Change of ~~correlation~~ statistical measures for LE modeling when switching on dynamic vegetation for all included sites and by using *default climatology* (left~~column~~) ~~, normalized standard deviation~~ or *MODIS climatology* (~~middle column) and relative bias (~~right~~column~~) ~~for different variable relationships in both models when activating dynamic vegetation~~as forcing.~~For reasons of practicability, elasticity is used reciprocal. Accordingly, the explanatory variable is the first one of each relationship showed on the y-axis. The grey shaded area marks the range between the thresholds of independence.~~

with an overall tighter relation, vegetation productivity and LAI peak together in spring (i.e., MAM). For these three sites, correlation coefficients range between ~~0.78 to 0.90~~ 0.80 to 0.86 indicating a clear but not perfect relation between LAI and GPP. However, the scatter of the observed relation is considerable with the standard deviation of the residuals (σ_r ~~values~~

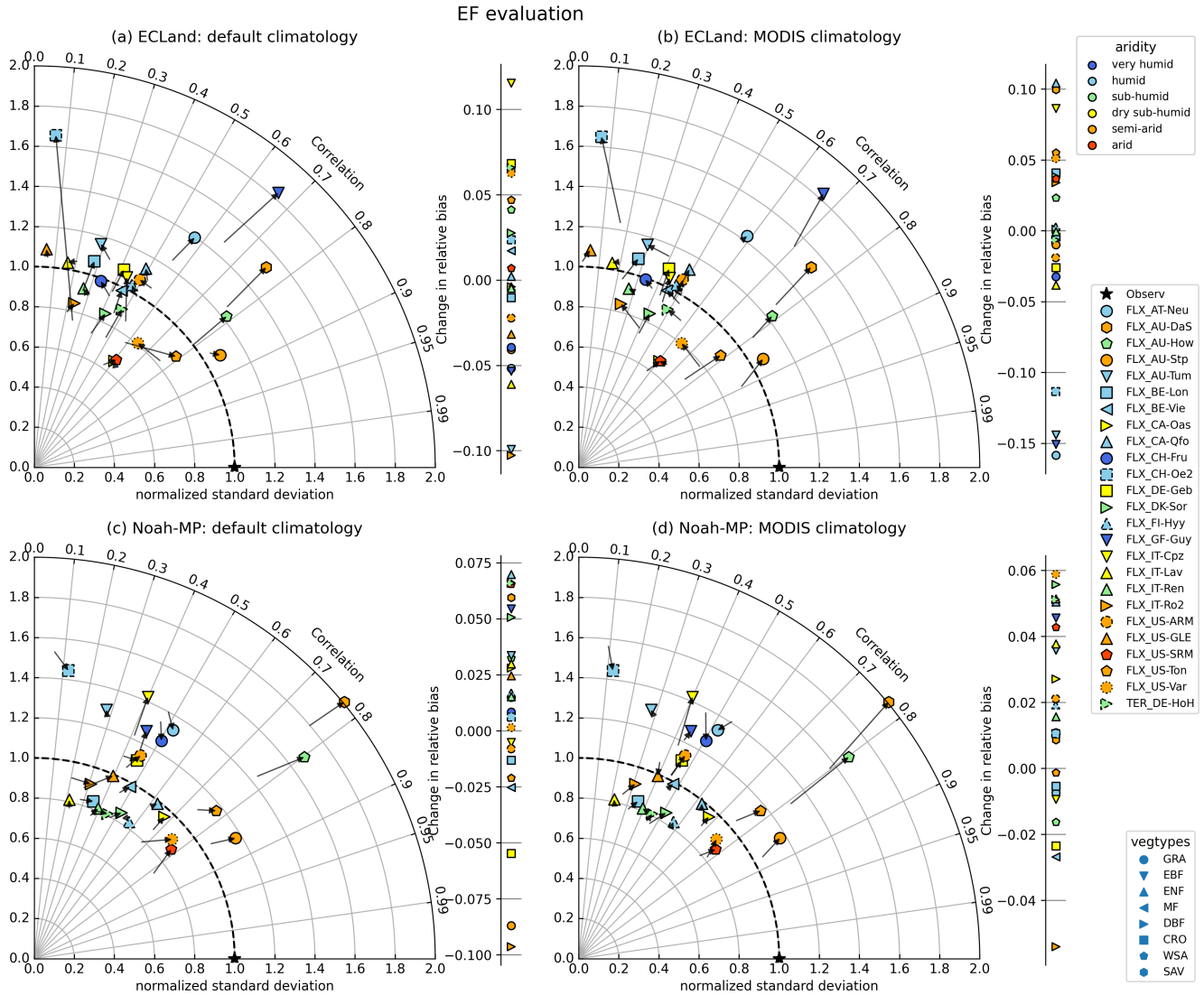

Figure 6. Same as before but for evaporative fraction which represents the turbulent flux partitioning.

~~between 53 and 105 $\cdot 10^{-6}$ $gCO_2m^{-2}s^{-1}$~~) being between 58 and 102 $\cdot 10^{-6}$ $gCO_2m^{-2}s^{-1}$. The variance is highest for the peak of the growing season, when GPP quickly responds to environmental conditions (e.g., cloudiness, precipitation, and soil moisture stress) that LAI responds much slower to. The tropical site in French Guiana (~~GF-Guy~~*GF-Guy*) shows, as expected, no seasonal cycle, leading to an extremely weak relation between LAI and GPP. The latter is comparatively high all year round (GPP ~~0.0002 and 0.0006 $gCO_2m^{-2}s^{-1}$~~between 250 and 600 $\cdot 10^{-6}$ $gCO_2m^{-2}s^{-1}$) although LAI values from the MODIS dataset surprisingly varied between 1 and 7 m^2m^{-2}. ~~In fact, the MODIS dataset generates some uncertainty through cloud coverage especially in the tropics.We tried to minimize this uncertainty by excluding all days from the dataset that were flagged~~

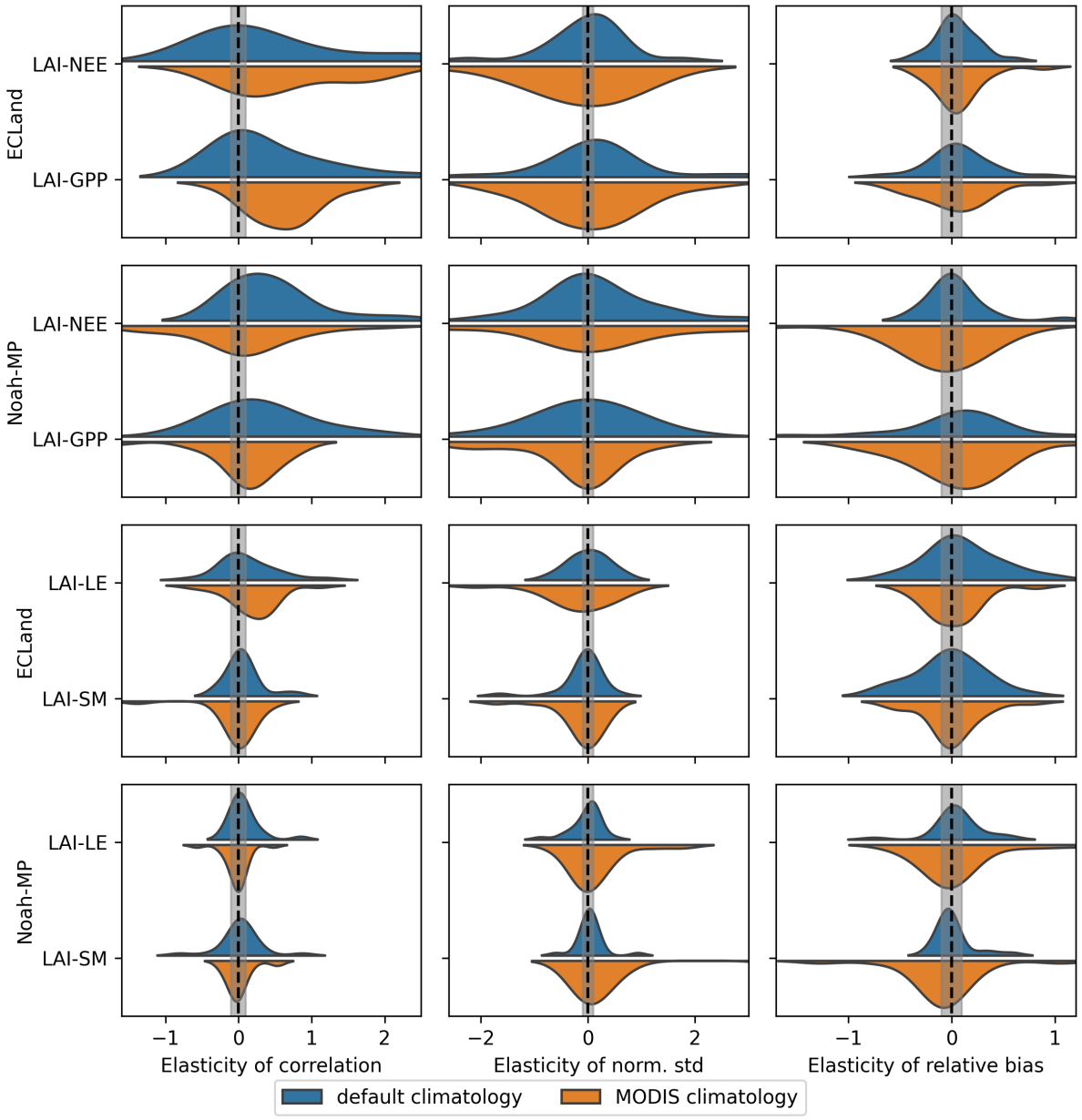

Figure 7. Density plots showing the elasticity of correlation (left column), normalized standard deviation (middle column) and relative bias (right column) for different variable relationships in both models when activating dynamic vegetation and using *default climatology* (blue) or *MODIS climatology* (orange) as forcing. For reasons of practicability, elasticity is used reciprocal. Accordingly, the explanatory variable is the first one of each relationship showed on the y-axis. The grey shaded area marks the range between the thresholds of independence.

~~with the value for significant cloudiness. For this~~ For this tropical site, GPP and LAI dynamics seem decoupled (Fig. 8 c).
Noah-MP shows a non-linear relationship with a pronounced hysteresis effect at all sites except the tropical one (Fig. 8 m-p). Thereby, GPP increases linearly with LAI during biomass built-up up to a point where allocation to leaves becomes minimal (vegetation type specific), and drops considerably without any substantial reductions in LAI towards the end of the growing season (e.g., Fig. 8 m). When GPP values reduce below approximately $100 \cdot 10^{-6}\ gCO_2 m^{-2} s^{-1}$, then LAI reduces from values about three towards zero. This hysteresis is shifted in seasons due to local climate as for the site *US-Var* (Fig. 8 p). At the tropical site, Noah-MP shows some variability in GPP, but almost no change in LAI which is around a value of five.
ECLand, in general, shows a linear relationship with considerable less variability compared to the observations. The slope and intercept of the linear regression is dependent on the choice of static or dynamic vegetation. Dynamic ECLand shows a very tight linear relation between LAI and GPP with much lower scatter compared to the observations (Fig. 8 third row) as R is larger than 0.99 and σ_r is between 10 and $14 \cdot 10^{-6}\ gCO_2 m^{-2} s^{-1}$ for all non-tropical sites. With slope values of 104 to $254 \cdot 10^{-6}\ gCO_2 m^{-2} s^{-1}$, that relationship is much steeper than in the observations. Even for the tropical site, ~~GPP and LAI dynamics seem decoupled~~ the relationship between LAI and GPP is clearly and tightly linear (Fig. **??**~~c).~~ 8 k).

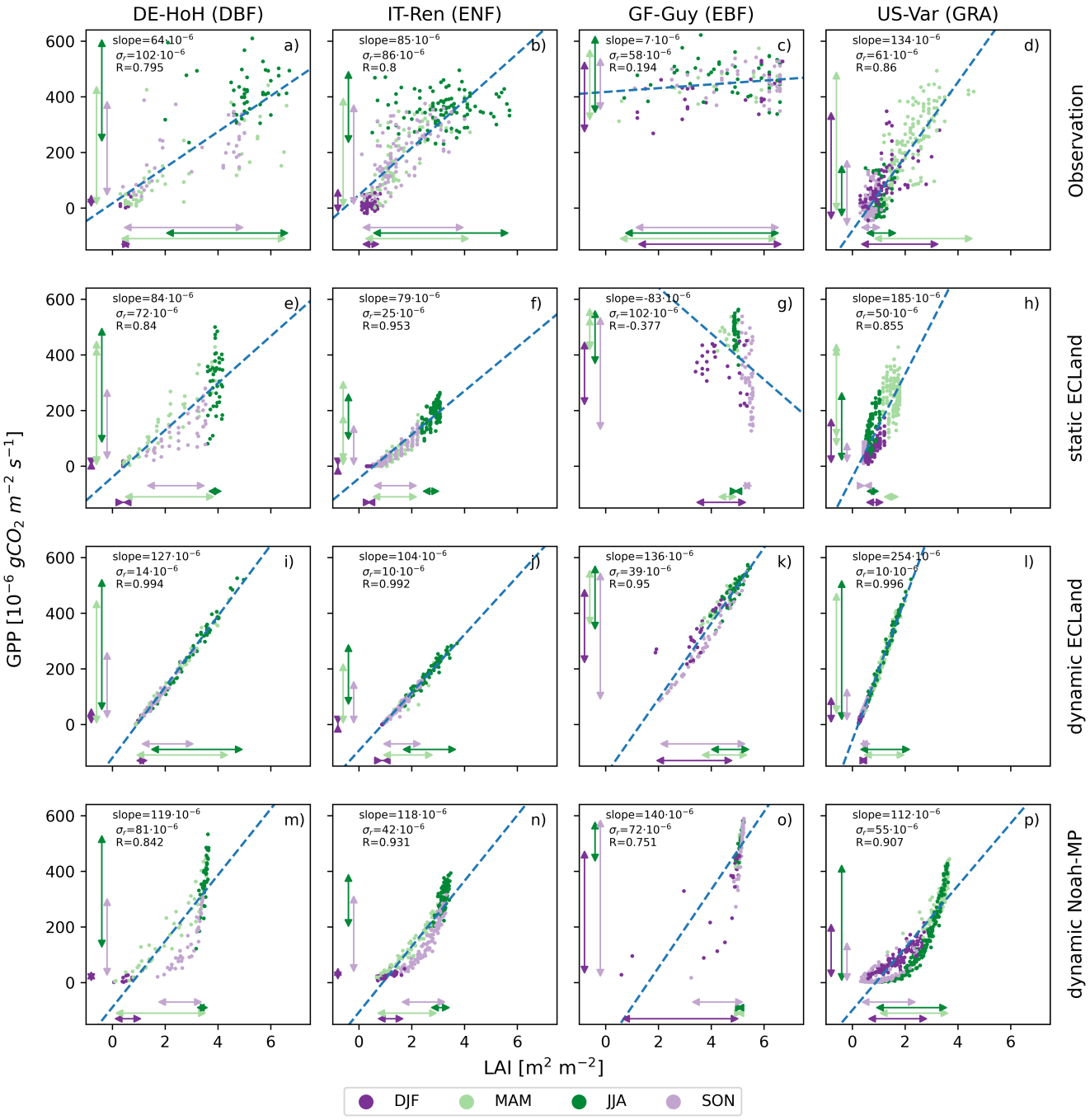

Figure 8. Scatter plots of the relationship between LAI on the x-axes and GPP on the y-axes as 8-day averages for four selected sites (columns). The rows from top to down show observations, static ECLand model output, dynamic ECLand model output, and dynamic Noah-MP model output. Seasons are represented by different dot colors. The arrows represent the range of GPP and LAI values for the individual seasons. A simple linear regression model was applied (blue dashed line) and its correlation coefficient (R), slope and standard deviation of the residuals (σ_r) are given for each relationship.

4 Discussion

4.1 Using LAI climatology for ECLand and Noah-MP runs is the best way to reproduce leaf area and carbon uptake

Comparison between model output and observational data of LAI, NEE or GPP on a daily basis is rarely done. The ability of the two models to reproduce these observed ecosystem variables ~~, i.e. LAI, NEE and GPP,~~ was in line with ~~results in the available literature~~previous results. For Noah-MP, model quality metrics were in the range of other studies ~~, although LAI and NEE~~ (Brunsell et al., 2020; Li et al., 2022a; Xu et al., 2021; Liang et al., 2020). However, dynamic LAI modelled by Noah-MP in our assessment ~~were more biased .~~ with a mean of $+70\,\%$ was more biased compared to a mean of $+20\,\%$ for annual LAI values reported by Li et al. (2022a). Ma et al. (2017) reported a relative bias in GPP of $40\,\%$ on average which is higher than the relative bias found here. For ECLand, we could not find any comparable study reporting the performance of daily LAI or NEE/GPP specifically, neither for dynamic nor static simulations. However, ~~correlation coefficients~~ for static ECLand, correlation coefficients between modeled and observed NEE and GPP were in line with ~~values for 10 day averages of NEE and GPP from static ECLand for a bunch of FLUXNET sitesanalyzed by Boussetta et al. (2013) and, by looking at~~ those obtained by Boussetta et al. (2013) for 10-day averages at several FLUXNET sites. Also, for the mean annual cycles of NEE and GPP, Stevens et al. (2020) found a lower prediction error (RMSD) when using MODIS LAI forcing compared to ~~LUT~~ default prescribed LAI, and, like in our study, a substantial bias in LAI.

~~Activating vegetation dynamics decreased the model~~ For both models, using *MODIS climatology* in static simulations resulted in the best performances concerning LAI. This agreed with expectations. Since all our simulations were validated with MODIS data, a better performance using static runs using *MODIS climatology* itself would likely yield better results than the default values in either model. For Noah-MP, static simulations with *MODIS climatology* indeed yielded the best performance regarding LAI ~~for both models, especially for short and sparse vegetationtypes. For static ECLand, changing LAI input to MODIS climatology instead of default LAI values improved LAI representations which is expected. The default climatological LAI in ECLand is~~ in some sites, but, interestingly, using the *default climatology* performed also well for others. LAI deviations with the *default climatology* occurred specifically in short vegetation, which was also true for the dynamic runs (see below). For ECLand, where the *default climatology* is already based on MODIS data (Boussetta et al., 2012)~~. Differing model performance regarding LAI between static runs of ECLand with default and MODIS climatological LAI, thus, has two reasons: First, the default climatological LAI~~ , the performance of the static run was generally improved compared to the validation dataset, as the higher spatial resolution allowed for a better geographical mapping. Also, ECLand *default climatology* was created by ~~the~~ disaggregating the total LAI in the MODIS data to the low and high vegetation type on the grid cell. ~~Second, these LAI values for high and low vegetation are gridded with $10\ km$ x $10\ km$ resolution and for the MODIS climatological LAI , here, we used data from the $500\ m$ x $500\ m$ grid cell in the MODIS dataset which was closest to the flux tower. As a result, a comparison of the performance of static ECLand with either using default or MODIS climatological LAI rather shows how representative the LAI climatology is for the vegetation on that grid cell.However, in this study, adding more detailed information by using MODIS single-year LAI forcing did not further improve modelperformance (not shown). Updating the LAI forcing on annual time scale is far from being a near real-time data assimilation which has been shown to improve the model performance of turbulent~~

~~fluxes, GPP and soil moisture for roughly 50% of the chosen sites (Boussetta et al., 2015).~~Both points together can explain the better performance for LAI of static ECLand simulations with *MODIS climatology* compared to *default climatology*.

~~For~~ Dynamic vegetation yielded no better LAI results compared to using static runs with *MODIS climatology* for either model. Evergreen broadleaf forests showed the lowest correlation coefficients for dynamic LAI predictions which was also shown by Yang et al. (2011) for tropical regions simulated by Noah-MP~~, static simulations with MODIS climatology had the best performance regarding LAI~~ . Additionally, Brunsell et al. (2020) reported overestimation of LAI with dynamic Noah-MP for the Eastern Amazonian Forest which we could not find here. ECland suffered from overall strong relative biases regarding LAI in dynamic simulations. The underestimation of prognostic LAI was already shown by Boussetta et al. (2021). ~~However, default LAI approach was performing equally well for some sites.~~ Substantial biases ~~occurred for simulations with and without vegetation dynamics especially~~ also occurred in Noah-MP (also shown by Huang et al., 2022), but especially so for short or sparse vegetation types~~, which~~ . The latter could be due to LAI overestimation in the early growing season as reported by Cai et al. (2014). Also, Liu et al. (2016) found that neither look-up table LAI nor predicted dynamic LAI annual cycles seemed to reproduce LAI observations for short vegetation. On the other hand, Pilotto et al. (2015) achieved satisfactory model predictions ~~also~~ for crop sites without vegetation dynamics. ~~For~~ Thus, for short vegetation such as grasslands, the Noah-MP Crop module ~~probably~~ maybe better represents LAI dynamics ~~but we did not use this option here~~(Liu et al., 2016), which should be tested in the future.

~~Whether switching on vegetation dynamics in Noah-MP improves NEE cannot be evaluated because it is only calculated for dynamic but not for static simulations there (see also section 2.2). Overall,~~ The performance of NEE and GPP in ECLand was not very sensitive to different vegetation dynamics. Generally, using static *MODIS climatology* yielded the best predictions of GPP and NEE, although the correlation between modeled and observed NEE was generally low (mean Pearson correlation coefficient was 0.44). In many sites, even static simulations with *default climatology* resulted in comparable performances. Interestingly, adding more detailed information by using *MODIS single-year* LAI forcing did not further improve model performance (not shown), as we would have expected if LAI dynamics contributed substantially to enhancing model performance for the carbon fluxes. However, other authors found improved model performance of turbulent fluxes, GPP and soil moisture for roughly 50% of their set of sites by updating the LAI forcing using near real-time data assimilation (Boussetta et al., 2015) . In other words, a more frequent reset of LAI to the correct value can improve the ECLand performance in general, but did not have an effect for the annual resolution applied here.

Assimilation of LAI during model runs and instead of fixed forcing (as in a static case) also improved LAI and GPP model quality in a study by Xu et al. (2021) using dynamic Noah-MP~~performed well in representing NEE for most forest sites. Thus, although some previous studies found substantial overestimation in GPP for the continental U. S. (Ma et al., 2017), predicting NEE using~~ . We, therefore, expected that LAI dynamics potentially improve model quality regarding carbon fluxes which was predominantly not the case. However, dynamic Noah-MP ~~could be useful in studies when LAI climatology cannot be used such as climate change impact studies. Nevertheless,~~ is already known to overestimate GPP (Ma et al., 2017; Liang et al., 2020; Brunsell et al., 2 . Especially short and sparse vegetation types suffered from low predictive ~~efficiencies by dynamic Noah-MP which is in accordance with findings from Yang et al. (2021) for ChinaFLUX. There, none~~ power mainly in NEE correlation (Yang et al., 2021)

and in GPP relative bias (Li et al., 2022a) which could be also observed here. None of the parameter sets ~~they~~ Yang et al. (2021) tested for simulations with dynamic Noah-MP resulted in ~~well fitting predictions of diurnal~~ well-fitting predictions of daily changes in NEE for three of the four sites with short vegetation ~~.An assimilation of LAIduring model runs and not only as fixed forcing (as in our case) might improve LAI and NEE representation which Xu et al. (2021) showed in their investigation with dynamic Noah-MP. Though~~within ChinaFLUX. Note, however, that LAI, NEE and GPP of short and sparse vegetation were also not well-represented in static runs either. Also, Kumar et al. (2019) could only achieve marginal improvements in GPP representation by dynamic Noah-MP due to LAI assimilation ~~which supports our detected limited effect of LAI~~ for crops and grasslands which suggests that LAI dynamics had only a limited effect on simulated NEE ~~. Similarly, the performance of NEE and GPP in ECLand was not very sensitive to different vegetation dynamics. Short~~ there. One possible reason for lower predictive power of the models regarding the carbon fluxes of short or sparse vegetation ~~types thereby were more affected by differing LAI estimates. Hence, a sensitivity analysis with respect to the impact of LAI and vegetation dynamics itself would be meaningful. In our investigation, using static ECLand simulations with MODIS climatology forcing seemed reliable in representing NEE although the correlation between modelled andobserved NEE was generally low (mean Pearson correlation coefficient was 0.44). For many sites, even using the default climatological LAI for simulations with static ECLand resulted in equally good performances in simulating NEE~~ could be that these vegetation types more quickly and dynamically respond to fluctuations in the environment (e.g. soil moisture limitations). Forest ecosystems might be able to compensate restrictions by a larger intrinsic carbon storage or deeper roots resulting in less variability of their productivity within and between the years. It seems that both models investigated here cannot mimic this differentiation. Nonetheless, it was shown here that correlation coefficients for GPP simulated with dynamic Noah-MP were high (also found by Liang et al., 2020; Li et al., 2022a) and, at the same time, relative bias was small for all forests except the evergreen broadleaf forests (see section 3.1 and Fig. A1). Thus, although some previous studies found substantial uncertainties in modeled GPP for different vegetation types (Ma et al., 2017; Liang et al., , predicting ecosystem variables using dynamic Noah-MP could be useful at least for forests in studies when LAI climatology cannot be used such as climate change impact studies.

Considering the opposing biases in NEE (and GPP) indicates that the models differ in their estimates of ecosystem respiration. One important difference is the sequence of the calculation of GPP, NEE and respiration. ECLand estimates net assimilation and respiration first separately whereby respiration is set to be 11% of net assimilation and, then, both are used to calculate GPP. In Noah-MP, the first estimate is for GPP which is reduced by respiration to gain a values for NEE and, additionally, respiration is scaled by GPP and available biomass inclusive of LAI. Including our findings, for dynamic ECLand, the underestimated LAI directly transfers into lower NEE values and, thus, also to GPP since respiration is a fixed fraction of NEE. Apart from the fraction of GPP that is directly needed for metabolism, the estimation of respiration in dynamic Noah-MP also considers leaf maintenance which is another difference compared to ECLand. As a result, respiration is slightly overestimated in ECLand, and ~~GPP~~slightly underestimated in Noah-MP. ~~For modelling LAI and NEE, using dynamic vegetation modules in their current implementation in either model is not yet efficient because they increase model complexity encompassing more dynamic processes andparameters without improving fluxes predictive skill. As the dynamic vegetation components in ECLand is still under development, findings from this study will help better understand and represent the processes involved to improve its~~

~~performance in modeling carbon and energy fluxes . Overall, we recommend using MODIS climatology forcing or alternative remote sensing LAI products for static simulations which yields reliable model performances for NEE and GPP.~~

4.2 ~~Modelled turbulent fluxes and soil moisture were almost unaffected by vegetation dynamics in both LSMs~~

~~Statistical measures for~~

4.2 Model performance of turbulent fluxes and soil moisture were almost unaffected by vegetation dynamics in both LSMs

The model performance of ECLand and Noah-MP regarding heat fluxes and soil moisture seems almost insensitive to vegetation dynamics. Correlation, variability and bias of turbulent fluxes in this study were comparable to other studies. While evaluating static ECLand with FLUXNET data, Stevens et al. (2020) found correlation coefficients of 0.79 and 0.77 for the annual cycle of latent and sensible heat, respectively, ~~when evaluating static ECLand simulations of the mean annual cycle with data from 17 FLUXNET stations,~~ and Boussetta et al. (2013) showed a mean correlation coefficient of 0.81 for ~~10 day~~ 10-day averages of latent heat~~for 32 FLUXNET sites modelled with static ECLand. We found no other studies looking explicitly at daily values for ECLand.~~ . For Noah-MP, statistical measures for turbulent fluxes and soil moisture were mostly in line with other studies ~~(Niu et al., 2011; Yang et al., 2021; Xu et al., 2021). We found no pronounced underestimations of latent heat fluxes for humid sites as Liang et al. (2020) did in their application of Noah-MP using static vegetation representation over China~~(Niu et al., 2011; Ma et al., 2017; Yang et al., 2018; Xu et al., 2021) although Pilotto et al. (2015) presented lower correlation coefficients between 0.20 and 0.43. Interestingly, Ma et al. (2017) showed opposing relative bias for evapotranspiration on annual time scale over the continental U.S. of 4% and 22% for static and dynamic simulations, respectively.

~~The impact of simulating vegetation dynamically on ECLand turbulent fluxes was small~~For ECLand, it had little impact on turbulent fluxes whether vegetation was simulated dynamically instead of statically. Model performance for ~~latent heat flux and evaporative fraction~~ LE and EF changed only for some sites and towards lower performance (see section 3.2). The predominant underestimation of ~~latent heat flux agrees with~~ LE agrees with the findings of Stevens et al. (2020). For dynamic ECLand, the underestimation of GPP and LAI ~~and might be also~~ (also in Boussetta et al., 2021) could also be the reason for the poor correlation of ~~evaporative fraction between modelled~~ EF between modeled and observed values ~~. However, at the same time,~~ because the energy fraction that is used for transpiration is underestimated. Boussetta et al. (2021) found that dynamic vegetation in ECLand improved ~~near surface temperature, sensible and turbulent heat fluxes and, hence, has the potential in improving numerical weather predictions~~numerical weather predictions. There, the main improvements in model performance were achieved through updating land cover maps and the LAI in the look-up table or by including LAI seasonality which both is comparable with our experiment using *MODIS climatology* in static ECLand simulations. Here, we could not confirm theses findings being related to improved performance in heat fluxes since model performance of LE and EF were almost unaffected by the used LAI forcing, which was already experienced by others (Stevens et al., 2020; Nogueira et al., 2021). The reason might be that parameters are adapted to the prior vegetation information (Ruiz-Vásquez et al., 2023) and, thus, the model needs a re-calibration.

~~Activating vegetation dynamics or changing LAI forcing had a small impact on latent heat and evaporative fraction predictionswith~~
~~Noah-MP. Slight~~ Also for Noah-MP, activating vegetation dynamics had mostly little impact on LE and EF predictions. A slight improvement in model performance was found for some sites with short vegetation types or semi-arid ~~climate. Ma et al. (2017) already concluded~~ climates. Ma et al. (2017) found that using LAI climatology resulted in better model performances for ~~latent heat flux~~ LE than simulations with activated vegetation dynamics for Noah-MP using the monthly FLUXNET Multi-Tree Ensemble data over the ~~US.~~U.S.. However, here, we did not find enhanced biases in ~~latent heat flux~~ LE predictions with dynamic Noah-MP compared to the static simulations as they did which could be due to the differing timescales for model evaluation. Both, overestimation and underestimation of LE predicted by dynamic Noah-MP is reported in the literature (Brunsell et al., 2020; Ma et al., 2017; Cai et al., 2014). Brunsell et al. (2020) showed a positive bias of monthly evapotranspiration in the Eastern Amazonian Forest simulated with dynamic Noah-MP while we found a negative bias of LE for the FLUXNET site *GF-Guy*. For short vegetation types, using the Noah-MP Crop module with activated vegetation dynamics might be ~~more~~ sufficient in predicting surface fluxes (Liu et al., 2016). Achieved improvement for LE might be not as large as for sensible heat flux (Liu et al., 2016) which could be a reason for poor performances in EF presented here.

Although vegetation and soil moisture state variables are directly coupled within land-surface models, we found almost no impact of different vegetation ~~modelling~~ modeling on soil moisture predictions for both models. Activating vegetation dynamics or changing LAI forcing did not improve soil moisture representation ~~. Moreover, modelled soil moisture~~ on average. The reason might be due to the implemented interaction of carbon and water processes. First, the potential photosynthetic activity in dependence of leaf area and radiative conditions is calculated. Then, the limitation factor of extractable water is estimated according to available soil water and roots. Lastly, the photosynthetic activity is adapted to that restriction and transpiration rate adapted to conductivity and atmospheric conditions. As a result, the only included path is that soil moisture impacts photosynthetic activity and biomass build-up. But there is no feedback that more biomass needs/loses more water that will be taken from the soil because photosynthetic activity in the models relates only to the carbon fluxes but not to the water fluxes. Additionally, modeled soil moisture suffers from substantial biases in both directions which was also found by Liang et al. (2020) for Noah-MP and by Garrigues et al. (2021) for ECLand although ~~in the latter case~~ correlation between observed and ~~modelled soil moisture was satisfactory (Beck et al., 2021)~~modeled soil moisture can be satisfactory (Beck et al., 2021; Xu et al., 2021; Pilo
. The reason might be underlying ~~LUT~~ default values for soil characteristics such as field capacity and permanent wilting point that possibly deviate from on-site soil conditions and optimal values for soil parameters are still uncertain (Li et al., 2020). Alternatively, it could be an effect of differing scales since the observation from FLUXNET refers to point measurements. The Multiscale parameter regionalization (MPR) might provide an improved way to estimate soil parameters by applying pedotransfer function on local soil characteristics and, recently, has been applied to Noah-MP in a proof-of-concept (Schweppe et al., 2022).

~~Notwithstanding that van den Hurk et al. (2003) at least~~ Overall, the model performance of soil moisture and heat fluxes was barely affected by vegetation dynamics or applied LAI forcing. However, the sensitivity to LAI might be given since van den Hurk et al. (2003) found some effect of changed LAI values given into TESSEL, a predecessor of ECLand, as well as Ma et al. (2017) and Zhang et al. (2016) did for Noah-MP~~, indicating that a certain sensitivity on evapotranspiration existed~~.

Xu et al. (2021) showed improved LE and soil moisture simulations with more realistic LAI although, also there, the effect was not only site-dependent but also differed with season and year. But those authors also highlighted that transpiration is only partly determined by LAI and ~~controls through~~ other factors controlling the canopy conductance ~~for water vapour~~ to water vapor might play a larger role. ~~However, canopy conductance is also scaled by LAI in ECland.~~ Therefore, other compensating mechanisms may explain low elasticity between LAI and ~~latent heat flux~~ LE or soil moisture ~~because the estimation of transpiration in the model remained almost the same as in older model versions and we also did not change any of the parameters that affect the canopy conductance.Overall, model performance regarding latent heat flux or soil moisture are independent of how LAI is represented~~(see section 3.2). Yang et al. (2011) demonstrated that the applied runoff scheme more strongly determined model performance of soil moisture and evapotranspiration than the schemes for dynamic vegetation, stomatal resistance and soil moisture stress. Still, optimizing parameters can be effective in improving model predictions which could be shown by several studies (Bohm et al., 2020; Li et al., 2021, 2020). Even more, the sensitivity of soil moisture to vegetation parameters was shown to enlarge with dynamic vegetation representation (Arsenault et al., 2018). Yet, uncertainty about the optimal values for especially soil and vegetation parameters remains (Li et al., 2020).

Overall, the impact of vegetation dynamics and LAI on turbulent heat fluxes and soil moisture in this investigation was slim across sites and seasons for both models. Thus, modelers who are mainly interested in the performance of carbon processes should be careful using performance metrics for hydrological variables as a proxy (e.g. ~~latent heat flux~~LE) because the model formulation for the latter might have controlling processes other than LAI or NEE which dominate the result. ~~In conclusion, an impact of vegetation dynamics and LAI on turbulent fluxes and soil moisture in this investigation was slim when considered across sites and seasons. However, the sensitivity to LAI might be given in some situations, since Xu et al. (2021) showed improving latent heat flux and soil moisture simulations with more realistic LAI although also there, the effect was not only site-dependent but also differed with season and year~~Whether applying vegetation dynamics in model simulations is advantageous might depend on the target variables. While, for heat flux predictions, using *MODIS climatology* might be sufficient, activating vegetation dynamics could play a role for improve carbon flux predictions at seasonal or annual timescale (Jarlan et al., 2008).

4.3 ~~Observed~~ Discrepancy between observed and simulated ~~relationships between ecohydrological variables~~GPP-LAI relationship is caused by model structure

The substantial scatter in the observed relation between GPP and LAI is in close agreement with previous work, showing that GPP ~~depends next to LAI also~~ also depends on the short-term availability of resources (e.g., light, soil water) (Hu et al., 2022). Additionally, Zhang et al. (2021) found that in LSMs the relation between LAI and GPP was too tight. We therefore checked the underlying relations in the models causing this.

GPP-LAI relationship in Noah-MP ~~shows a marked hysteresis effect at all sites except the tropical one (Fig. ?? c-h), with GPP linearly increasing with LAI during biomass built-up up to a point where allocation to leaves becomes minimal (vegetation type specific), and a substantial drop in GPP without any substantial reductions in LAI towards the end of the growing season (e.g., Fig. ?? e). When GPP values reduce below approximately $0.0001\ gCO_2m^{-2}s^{-1}$, then LAI reduces from values about~~

three towards zero. A similar behaviour is observed at the grassland site in the U.S. with a shift in seasons due to local climate (Fig. ?? h). At the tropical site, Noah-MP shows some variability in GPP, but almost no change in LAI which is around a value of five.The LAI dynamics in Noah-MP depend on a number of processes. Allocation of carbon to the leaves increases LAI, while leaf turnover and leaf showed a clear exponential hysteresis (see section 3.3). This hysteresis is related to the partitioning of GPP to the carbon pools in the plants and to LAI reducing processes as leaf turnover and leaf die-backreduce LAI. Leaf turnover . Noah-MP uses a non-linear function for allocation of GPP to the leaves that limits the maximum LAI the model can grow resulting in the LAI saturation in summer that can be seen in Figure 8 m-p. On the other hand, leaf turnover due to leaf aging is implemented as a linear function of leaf mass . Leaf while leaf die-back due to environmental limitations follows exponential functions. Taken together, leaf die-back dominates , in the later growing season which results in the hysteresis. The reduction of LAI (i.e., leaf die-back) is implemented to be dependent both on water and temperature stress, but temperature stress is the main driver. In the specific implementation used here, water stress only occurs at a very low soil saturation of $0.1\ vol\%$ for silt loam exemplarily which is even below the permanent wilting point of this soil texture type according to the LUT look-up table value. These values are rarely reached and, thus, water stress is negligible most of the time. In contrast, temperature stress is implemented as an exponential function causing the late growing season non-linear decline of GPP observed throughout the non-tropical sites. Temperature stress is at maximum at 5 °C 5 $°C$ for forest ecosystems resulting in no active biomass below this threshold. For this reason, LAI values are almost constant at the tropical forest site because temperature is never limiting there.

ECLand shows a very tight linear relation between LAI and GPP with much lower scatter compared to the observations (Fig. ?? third and fourth row). ECLand with ECLand with static vegetation shows a similar pattern of seasonal dynamics as Noah-MP with vegetation dynamics but with less pronounced exponential relationship. In contrast, dyanmic dynamic ECLand simulates LAI that is strongly coupled to daily meteorological conditions, leading to higher daily fluctuations of LAI than expected, including strong drops of LAI in summer. Three processes govern this these daily LAI dynamics: GPP, respiration and senescence. GPP relates linear is linearily related to LAI and varies with environmental and meteorological conditions causing the variability in static runs. In dynamic runs, losses in biomass due to high or low daily GPP linearly affect LAI. In other words, unfavourable GPP can reduce LAI almost immediately. The second process affecting LAI is senescence. ECLand distinguishes growing and senescence phase phases by comparing active biomass due to assimilation with biomass from the biomass from the previous time step. If active, then senescence is a linear function of active biomass and a folding-factor. The folding-factor reduces part of the senescent biomass, depending on photosynthesis (reduced in the case of high assimilation) and LAI. Overall, the folding-factor changes only slightly with LAI. Additionally, a reduction of LAI and, thus, active biomass due to reduced GPP (as explained before) causes the model to trigger senescence because the active biomass of the previous time step was higher. The third process is respiration. About 11% of physiologically possible assimilation is used for dark respiration without considering actual light conditions. This might cause high values of dark respiration compared with possible assimilation based on meteorological conditions and, thus, minimize reduce net primary productionor even produce , even producing negative values. Notably, no aboveground biomass storage is built up and there is no turnover. Most locations show a linear relationship comparable to ECLand but with a higher variability (Fig. ?? first and fourth 8 first and third row). This might be due to the fact

that leaf growth and leaf fall, in particular for trees, happen on longer timescales than the daily one as implemented in ECLand which inhibits immediate effects of GPP on LAI.

Overall, the current implementations of leaf dynamics in both models use very different approaches to represent LAI dynamics. In Noah-MP it is mainly temperature-driven, and GPP depends little on LAI once the canopy is fully developed. In contrast, in ECLand, LAI and GPP are coupled very tightly and, thus, the LAI dynamics follow almost the same sensitivities to water limitation and radiation as turbulent fluxes, which is unrealistic. ~~However, real~~ Realistic LAI is less dynamic and less sensitive to environmental conditions, as also indicated by the observations. Hence for very different reasons, in both models the performance regarding LAI and turbulent and carbon fluxes is disconnected.

4.4 Implications and limitations

For modeling LAI and carbon fluxes, using dynamic vegetation modules in their current implementation in either model is not yet efficient because they increase model complexity encompassing more dynamic processes and parameters without improving the predictive skill. As the dynamic vegetation components in ECLand are still under development, findings from this study can help better understand and represent the processes involved to improve its performance in modeling carbon and energy fluxes. But also for Noah-MP, we showed that the dynamic vegetation module has potential for improvement especially related to the relationship between GPP (and thus also NEE) and LAI. Underlying processes such as carbon allocation, root dynamics, plant hydraulics, feedbacks on photosynthesis and their parameterization can still be worked on (Ma et al., 2017; Li et al., 2021). Overall, we recommend using *MODIS climatology* forcing for static simulations which yielded the best model performances for carbon and water fluxes. This might be valid for other remote sensing LAI products as well but would need to be tested beforehand.

The value of a model evaluation like in this study depends on the reliability of the included datasets. Uncertainty in the forcing data might have a larger impact on the model runs than processes within the models (Zhang et al., 2016), but Haughton et al. (2016) demonstrated that observational errors, in general, are unlikely to cause poor model performance. Nonetheless, model evaluations are also restricted by uncertainty in the reference data (Li et al., 2022a) especially when considering flux measurements (Li et al., 2019) . We tried to address by carefully inspecting the time series data from FLUXNET2015 before their usage. However, as in all measurements, there are still uncertainties, e.g. from instrumental errors or incomplete energy balance closure.

Also, the MODIS dataset harbors uncertainty originating from cloud coverage, especially in the tropics. We tried to minimize this uncertainty by excluding all days from the dataset that were flagged with significant cloudiness. But saturation also limits the representativeness of the LAI measurements. Even when using only data with the highest possible quality flag, we found suspiciously low LAI values in summer for temperate forests and grasslands, and especially for tropical forests throughout the year (Fig. 8 c). Noisy and uncertain LAI data from MODIS for tropical forests was already reported among the literature (Weiss et al., 2007; Garrigues et al., 2008; Xiao et al., 2016; Zhang et al., 2024). As a result, reference data remains a source for uncertainty and a deviation in model outputs from it is expected. In any case, reference data is essential for model verification, calibration, and validation but should be treated carefully concerning its reliability and uncertainty.

5 Conclusions

Land-surface models often include modules for dynamic vegetation processes. ~~However~~Yet, an evaluation of the representativeness of key variables ~~like~~ such as leaf area index or net ecosystem exchange is rarely done on high temporal resolution. The impact of different parameterization of vegetation processes on water and carbon flux estimates by land-surface models is still poorly understood. ~~Additionally, multi-model comparison studies mainly focus on internal performance rankings without deeper investigations into the reasons of performance results.~~ Therefore, we evaluated the change in model performance of ecohydrological target variables when dynamic vegetation processes are included for two land-surface models and further gained insight into critical process implementations that lead to the observed patterns.

Surprisingly, neither for ECLand nor for Noah-MP, including modules for dynamic vegetation in their implementation improved the model predictions of ecohydrological variables. We expected vegetation dynamics in these land-surface models to better capture the higher variability in ~~the ecosystem exchangeespecially of~~ ecosystem exchange, especially that of highly dynamic short or sparse vegetation types, but this was predominantly not the case. Using alternative input for leaf area index other than default ~~climatological values also had an~~ climatology also had a negligible effect on the model performance but this needs to be evaluated in more detail since we were limited in data sources. Moreover, model performances of carbon and hydrological fluxes appeared to be weakly coupled. Therefore, the question arose whether exchange fluxes themselves in these land surface models are sensitive to changes in leaf area index estimates and not only to changing parameter sets. Indeed, different leaf area index estimates lead to different predictions in exchange fluxes but without affecting the overall model performance of these variables. This might be caused by the mismatch in the seasonal patterns between ~~observation~~ observations and models for the relationship of gross primary productivity and leaf area index. While this ~~relation~~ relationship in dynamic Noah-MP showed a logarithmic hysteresis, mainly driven by temperature, both variables are tightly ~~linear~~ linearly coupled in dynamic ECLand without allowing for ~~LAI~~ the leaf area index to remain unchanged in suboptimal conditions for photosynthesis.

This deeper analysis of the model performance for ecohydrological fluxes that pinpoints to the reasons ~~of~~ for model behavior was only possible with a reduced number of models. We used specific setups for the two land surface models evaluated here. Adapting or changing parameters and investigating the effect of other processes within the models were beyond the scope of this study. At this point, it remains unclear how representative our model selection is for the performance and process evaluation of other land surface models since they have processes implemented differently. Nonetheless, we highlighted some crucial relationships in the implementation of vegetation processes that have the potential for further improvement. Additionally, they might be a good starting point for a similar intensive investigation with other land surface models or other alternative LAI climatology.

Code and data availability. Observational data from the FLUXNET2015 dataset were accessed via FLUXNET data portal (fluxnet.org, 2020). Observational data for TERENO observatory "Hohes Holz" can be found at PANGAEA (Rebmann and Pohl, 2023). IGBP Land Classification is published by National Center for Atmospheric Research (2022). Aridity index was taken from Trabucco and Zomer (2018). Gap-filling of meteorological data was done by using ERA5 re-analysis product (Hersbach et al., 2020), accessed by Climate Data Store API

(Copernicus, 2018). USGS vegetation types can be found at University Corporation for Atmospheric Research (2023). Global gridded soil information (Hengl et al., 2014) is available at https://soilgrids.org. MODIS Leaf area index was retrieved via Earth Data Portal from NASA (Myneni et al., 2015).

Appendix

A.01 Dynamic ECLand processes

For more details, see the published model descriptions (Boussetta et al., 2012, 2013, 2021). Photosynthesis model is based on Calvet et al. (1998). Therein, potential net assimilation A_n is estimated from physiological constrains as

$$A_n = A_{max} \cdot (1 - e^{-\frac{g_{meso} \cdot (c_i - c_{comp})}{A_{max}}}) \tag{A.1}$$

where A_{max} is the leaf photosynthetic capacity, g_{meso} is the mesophyll conductance, c_i is the leaf-internal CO_2 concentration and c_{comp} is the CO_2 compensation point. Potential gross assimilation A_g, then, is calculated as

$$A_g = (A_n + R_d) \cdot \epsilon \tag{A.2}$$

where R_d is the dark respiration from

$$R_d = A_n \cdot f_R \tag{A.3}$$

with $f_R = \frac{1}{9}$ as dark respiration factor, and where ϵ is a quantum use efficiency factor, estimated as

$$\epsilon = 1 - e^{-\frac{\epsilon_0 \cdot E_{PAR}}{A_n + R_d}} \tag{A.4}$$

where ϵ_0 is the maximum quantum use efficiency and E_{PAR} is the absorbed photosynthetic active radiation. Actual gross assimilation GPP results from

$$GPP = A_g \cdot LAI \cdot \rho_a \tag{A.5}$$

where LAI is the leaf area index of the prior time step and ρ_a is the air density corrected for humidity.
A_n is used as the maximum leaf assimilation for the senescence model (Calvet and Soussana, 2001). To avoid immediate leaf die-back, a damping factor for senescence f_s is introduced as

$$f_s = \max(\frac{\tau_{lim} \cdot t_s}{100 \cdot N_{day}}, \max(10^{-8}, \frac{t_s}{N_{day}} \cdot \min(1, \frac{A_n}{A_{max}}) \cdot \frac{\max((r_{meso} \cdot 1000)^{0.321} \cdot LAI}{f_{LAI}}, 1))) \tag{A.6}$$

where τ_{lim} is a limiting factor for immediate biomass loss, t_s is the damping time for senescence, which basically is the amount of seconds per year, N_{day} is the amount of seconds per day, A_{max} is the maximum photosynthesis rate with optimal conditions and f_{LAI} is a LAI correction parameter that reduces mortality at high LAI values which would occur due to shadowing. The amount of biomass loss B_{loss} then is

$$B_{loss} = \min(B - LAI_{min} \cdot f_{LAI-B}, B \cdot (1 - e^{-\frac{1}{f_s}})) \tag{A.7}$$

where B is the biomass of the prior time step and f_{LAI-B} is a conversion factor between LAI and B. Then, biomass B is updated by subtracting B_{loss}. The change in biomass due to assimilation B_{gain} results from

$$B_{gain} = \max(LAI_{min} \cdot f_{LAI-B} - B, A_n \cdot f_{Cbiom}) \tag{A.8}$$

where $f_{Cbiom} \approx 0.68$ is a factor converting the amount of CO_2 uptake from assimilation to carbon in dry biomass. Biomass B is updated again by adding B_{gain}. In the end, this updated biomass is transferred into an updated LAI value by

$$LAI = \frac{B}{f_{LAI-B}} \tag{A.9}$$

LAI determines the interception reservoir W by

$$W = W_{max} \cdot (c_B + c_H \cdot LAI_H + c_L \cdot LAI_L) \tag{A.10}$$

where W_{max} is the maximum thickness of the water layer on leafs or bare ground, c_B, c_H and c_L are the fractions for bare soil, high vegetation and low vegetation on a grid cell and LAI_H and LAI_L are the LAI values for high and low vegetation, respectively (Boussetta et al., 2012). Additionally, canopy resistance r_c depends on LAI via

$$r_c = f_1 f_2 f_3 \cdot \frac{r_{s,min}}{LAI} \tag{A.11}$$

where $r_{s,min}$ is the minimum stomatal resistance and f_n are the restriction factors for low input in shortwave radiation, soil moisture stress and saturated atmospheric conditions (Boussetta et al., 2012).

A.02 Dynamic Noah-MP processes

For more details, see the published model descriptions (Niu et al., 2011; Ma et al., 2017; Oleson et al., 2012). The model for leaf dynamics within Noah-MP is based on Dickinson et al. (1998). Leaf biomass C_{leaf} is balanced over time with

$$\frac{\delta C_{leaf}}{\delta t} = f_{leaf} \cdot A_{tot} - (d_{stress} + d_{turnover} + R_{leaf}) \cdot C_{leaf} \tag{A.12}$$

where A_{tot} is the total carbon assimilation rate, f_{leaf} is the fraction of allocation to the leaves, d_{stress} is the dying rate caused by cold and drought stress, $d_{turnover}$ is the turnover rate due to senescence, herbivory or mechanical loss as a vegetation-type dependent parameter and R_{leaf} is the respiration rate of the leaf biomass. f_{leaf} is determined by LAI via

$$f_{leaf} = e^{0.01 \cdot LAI(1-e^{\chi \cdot LAI})} \tag{A.13}$$

where $\chi = 0.75$ is a parameter defining the partitioning of carbon allocation between leaves and stem. A_{tot} is split up to photosynthesis rates from sunlit and shaded leaves, respectively:

$$A_{tot} = 12 \cdot 10^{-6} \cdot (A_{sunlit} \cdot LAI_{sunlit} + A_{shaded} \cdot LAI_{shaded}) \tag{A.14}$$

where the first factor is for unit conversion. The partitioning of sunlit and shaded LAI results from a two-stream radiation transfer scheme (Niu et al., 2011). Assimilation rate for sunlit and shaded leaves, respectively, is estimated with a bottle-neck principle as

$$A = I_g \min(A_L, A_C, A_S) \tag{A.15}$$

where I_g is a growing season index according to leaf temperature and A_L, A_C, A_S are the photosynthesis rates limited by light, Rubisco and export, respectively (Bonan, 1996). A_L results from

$$A_L = \frac{4.6 \cdot \epsilon \cdot E_{PAR}(c_i - c_{comp})}{c_i + 2c_{comp}} \tag{A.16}$$

with c_i being the leaf-internal CO_2 concentration, c_{comp} being the CO_2 compensation point, ϵ being the quantum use efficiency and E_{PAR} being the absorbed photosynthetic active radiation. Additionally, $A_S = 0.5 \cdot V_{max}$ and

$$A_C = \frac{V_{max}(c_i - c_{comp})}{c_i + K_c(1 + \frac{c_o}{K_o})} \tag{A.17}$$

where c_o is the atmospheric O_2 concentration, K_c and K_o are the Michaelis-Menton constants for CO_2 and O_2 (Collatz et al., 1991), respectively, and V_{max} is the maximum carboxylation rate, defined by

$$V_{max} = V_{max,25} \cdot \alpha_{max}^{\frac{T_v - 25}{10}} \cdot f_N f_{T_v} \beta \tag{A.18}$$

where $V_{max,25}$ is the maximum carboxylation rate at 25 °C, α_{max} is a temperature conversion factor, T_v is the vegetation temperature, f_N is a factor for nitrogen limitation of the leaves, f_{T_v} is a factor for temperature limitation (Collatz et al., 1991) and β represents the limitation by available soil moisture.
d_{stress} for the leaf mass balance is estimated from

$$d_{stress} = d_{cold} \cdot e^{-0.3 \cdot \max(0, T_v - T_{min})} \frac{C_{leaf}}{120} + d_{dry} \cdot e^{-100\beta} \tag{A.19}$$

where T_{min} is a vegetation type dependent threshold temperature for leaf survival, β is the soil moisture limitation factor and d_{cold} and d_{dry} are vegetation type dependent dying rates (prescribed parameter) for temperature and dryness stress, respectively. Leaf respiration R_{leaf} is calculated with

$$R_{leaf} = f_{res}((f_{leaf} - \frac{LAI}{\chi \cdot f_{leaf}}) \cdot A_{tot} - R_l \tag{A.20}$$

where f_{res} is a factor defining the fraction of assimilation that is used for respiration and R_l is the respiration for leaf maintenance from

$$R_l = \min(\frac{C_{leaf} - C_{leaf,min}}{\Delta t}, 0.5 \cdot 12 \cdot 10^{-6} \cdot r_l(T_v) \cdot LAI \cdot \beta \cdot \frac{c_N}{c_{N,max}}) \tag{A.21}$$

where $C_{leaf,min}$ is the minimum leaf biomass, Δt is the time step duration, 0.5 is a reduction factor for respiration during non-growing season, $r_l(T_v)$ is the vegetation type dependent respiration rate for leaf maintenance at T_v and $\frac{c_N}{c_{N,max}}$ is the nitrogen saturation within the leaves. Afterwards, net primary production NPP is estimated as

$$NPP = (f_{leaf} - \frac{LAI}{\chi \cdot f_{leaf}}) \cdot A_{tot} - R_{leaf} - R_l \tag{A.22}$$

GPP is set to A_{tot} and LAI is updated with

$$LAI = C_{leaf} \cdot f_{LAI-B} \tag{A.23}$$

where f_{LAI-B} is the leaf area per biomass.
Assimilation rate A determines the stomatal resistance r_s by

$$\frac{1}{r_s} = g_{min} + \frac{m \cdot p_{air} \cdot A}{c_{air}} \frac{e_{air}}{e_{sat}(T_v)} \tag{A.24}$$

where g_{min} is the minimum stomatal conductance, m is an empirical parameter for the relationship between transpiration and CO_2 flux, p_{air} is the surface air pressure, c_{air} is the CO_2 concentration at leaf surface, e_{air} is the vapor pressure at leaf surface and $e_{sat}(T_v)$ is the saturation vapor pressure inside the leaves (Ball et al., 1987; Bonan, 1996). r_s then is used to estimate latent heat flux and, thus, evapotranspiration.

A.03 Additional figures

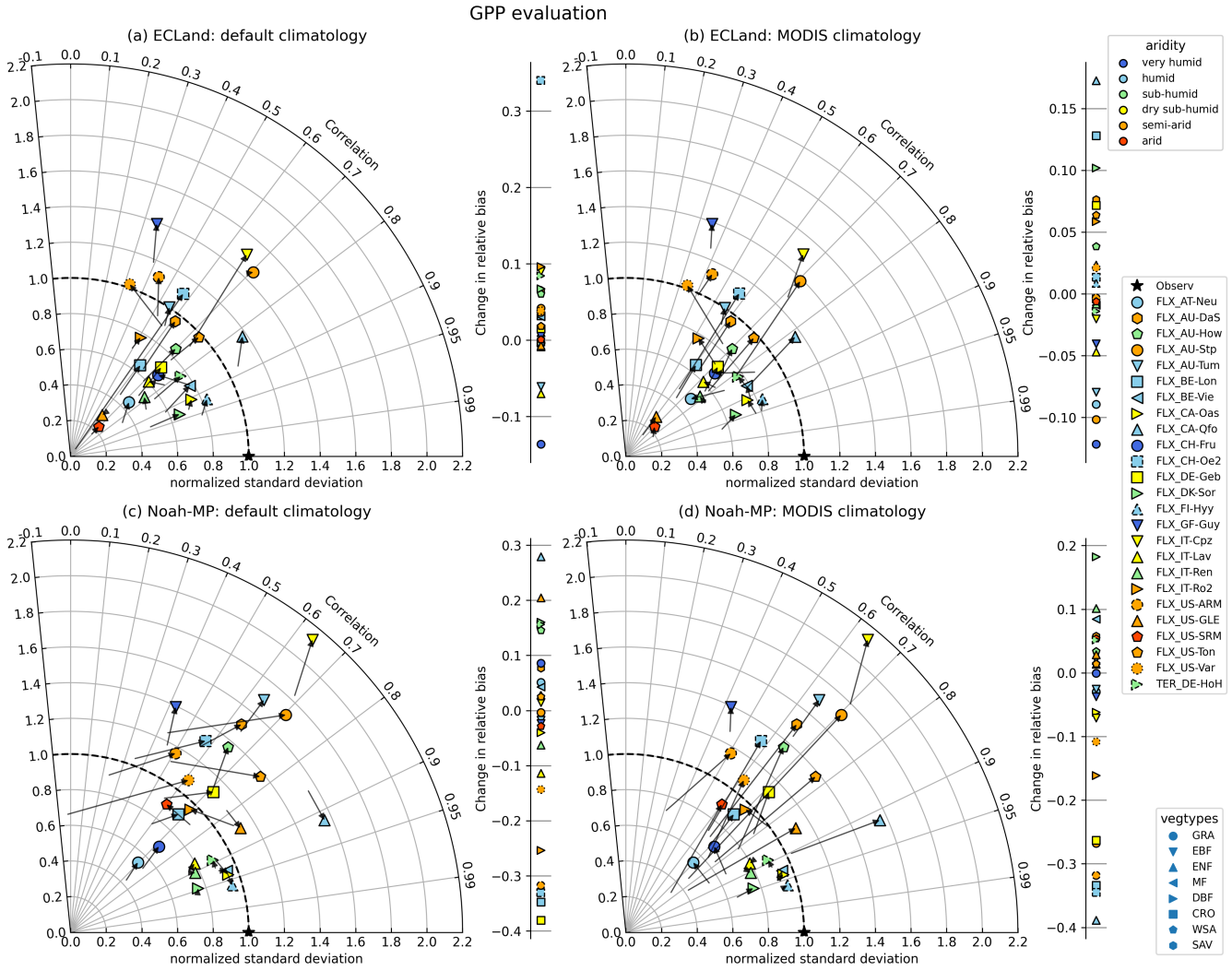

Figure A1. Change of model quality metrics for GPP prediction when switching on dynamic vegetation for all included sites and by using ~~LUT LAI forcing~~ *default climatology* (left) or ~~MODIS LAI climatology~~ MODIS climatology (right). The star ("Observ") marks the location of the perfect correlation between observation and model and perfect agreement between observed and modelled variance. The model performance of the static runs can be read from the start of each arrow. The point colors indicate the site aridity (top right legend). Vegetation types are symbolized by different marker types (bottom right legend).~~Since GPP is not generated as variable from Noah-MP when running the model without dynamics, no change in statistical measures can be presented. Additionally, because all the simulations with dynamic vegetation created the same output for Noah-MP, only one Taylor diagram is shown.~~

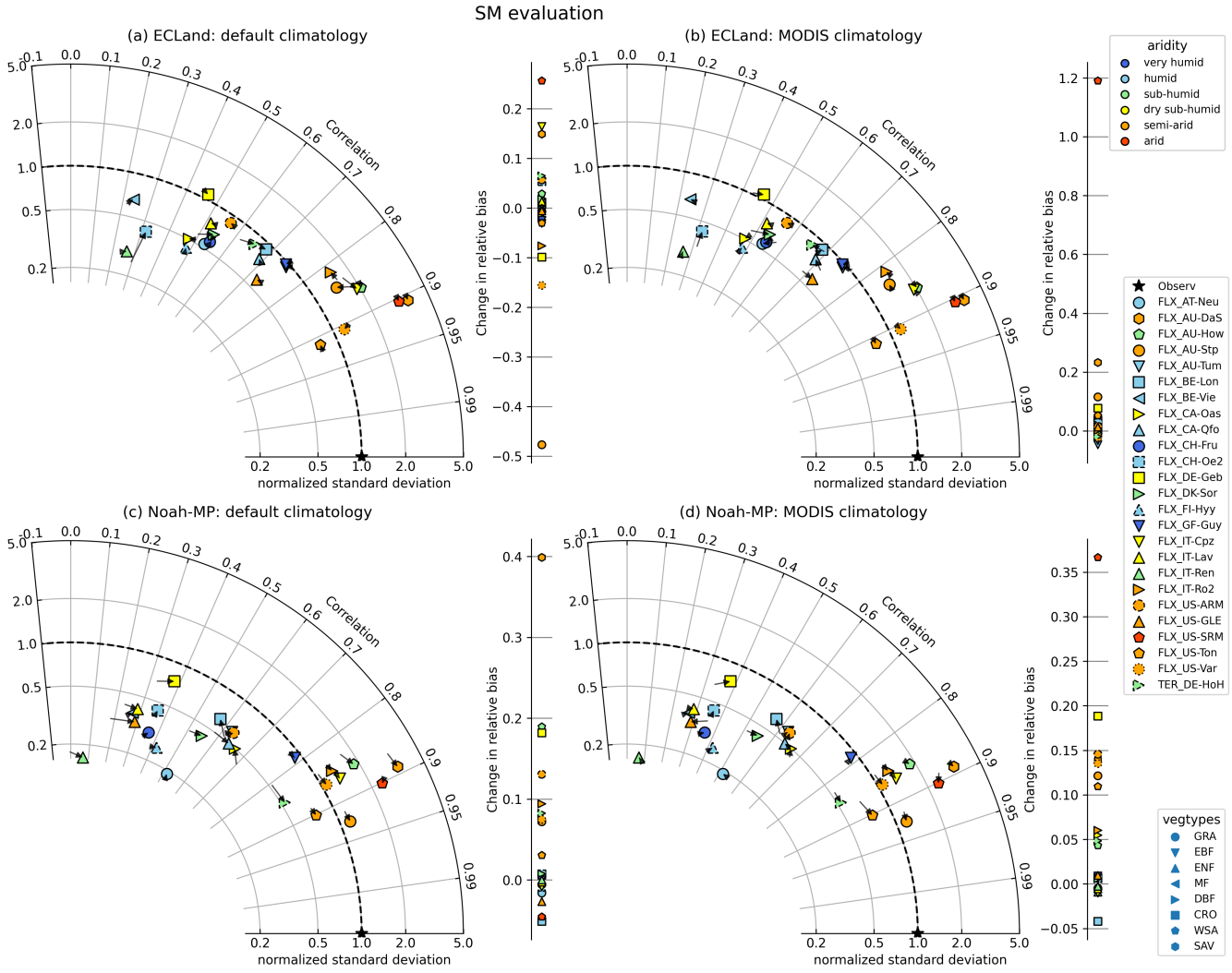

Figure A2. Same as before but for soil moisture.

A.04 Performance metrics tables

Table A1. Relative bias for LAI. The word climatology is shortened with clim.. MODIS single refers to the MODIS single-year setup.

ECLand						Location				
sim00	default clim.	sim02	MODIS clim.	sim40	MODIS single	sim42	sim50	default clim.	sim52	M
0% static	0% dynamic	0% static	0% dynamic	0% static	0% dynamic	Obs	0% static	0% dynamic	0% static	
-11height-68%	-34-77%	-26-28%	-73%	-32-31%	-74-73%	AT-Neu	-54%	-14%	65%	
0%	1822%	-22-24%	20%	-36-42%	19%	AU-DaS	-54%	2151%	-4-9%	
-8-7%	-20%	-15-17%	0-1%	-16-17%	-1%	AU-How	-75%	9127%	1-3%	
153%	-24%	-49-51%	-36%	-49-50%	-36%	AU-Stp	176%	214231%	-5-4%	
-31%	-74%	-3-1%	-72%	-20%	-72-71%	AU-Tum	0%	-5%	-20%	
2729%	4851%	-10-7%	48%	-9-10%	4847%	BE-Lon	-28%	110%	03%	
-18-26%	-23-19%	-8-16%	-18%	-9-15%	-18%	BE-Vie	3%	9%	1-6%	
-4%	-13-10%	-12%	-11%	-13-14%	-11%	CA-Oas	-3%	-7%	-2-3%	
551%	52%	-17%	47%	-17%	47%	CA-Qfo	200%	92%	-7%	
-19%	-67%	-32-35%	-67%	-34%	-67%	CH-Fru	-44%	-3%	-3-5%	
127-95%	133141%	-8-10%	148%	-6-10%	148%	CH-Oe2	6%	146%	20%	
5156%	4730%	-4-8%	26%	-6-11%	26%	DE-Geb	-20%	99%	83%	
-51-52%	-35-32%	-15-20%	-32-30%	-11-10%	-32-29%	DE-HoH	-45%	-18-16%	-6-9%	
521%	1644%	-9-11%	42%	-9-11%	42%	DK-Sor	13%	62%	1-1%	
-8%	-9%	-11-16%	-10%	-10-15%	-9-10%	FI-Hyy	62%	-11%	-1-6%	
-5%	-16%	64%	-16%	121%	-15-16%	GF-Guy	-7%	4%	85%	
31-32%	-14-9%	-105%	-25-7%	-10-1%	-25-7%	IT-Cpz	57%	21%	5%	
32%	-22%	0%	-24%	-3%	-24%	IT-Lav	109%	14%	212%	
52%	4-9%	-12-15%	-9%	-12-14%	-9%	IT-Ren	129%	29%	-1-5%	
-478%	-46-1%	-13%	-7%	-13-14%	-8%	IT-Ro2	-38%	22%	-10%	
32-9%	-1-51%	-36%	-53%	-37-36%	-53%	US-ARM	12%	144%	01%	
263266%	150152%	-15-14%	135%	-15-16%	136135%	US-GLE	872%	348%	-6-3%	
162182%	11231%	-14-13%	221%	-14%	220%	US-SRM	365%	186%	-6%	
29149%	-2887%	-14-15%	77%	-13-14%	77%	US-Ton	38%	93%	-2-3%	
818%	-44-57%	-39-40%	-61%	-40%	-61%	US-Var	-2%	100%	3-2%	

Relative bias for LAI.

Table A2. Relative bias for NEE. Note that a positive bias in NEE means an underestimation of carbon uptake by the ecosystem. Abbreviations in the headings are as before.

ECLand						Location				
sim00	default clim.	sim02	MODIS clim.	sim40	MODIS single	sim42	sim50	default clim.	sim52	M
0% static	0% dynamic	0% static	0% dynamic	0% static	0% dynamic	Obs	0% static	0% dynamic	0% static	
-10height-21%	-9-20%	-33-34%	-22%	-33%	-22%	AT-Neu	---19%	-23%	---25%	
6567%	6162%	6869%	62%	7072%	62%	AU-DaS	---9%	-4-6%	---11%	
6470%	6065%	6268%	6065%	6268%	6065%	AU-How	--8%	314%	--0%	
5657%	59%	65%	5960%	6465%	5960%	AU-Stp	---22%	42%	---22%	
-2%	2%	-3%	2%	-3%	2%	AU-Tum	---34%	-32%	---34%	
-6%	-6%	-3%	-6%	-3%	-6%	BE-Lon	---12%	-17%	---16%	
-818%	-616%	1415%	16%	15%	16%	BE-Vie	---6%	-6%	---5%	
-6%	-6%	-6-5%	-5%	-5%	-5%	CA-Oas	---23%	-9%	---22%	
-4-1%	-2%	-1410%	-4-1%	-1411%	-4-1%	CA-Qfo	-32%	-31%	-22%	
-17%	-6%	-15%	-6%	-15%	-6%	CH-Fru	---2%	-4-6%	---6%	
-125%	-11-20%	-9%	-20%	-9%	-20%	CH-Oe2	---20%	-26%	---21%	
-6-7%	-6-7%	-5-4%	-7%	-4%	-7%	DE-Geb	---15%	-18%	---19%	
87%	53%	3%	53%	32%	43%	DE-HoH	---16%	-6%	---21%	
-11-1%	-11-4%	0%	-4%	0%	-4%	DK-Sor	---20%	-7%	---19%	
5%	6%	56%	6%	6%	6%	FI-Hyy	---3%	-4%	---6%	
13%	14%	13%	14%	1314%	14%	GF-Guy	---62%	-54%	---62%	
4415%	4710%	497%	9%	8%	9%	IT-Cpz	-40%	-30%	-36%	
45%	49%	46%	49%	47%	49%	IT-Lav	--30%	32%	--32%	
320%	220%	1320%	1420%	1320%	1420%	IT-Ren	--0%	--5%	07%	
1214%	1419%	22%	19%	22%	1920%	IT-Ro2	---9%	3%	---18%	
4-3%	3-1%	-1%	-1%	-2%	-1%	US-ARM	---2%	-9%	---2%	
-1%	-10%	12%	0%	12%	0%	US-GLE	--27%	-19%	---7%	
2860%	3059%	59%	59%	59%	59%	US-SRM	---8%	-6%	---3%	
210%	28%	15%	9%	15%	9%	US-Ton	---7%	-9%	---8%	
-2-11%	-2-7%	-8-9%	-6-7%	-8-9%	-6-7%	US-Var	---4%	-13%	---9%	

Relative bias for NEE. Note that for static Noah-MP no NEE output is created.

Table A3. Relative bias for GPP. Abbreviations in the headings are as before.

ECLand						Location				
sim00	default clim.	sim02	MODIS clim.	sim40	MODIS single	sim42	sim50	default clim.	sim52	MODIS
0% static	0% dynamic	0% static	0% dynamic	0% static	0% dynamic	Obs	0% static	0% dynamic	0% static	0% dy
-25%	-26-25%	-15%	-24-23%	-15%	-24%	AT-Neu	--25%	-20%	--17%	
-36-38%	-30-31%	-38-39%	-31%	-41-42%	-31%	AU-DaS	--24%	-21-16%	--22%	-2
-41-44%	-35% -38%	-34-41%	-38%	-34-42%	-38%	AU-How	--33%	3-18%	--22%	
2116%	1712%	50%	1610%	60%	1610%	AU-Stp	-30%	3230%	--3%	
-8%	-14%	-6%	-14%	-6%	-14%	AU-Tum	-21%	23%	-21%	
-10-8%	-6-5%	-19-18%	-6%	-19%	-6%	BE-Lon	--7%	42%	-9%	
-19-27%	-21-24%	-22-23%	-24%	-22-24%	-24%	BE-Vie	--7%	-3%	--11%	
-14-13%	-15-14%	-13%	-14%	-14-15%	-14%	CA-Oas	-4%	8%	-2%	
-27-4%	-3%	-21%	-4%	-22%	-4%	CA-Qfo	69%	41%	2%	
-15%	-29%	-19-17%	-31-29%	-18-17%	-31-29%	CH-Fru	--32%	-25-23%	--23%	-2
-5-49%	-515%	-17%	16%	-17%	16%	CH-Oe2	--2%	35%	--1%	
-5-6%	-4-5%	-12%	-5%	-13%	-5%	DE-Geb	-4%	42%	-16%	
-24-25%	-18-17%	-15%	-18-16%	-14-13%	-18-16%	DE-HoH	--16%	0%	--5%	
-36-34%	-34-27%	-37-38%	-27%	-37-38%	-27%	DK-Sor	--27%	11-11%	--29%	
-25%	-25%	-25-26%	-25%	-25-27%	-25%	FI-Hyy	-10%	-8%	--10%	
-12%	-12%	-6-8%	-11-12%	-6-10%	-11-12%	GF-Guy	--2%	4%	-0%	
-45-22%	-49-13%	-10%	-12%	-12%	-12%	IT-Cpz	16%	14%	7%	
-51%	-58%	-53%	-58%	-59-54%	-58%	IT-Lav	--17%	-29%	--30%	
-20-39%	-18-40%	-29-39%	-30-40%	-29-39%	-30-40%	IT-Ren	-4%	3-11%	--21%	
-411%	-9-1%	-9%	-3%	-8-9%	-3%	IT-Ro2	--5%	30%	-14%	
-512%	-49%	8%	8%	10%	8%	US-ARM	-7%	38%	-7%	
-21-22%	-22-23%	-24-25%	-22-23%	-24-25%	-22-23%	US-GLE	-33%	13%	--15%	
-17-23%	-20-23%	-22%	-23%	-22%	-23%	US-SRM	-2%	5%	--11%	
-6-7%	-6-5%	-11%	-5%	-11%	-5%	US-Ton	--6%	3%	--5%	
-212%	-38%	9%	67%	9%	67%	US-Var	--1%	1516%	-5%	

Relative bias for GPP. Note that for static Noah-MP no GPP output is produced.

Table A4. Relative bias for latent heat flux. Abbreviations in the headings are as before.

ECLand						Location			
sim00	default clim.	sim02	MODIS clim.	sim40	MODIS single	sim42	sim50	default clim.	sim52
0% static	0% dynamic	0% static	0% dynamic	0% static	0% dynamic	Obs	0% static	0% dynamic	0% static
-36height-27%	-40-31%	-13%	-28%	-13%	-28%	AT-Neu	-25%	-19%	-21%
-25-27%	-17-18%	-28-30%	-18%	-34-37%	-18-19%	AU-DaS	-24-14%	-23-13%	-20-12%
-53%	-49%	-50-51%	-48%	-51%	-48%	AU-How	-31-43%	-29-43%	-29-40%
82%	4-1%	3-3%	4-1%	2-3%	4-1%	AU-Stp	78%	1-1%	-4-3%
-11%	-17%	-7%	-17%	-7%	-17%	AU-Tum	5%	7%	4%
-16%	-14%	-24-22%	-14%	-24%	-14%	BE-Lon	-3%	0%	-4-3%
8-27%	7-20%	-18-19%	-20%	-18-20%	-20%	BE-Vie	-5%	1%	-4%
-5-9%	-6-9%	-9%	-9%	-10%	-10%	CA-Oas	3%	8%	4%
-22%	-21%	-35%	-22%	-36%	-37-22%	-24CA-Qfo	-36%	-31-36%	-24-38%
-21%	-28%	-22%	-29%	-22%	-29%	CH-Fru	-32-30%	-26-25%	-31-29%
-14-65%	-15-1%	-26-25%	0%	-25%	0%	CH-Oe2	3%	9%	2%
-28%	-23%	-4-5%	2%	-8%	2%	DE-Geb	-2%	5%	-1%
-34-41%	-29-33%	-26-30%	-29-32%	-26-29%	-29-32%	DE-HoH	-17-12%	-14-8%	-16-11%
-7-37%	-4-29%	-37-36%	-29%	-37%	-29%	DK-Sor	-19%	-12%	-21%
-22%	-21%	-21-22%	-21%	-21-22%	-21%	FI-Hyy	-34%	-32%	-35%
-31%	-36%	-25-26%	-35%	-24-30%	-35-36%	GF-Guy	-17%	-15%	-17%
-41-21%	-43-8%	-47-1%	-7%	-3%	-7%	IT-Cpz	17%	16%	16%
-40%	-46%	-42%	-47%	-48-43%	-47%	IT-Lav	-50%	-47%	-50%
-16-41%	-14-41%	-34-41%	-35-41%	-34-41%	-35-41%	IT-Ren	-37-43%	-35-41%	-38-43%
-12-30%	-17-38%	-39%	-39%	-39%	-39%	IT-Ro2	-9%	-6%	-8%
76%	34%	7%	4%	6%	4%	US-ARM	6%	11%	87%
-58-62%	-60-64%	-66-68%	-61-64%	-66-68%	-61-64%	US-GLE	-52-54%	-59-63%	-69-73%
-21-22%	-21%	-27%	-21%	-26%	-22%	US-SRM	-20%	-19%	-21%
-5%	-6-12%	-20-19%	-14-13%	-20-19%	-14-13%	US-Ton	-10-8%	-10-7%	-12% -10%
29%	28%	2729%	27%	2628%	27%	26% US-Var	2021%	2223%	1617%

Relative bias for latent heat flux.

Table A5. Relative bias for evaporative fraction. Abbreviations in the headings are as before.

ECLand						Location			
sim00	default clim.	sim02	MODIS clim.	sim40	MODIS single	sim42	sim50	default clim.	sim52
0% static	0% dynamic	0% static	0% dynamic	0% static	0% dynamic	Obs	0% static	0% dynamic	0% static
-37height-34%	-41-39%	-21%	-37%	-22%	-37%	AT-Neu	-12%	-10%	-10-9%
-40-43%	-35-36%	-45-47%	-37%	-50-53%	-37%	AU-DaS	-51-40%	-43-34%	-43-35%
-49%	-45%	-46-47%	-45%	-47%	-45%	AU-How	-29-43%	-22-40%	-25-38%
-7-14%	-12-18%	-10-16%	-12-17%	-11-17%	-12-17%	AU-Stp	0-1%	-6-10%	-9-10%
-50%	-60%	-46-45%	-60%	-46-45%	-60%	AU-Tum	-26%	-23%	-27%
-4%	-5%	-10%	-6%	-11%	-6%	BE-Lon	8%	10%	9%
8-12%	5-10%	-9-10%	-10%	-9-10%	-10%	BE-Vie	0%	3%	0%
-3-4%	-3-5%	-5%	-5%	-5%	-5%	CA-Oas	-4%	-1%	-4%
-15-21%	-16-21%	-9-32%	-12-22%	-33%	-22%	CA-Qfo	-33%	-26%	-31%
-8%	-12%	CH-Fru -9%	-12%	-9%	-8-12%	CH-Fru	-10%	-9%	-8-10%
-43-32%	-45-30%	-18%	-29%	-18%	-29%	CH-Oe2	-4%	-4%	-5%
410%	14%	10%	3%	-2%	3%	DE-Geb	8%	13%	11%
-56-52%	-51-46%	-49-45%	-51-45%	-48-43%	-51-45%	DE-HoH	-27%	-20-21%	-25-26%
2-14%	2-11%	-15%	-11%	-15%	-11%	DK-Sor	-9%	-4%	-10%
-5%	-6%	-5-6%	-6%	-6%	-6%	FI-Hyy	-11%	-10%	-12%
-73%	-78%	-60-63%	-78%	-59-67%	-77-78%	GF-Guy	-48%	-42%	-47%
-25-12%	-2900%	9%	1%	7%	1%	IT-Cpz	34%	34%	33%
-25%	-31%	-32-28%	-32%	-29%	-32%	IT-Lav	-33%	-30%	-34%
5-7%	5-8%	-6-8%	-6-8%	-6-8%	-6-8%	IT-Ren	-11-13%	-9-12%	-11-13%
18-7%	11-17%	-22%	-18%	-22%	-18%	IT-Ro2	6%	16%	11%
-7%	-13-9%	-7%	-9%	-8%	-9%	US-ARM	1%	2%	4%
-35-41%	-39-44%	-48-50%	-43-45%	-48-50%	-43-45%	US-GLE	-29%	-27-26%	-30-31%
-4-8%	-2-7%	-11%	-7%	-11%	-7%	US-SRM	-15%	-9%	-13%
95%	80%	-6%	0%	-6%	0%	US-Ton	1%	3%	23%
98%	72%	67%	12%	6%	12%	US-Var	89%	89%	1415%

Relative bias for evaporative fraction.

Table A6. Relative bias of soil moisture. Abbreviations in the headings are as before.

ECLand						Location				
sim00	default clim.	sim02	MODIS clim.	sim40	MODIS single	sim42	sim50	default clim.	sim52	MOD
0% static	0% dynamic	0% static	0% dynamic	0% static	0% dynamic	Obs	0% static	0% dynamic	0% static	0% d
5height1%	62%	-5%	1%	-4%	1%	AT-Neu	-10%	-11%	-10-11%	
687695%	674680%	704%	681%	709711%	681%	AU-DaS	371481%	353441%	357455%	3
194196%	191193%	197198%	193%	197198%	193%	AU-How	192129%	146110%	169114%	1
102116%	147163%	161180%	151169%	160179%	151169%	AU-Stp	4762%	4154%	5266%	
54%	57%	52%	57%	52%	57%	AU-Tum	29%	28%	29%	
10%	9%	1413%	9%	14%	9%	BE-Lon	-8%	-13%	-8%	
2937%	2936%	3536%	36%	3536%	36%	BE-Vie	7%	7%	7%	
127131%	130133%	132133%	133%	133%	134%	CA-Oas	73%	65%	71%	
-2884%	-2883%	86%	83%	86%	83%	CA-Qfo	97%	96%	95%	
-33%	-32%	-31-33%	-32%	-33%	-31-32%	CH-Fru	-44%	-44%	-44%	
5053%	5047%	50%	47%	50%	47%	CH-Oe2	29%	28%	29%	
9782%	9892%	100101%	93%	102%	93%	DE-Geb	45%	27%	4445%	
167161%	163154%	158152%	163154%	157150%	162153%	DE-HoH	111109%	103101%	107106%	1
6980%	6878%	7980%	7778%	7880%	7778%	DK-Sor	1112%	11%	11%	
51%	50%	5051%	50%	50%	50%	FI-Hyy	-3%	-4%	-3%	
251%	253%	250%	253%	250251%	253%	GF-Guy	160159%	159%	160%	1
246%	160% 230%	228%	229%	230%	239%	IT-Cpz	124%	125%	124%	
-86-87%	-85%	-85-86%	-85%	-85-86%	-85%	IT-Lav	-25%	-25%	-25%	
-44-42%	-44-42%	-42%	-42%	-42%	-42%	IT-Ren	-11%	-11%	-11%	
-1275%	-1083%	1384%	1283%	1383%	1283%	IT-Ro2	-1825%	-2216%	-1922%	
17-7%	21-1%	-2%	0%	-2%	0%	US-ARM	14%	1%	16%	
48%	48%	50%	49%	50%	49%	US-GLE	36%	38%	39%	
314455%	398429%	552%	433%	552%	433%	US-SRM	298%	303%	339%	
736%	1039%	45%	40%	45%	40%	US-Ton	6%	3%	14%	
58%	6274%	72%	74%	72%	74%	US-Var	60%	53%	6566%	

Relative bias of soil moisture

Author contributions. SW prepared model setups for the selected sites and prepared input data from available datasets in consultation with ST and AH. Model source code was provided by ST. SB supported setup of ECLand model runs. Simulations, analysis and plotting were done by SW with the involvement of AH and ST. SW took the lead in writing the manuscript with contributions from all authors.

Competing interests. The authors declare that they have no conflict of interest.

Acknowledgements. This work used eddy covariance data acquired and shared by the FLUXNET community and by the TERENO network. On-site LAI data from site "Hohes Holz" was acquired, analyzed, and shared by the working group Model Driven Monitoring ~~lead by~~ led by site PI Corinna Rebmann at ~~UFZ~~Helmholtz-Centre for Environmental Research - UFZ. We thank all station PIs, scientists, and technicians for their efforts in collecting, processing, and sharing their data.

References

Arsenault, K. R., Nearing, G. S., Wang, S., Yatheendradas, S., and Peters-Lidard, C. D.: Parameter Sensitivity of the Noah-MP Land Surface Model with Dynamic Vegetation, Journal of Hydrometeorology, 19, 815 –830, https://doi.org/10.1175/jhm-d-17-0205.1, 2018.

Ashaolu, E. D. and Iroye, K. A.: Rainfall and potential evapotranspiration patterns and their effects on climatic water balance in the Western Lithoral Hydrological Zone of Nigeria, Ruhuna Journal of Science, 9, https://doi.org/10.4038/rjs.v9i2.45, 2018.

Ball, J. T., Woodrow, I. E., and Berry, J. A.: A Model Predicting Stomatal Conductance and its Contribution to the Control of Photosynthesis under Different Environmental Conditions, pp. 221–224, Springer Netherlands, Dordrecht, https://doi.org/10.1007/978-94-017-0519-6_48, 1987.

Balsamo, G., Viterbo, P., Beljaars, A., van den Hurk, B., Hirschi, M., Betts, A. K., and Scipal, K.: A Revised Hydrology for the ECMWF Model: Verification from Field Site to Terrestrial Water Storage and Impact in the Integrated Forecast System, Journal of Hydrometeorology, 10, 623–643, https://doi.org/10.1175/2008jhm1068.1, 2009.

Beck, H. E., Pan, M., Miralles, D. G., Reichle, R. H., Dorigo, W. A., Hahn, S., Sheffield, J., Karthikeyan, L., Balsamo, G., Parinussa, R. M., van Dijk, A. I. J. M., Du, J., Kimball, J. S., Vergopolan, N., and Wood, E. F.: Evaluation of 18 satellite- and model-based soil moisture products using in situ measurements from 826 sensors, Hydrology and Earth System Sciences, 25, 17–40, https://doi.org/10.5194/hess-25-17-2021, 2021.

Benesty, J., Chen, J., Huang, Y., and Cohen, I.: Pearson correlation coefficient, in: Noise reduction in speech processing, pp. 37–40, Springer, 2009.

Best, M. J., Abramowitz, G., Johnson, H. R., Pitman, A. J., Balsamo, G., Boone, A., Cuntz, M., Decharme, B., Dirmeyer, P. A., Dong, J., Ek, M., Guo, Z., Haverd, V., van den Hurk, B. J. J., Nearing, G. S., Pak, B., Peters-Lidard, C., Santanello, J. A., Stevens, L., and Vuichard, N.: The Plumbing of Land Surface Models: Benchmarking Model Performance, Journal of Hydrometeorology, 16, 1425–1442, https://doi.org/10.1175/jhm-d-14-0158.1, 2015.

Blyth, E. M., Arora, V. K., Clark, D. B., Dadson, S. J., De Kauwe, M. G., Lawrence, D. M., Melton, J. R., Pongratz, J., Turton, R. H., Yoshimura, K., and Yuan, H.: Advances in Land Surface Modelling, Current Climate Change Reports, 7, 45–71, https://doi.org/10.1007/s40641-021-00171-5, 2021.

Bohm, K., Ingwersen, J., Milovac, J., and Streck, T.: Distinguishing between early- and late-covering crops in the land surface model Noah-MP: impact on simulated surface energy fluxes and temperature, Biogeosciences, 17, 2791–2805, https://doi.org/10.5194/bg-17-2791-2020, 2020.

Bonan, G. B.: Land surface model (LSM version 1.0) for ecological, hydrological, and atmospheric studies: Technical description and user's guide., Technical Note PB-97-131494/XAB; NCAR/TN-417-STR; TRN: 70341497, U.S. Department of Energy, Office of Scientific and Technical Information, https://www.osti.gov/biblio/442360, 1996.

Boussetta, S., Balsamo, G., Beljaars, A., Kral, T., and Jarlan, L.: Impact of a satellite-derived leaf area index monthly climatology in a global numerical weather prediction model, International Journal of Remote Sensing, 34, 3520–3542, https://doi.org/10.1080/01431161.2012.716543, 2012.

Boussetta, S., Balsamo, G., Beljaars, A., Panareda, A.-A., Calvet, J.-C., Jacobs, C., van den Hurk, B., Viterbo, P., Lafont, S., Dutra, E., Jarlan, L., Balzarolo, M., Papale, D., and van der Werf, G.: Natural land carbon dioxide exchanges in the ECMWF integrated forecasting system: Implementation and offline validation, Journal of Geophysical Research: Atmospheres, 118, 5923–5946, https://doi.org/https://doi.org/10.1002/jgrd.50488, 2013.

Boussetta, S., Balsamo, G., Dutra, E., Beljaars, A., and Albergel, C.: Assimilation of surface albedo and vegetation states from satellite observations and their impact on numerical weather prediction, Remote Sensing of Environment, 163, 111–126, https://doi.org/10.1016/j.rse.2015.03.009, 2015.

Boussetta, S., Balsamo, G., Arduini, G., Dutra, E., McNorton, J., Choulga, M., Agustí-Panareda, A., Beljaars, A., Wedi, N., Munõz-Sabater, J., de Rosnay, P., Sandu, I., Hadade, I., Carver, G., Mazzetti, C., Prudhomme, C., Yamazaki, D., and Zsoter, E.: ECLand: The ECMWF Land Surface Modelling System, Atmosphere, 12, https://doi.org/10.3390/atmos12060723, 2021.

Brunsell, N. A., de Oliveira, G., Barlage, M., Shimabukuro, Y., Moraes, E., and Aragão, L.: Examination of seasonal water and carbon dynamics in eastern Amazonia: a comparison of Noah-MP and MODIS, Theoretical and Applied Climatology, 143, 571–586, https://doi.org/10.1007/s00704-020-03435-6, 2020.

Budyko, M. I.: Climate and Life: English Ed. edited by David H. Miller, Academic Press, New York, 1974.

Cai, X., Yang, Z.-L., Xia, Y., Huang, M., Wei, H., Leung, L. R., and Ek, M. B.: Assessment of simulated water balance from Noah, Noah-MP, CLM, and VIC over CONUS using the NLDAS test bed, Journal of Geophysical Research: Atmospheres, 119, 13,751–13,770, https://doi.org/10.1002/2014jd022113, 2014.

Calvet, J. C. and Soussana, J. F.: Modelling CO2-enrichment effects using an interactive vegetation SVAT scheme, Agricultural and Forest Meteorology, 108, 129–152, https://doi.org/Doi 10.1016/S0168-1923(01)00235-0, 2001.

Calvet, J. C., Noilhan, J., Roujean, J. L., Bessemoulin, P., Cabelguenne, M., Olioso, A., and Wigneron, J. P.: An interactive vegetation SVAT model tested against data from six contrasting sites, Agricultural and Forest Meteorology, 92, 73–95, https://doi.org/Doi 10.1016/S0168-1923(98)00091-4, 1998.

Chen, F. and Dudhia, J.: Coupling an advanced land surface-hydrology model with the Penn State-NCAR MM5 modeling system. Part I: Model implementation and sensitivity, Monthly Weather Review, 129, 569–585, https://doi.org/Doi 10.1175/1520-0493(2001)129<0569:Caalsh>2.0.Co;2, 2001.

Copernicus: Climate Data Store, https://cds.climate.copernicus.eu/, accessed via: CDS API, last access: 2024-04-23, 2018.

Copin, Y.: Taylor diagram for python/matplotlib, https://doi.org/10.5281/zenodo.5548061, 2021.

De Kauwe, M. G., Zhou, S. X., Medlyn, B. E., Pitman, A. J., Wang, Y. P., Duursma, R. A., and Prentice, I. C.: Do land surface models need to include differential plant species responses to drought? Examining model predictions across a mesic-xeric gradient in Europe, Biogeosciences, 12, 7503–7518, https://doi.org/10.5194/bg-12-7503-2015, 2015.

Dickinson, R. E., Shaikh, M., Bryant, R., and Graumlich, L.: Interactive canopies for a climate model, Journal of Climate, 11, 2823–2836, https://doi.org/Doi 10.1175/1520-0442(1998)011<2823:Icfacm>2.0.Co;2, 1998.

Dirmeyer, P. A., Chen, L., Wu, J., Shin, C. S., Huang, B., Cash, B. A., Bosilovich, M. G., Mahanama, S., Koster, R. D., Santanello, J. A., Ek, M. B., Balsamo, G., Dutra, E., and Lawrence, D. M.: Verification of land-atmosphere coupling in forecast models, reanalyses and land surface models using flux site observations, J Hydrometeorol, 19, 375–392, https://doi.org/10.1175/JHM-D-17-0152.1, 2018.

Dirmeyer, P. A., Balsamo, G., Blyth, E. M., Morrison, R., and Cooper, H. M.: Land-Atmosphere Interactions Exacerbated the Drought and Heatwave Over Northern Europe During Summer 2018, AGU Advances, 2, https://doi.org/10.1029/2020av000283, 2021.

Dutra, E., Balsamo, G., Viterbo, P., Miranda, P. M. A., Beljaars, A., Schär, C., and Elder, K.: An Improved Snow Scheme for the ECMWF Land Surface Model: Description and Offline Validation, Journal of Hydrometeorology, 11, 899–916, https://doi.org/10.1175/2010jhm1249.1, 2010.

Ek, M. B., Mitchell, K. E., Lin, Y., Rogers, E., Grunmann, P., Koren, V., Gayno, G., and Tarpley, J. D.: Implementation of Noah land surface model advances in the National Centers for Environmental Prediction operational mesoscale Eta model, Journal of Geophysical Research: Atmospheres, 108, https://doi.org/10.1029/2002jd003296, 2003.

Fang, H., Wei, S., and Liang, S.: Validation of MODIS and CYCLOPES LAI products using global field measurement data, Remote Sensing of Environment, 119, 43–54, https://doi.org/10.1016/j.rse.2011.12.006, 2012.

Fisher, J. B., Huntzinger, D. N., Schwalm, C. R., and Sitch, S.: Modeling the Terrestrial Biosphere, Annual Review of Environment and Resources, 39, 91–123, https://doi.org/10.1146/annurev-environ-012913-093456, 2014.

fluxnet.org: FLUXNET2015 Dataset, https://fluxnet.org/data/fluxnet2015-dataset/, last access: 2024-04-23, 2020.

Forzieri, G., Miralles, D. G., Ciais, P., Alkama, R., Ryu, Y., Duveiller, G., Zhang, K., Robertson, E., Kautz, M., Martens, B., Jiang, C. Y., Arneth, A., Georgievski, G., Li, W., Ceccherini, G., Anthoni, P., Lawrence, P., Wiltshire, A., Pongratz, J., Piao, S. L., Sitch, S., Goll, D. S., Arora, V. K., Lienert, S., Lombardozzi, D., Kato, E., Nabel, J. E. M. S., Tian, H. Q., Friedlingstein, P., and Cescatti, A.: Increased control of vegetation on global terrestrial energy fluxes, Nature Climate Change, 10, 356–+, https://doi.org/10.1038/s41558-020-0717-0, 2020.

Garrigues, S., Lacaze, R., Baret, F., Morisette, J. T., Weiss, M., Nickeson, J. E., Fernandes, R., Plummer, S., Shabanov, N. V., Myneni, R. B., Knyazikhin, Y., and Yang, W.: Validation and intercomparison of global Leaf Area Index products derived from remote sensing data, Journal of Geophysical Research: Biogeosciences, 113, https://doi.org/10.1029/2007jg000635, 2008.

Garrigues, S., Verhoef, A., Blyth, E., Wright, A., Balan-Sarojini, B., Robinson, E. L., Dadson, S., Boone, A., Boussetta, S., and Balsamo, G.: Capability of the variogram to quantify the spatial patterns of surface fluxes and soil moisture simulated by land surface models, Progress in Physical Geography: Earth and Environment, 45, 279–293, https://doi.org/10.1177/0309133320986147, 2021.

Harrigan, S., Zoster, E., Cloke, H., Salamon, P., and Prudhomme, C.: Daily ensemble river discharge reforecasts and real-time forecasts from the operational Global Flood Awareness System, Hydrology and Earth System Sciences Discussions, pp. 1–22, https://doi.org/10.5194/hess-2020-532, publisher: Copernicus GmbH, 2020.

Haughton, N., Abramowitz, G., Pitman, A. J., Or, D., Best, M. J., Johnson, H. R., Balsamo, G., Boone, A., Cuntz, M., Decharme, B., Dirmeyer, P. A., Dong, J., Ek, M., Guo, Z., Haverd, V., van den Hurk, B. J. J., Nearing, G. S., Pak, B., Santanello, J. A., J., Stevens, L. E., and Vuichard, N.: The plumbing of land surface models: is poor performance a result of methodology or data quality?, J Hydrometeorol, 17, 1705–1723, https://doi.org/10.1175/JHM-D-15-0171.1, 2016.

Haughton, N., Abramowitz, G., De Kauwe, M. G., and Pitman, A. J.: Does predictability of fluxes vary between FLUXNET sites?, Biogeosciences, 15, 4495–4513, https://doi.org/10.5194/bg-15-4495-2018, 2018a.

Haughton, N., Abramowitz, G., and Pitman, A. J.: On the predictability of land surface fluxes from meteorological variables, Geoscientific Model Development, 11, 195–212, https://doi.org/10.5194/gmd-11-195-2018, 2018b.

Haverd, V., Smith, B., Nieradzik, L., Briggs, P. R., Woodgate, W., Trudinger, C. M., Canadell, J. G., and Cuntz, M.: A new version of the CABLE land surface model (Subversion revision r4601) incorporating land use and land cover change, woody vegetation demography, and a novel optimisation-based approach to plant coordination of photosynthesis, Geoscientific Model Development, 11, 2995–3026, https://doi.org/10.5194/gmd-11-2995-2018, 2018.

Hengl, T., de Jesus, J. M., MacMillan, R. A., Batjes, N. H., Heuvelink, G. B., Ribeiro, E., Samuel-Rosa, A., Kempen, B., Leenaars, J. G., Walsh, M. G., and Gonzalez, M. R.: SoilGrids1km–global soil information based on automated mapping, PLoS One, 9, e105 992, https://doi.org/10.1371/journal.pone.0105992, 2014.

Hersbach, H., Bell, B., Berrisford, P., Hirahara, S., Horányi, A., Muñoz-Sabater, J., Nicolas, J., Peubey, C., Radu, R., Schepers, D., Simmons, A., Soci, C., Abdalla, S., Abellan, X., Balsamo, G., Bechtold, P., Biavati, G., Bidlot, J., Bonavita, M., De Chiara, G., Dahlgren, P., Dee,

D., Diamantakis, M., Dragani, R., Flemming, J., Forbes, R., Fuentes, M., Geer, A., Haimberger, L., Healy, S., Hogan, R. J., Hólm, E., Janisková, M., Keeley, S., Laloyaux, P., Lopez, P., Lupu, C., Radnoti, G., de Rosnay, P., Rozum, I., Vamborg, F., Villaume, S., and Thépaut, J.-N.: The ERA5 global reanalysis, Q. J. Roy. Meteor. Soc., n/a, https://doi.org/10.1002/qj.3803, 2020.

Hu, Z., Piao, S., Knapp, A. K., Wang, X., Peng, S., Yuan, W., Running, S., Mao, J., Shi, X., Ciais, P., Huntzinger, D. N., Yang, J., and Yu, G.: Decoupling of greenness and gross primary productivity as aridity decreases, Remote Sensing of Environment, 279, 113 120, https://doi.org/10.1016/j.rse.2022.113120, 2022.

Huang, A., Shen, R., Di, W., and Han, H.: A methodology to reconstruct LAI time series data based on generative adversarial network and improved Savitzky-Golay filter, International Journal of Applied Earth Observation and Geoinformation, 105, https://doi.org/10.1016/j.jag.2021.102633, 2021.

Huang, A., Shen, R., Shi, C., and Sun, S.: Effects of satellite LAI data on modelling land surface temperature and related energy budget in the Noah-MP land surface model, Journal of Hydrology, 613, https://doi.org/10.1016/j.jhydrol.2022.128351, 2022.

Jarlan, L., Balsamo, G., Lafont, S., Beljaars, A., Calvet, J. C., and Mougin, E.: Analysis of leaf area index in the ECMWF land surface model and impact on latent heat and carbon fluxes: Application to West Africa, Journal of Geophysical Research: Atmospheres, 113, https://doi.org/10.1029/2007jd009370, 2008.

Jung, M., Koirala, S., Weber, U., Ichii, K., Gans, F., Camps-Valls, G., Papale, D., Schwalm, C., Tramontana, G., and Reichstein, M.: The FLUXCOM ensemble of global land-atmosphere energy fluxes, Scientific Data, 6, 74, https://doi.org/10.1038/s41597-019-0076-8, 2019.

Krinner, G., Derksen, C., Essery, R., Flanner, M., Hagemann, S., Clark, M., Hall, A., Rott, H., Brutel-Vuilmet, C., Kim, H., Ménard, C. B., Mudryk, L., Thackeray, C., Wang, L., Arduini, G., Balsamo, G., Bartlett, P., Boike, J., Boone, A., Chéruy, F., Colin, J., Cuntz, M., Dai, Y., Decharme, B., Derry, J., Ducharne, A., Dutra, E., Fang, X., Fierz, C., Ghattas, J., Gusev, Y., Haverd, V., Kontu, A., Lafaysse, M., Law, R., Lawrence, D., Li, W., Marke, T., Marks, D., Ménégoz, M., Nasonova, O., Nitta, T., Niwano, M., Pomeroy, J., Raleigh, M. S., Schaedler, G., Semenov, V., Smirnova, T. G., Stacke, T., Strasser, U., Svenson, S., Turkov, D., Wang, T., Wever, N., Yuan, H., Zhou, W., and Zhu, D.: ESM-SnowMIP: assessing snow models and quantifying snow-related climate feedbacks, Geoscientific Model Development, 11, 5027–5049, https://doi.org/10.5194/gmd-11-5027-2018, 2018.

Kumar, S. V., M. Mocko, D., Wang, S., Peters-Lidard, C. D., and Borak, J.: Assimilation of Remotely Sensed Leaf Area Index into the Noah-MP Land Surface Model: Impacts on Water and Carbon Fluxes and States over the Continental United States, Journal of Hydrometeorology, 20, 1359–1377, https://doi.org/10.1175/jhm-d-18-0237.1, 2019.

Lawrence, D. M., Fisher, R. A., Koven, C. D., Oleson, K. W., Swenson, S. C., Bonan, G., Collier, N., Ghimire, B., van Kampenhout, L., Kennedy, D., Kluzek, E., Lawrence, P. J., Li, F., Li, H., Lombardozzi, D., Riley, W. J., Sacks, W. J., Shi, M., Vertenstein, M., Wieder, W. R., Xu, C., Ali, A. A., Badger, A. M., Bisht, G., van den Broeke, M., Brunke, M. A., Burns, S. P., Buzan, J., Clark, M., Craig, A., Dahlin, K., Drewniak, B., Fisher, J. B., Flanner, M., Fox, A. M., Gentine, P., Hoffman, F., Keppel-Aleks, G., Knox, R., Kumar, S., Lenaerts, J., Leung, L. R., Lipscomb, W. H., Lu, Y., Pandey, A., Pelletier, J. D., Perket, J., Randerson, J. T., Ricciuto, D. M., Sanderson, B. M., Slater, A., Subin, Z. M., Tang, J., Thomas, R. Q., Val Martin, M., and Zeng, X.: The Community Land Model Version 5: Description of New Features, Benchmarking, and Impact of Forcing Uncertainty, Journal of Advances in Modeling Earth Systems, 11, 4245–4287, https://doi.org/10.1029/2018MS001583, _eprint: https://onlinelibrary.wiley.com/doi/pdf/10.1029/2018MS001583, 2019.

Lawrence, P. J., Lawrence, D. M., and Hurtt, G. C.: Attributing the Carbon Cycle Impacts of CMIP5 Historical and Future Land Use and Land Cover Change in the Community Earth System Model (CESM1), Journal of Geophysical Research: Biogeosciences, 123, 1732–1755, https://doi.org/10.1029/2017jg004348, 2018.

Li, J., Zhang, G., Chen, F., Peng, X., and Gan, Y.: Evaluation of Land Surface Subprocesses and Their Impacts on Model Performance With Global Flux Data, Journal of Advances in Modeling Earth Systems, 11, 1329–1348, https://doi.org/10.1029/2018ms001606, 2019.

Li, J., Chen, F., Lu, X., Gong, W., Zhang, G., and Gan, Y.: Quantifying Contributions of Uncertainties in Physical Parameterization Schemes and Model Parameters to Overall Errors in Noah-MP Dynamic Vegetation Modeling, Journal of Advances in Modeling Earth Systems, 12, https://doi.org/10.1029/2019ms001914, 2020.

Li, J., Miao, C., Zhang, G., Fang, Y., Shangguan, W., and Niu, G.: Global Evaluation of the Noah-MP Land Surface Model and Suggestions for Selecting Parameterization Schemes, Journal of Geophysical Research: Atmospheres, 127, https://doi.org/10.1029/2021jd035753, 2022a.

Li, L., Yang, Z., Matheny, A. M., Zheng, H., Swenson, S. C., Lawrence, D. M., Barlage, M., Yan, B., McDowell, N. G., and Leung, L. R.: Representation of Plant Hydraulics in the Noah-MP Land Surface Model: Model Development and Multiscale Evaluation, Journal of Advances in Modeling Earth Systems, 13, https://doi.org/10.1029/2020ms002214, 2021.

Li, W., Migliavacca, M., Forkel, M., Denissen, J. M. C., Reichstein, M., Yang, H., Duveiller, G., Weber, U., and Orth, R.: Widespread increasing vegetation sensitivity to soil moisture, Nat Commun, 13, 3959, https://doi.org/10.1038/s41467-022-31667-9, 2022b.

Liang, J., Yang, Z., and Lin, P.: Systematic Hydrological Evaluation of the Noah-MP Land Surface Model over China, Advances in Atmospheric Sciences, 36, 1171–1187, https://doi.org/10.1007/s00376-019-9016-y, 2019.

Liang, J., Yang, Z.-L., Cai, X., Lin, P., Zheng, H., and Bian, Q.: Modeling the Impacts of Nitrogen Dynamics on Regional Terrestrial Carbon and Water Cycles over China with Noah-MP-CN, Advances in Atmospheric Sciences, 37, 679–695, https://doi.org/10.1007/s00376-020-9231-6, 2020.

Liu, X., Chen, F., Barlage, M., Zhou, G., and Niyogi, D.: Noah-MP-Crop: Introducing dynamic crop growth in the Noah-MP land surface model, Journal of Geophysical Research: Atmospheres, 121, 13,953–13,972, https://doi.org/10.1002/2016jd025597, 2016.

Luo, J., Ying, K., and Bai, J.: Savitzky-Golay smoothing and differentiation filter for even number data, Signal Processing, 85, 1429–1434, https://doi.org/10.1016/j.sigpro.2005.02.002, 2005.

Ma, N., Niu, G.-Y., Xia, Y., Cai, X., Zhang, Y., Ma, Y., and Fang, Y.: A Systematic Evaluation of Noah-MP in Simulating Land-Atmosphere Energy, Water, and Carbon Exchanges Over the Continental United States, Journal of Geophysical Research: Atmospheres, 122, 12,245–12,268, https://doi.org/10.1002/2017jd027597, 2017.

Menard, C. B., Essery, R., Krinner, G., Arduini, G., Bartlett, P., Boone, A., Brutel-Vuilmet, C., Burke, E., Cuntz, M., Dai, Y., Decharme, B., Dutra, E., Fang, X., Fierz, C., Gusev, Y., Hagemann, S., Haverd, V., Kim, H., Lafaysse, M., Marke, T., Nasonova, O., Nitta, T., Niwano, M., Pomeroy, J., Schädler, G., Semenov, V. A., Smirnova, T., Strasser, U., Swenson, S., Turkov, D., Wever, N., and Yuan, H.: Scientific and Human Erros in a Snow Model Intercomparison, https://doi.org/https://doi.org/10.1175/BAMS-D-19-0329.1, 2021.

Myneni, R., Knyazikhin, Y., and Park, T.: MOD15A2H MODIS/Terra Leaf Area Index/FPAR 8-Day L4 Global 500m SIN Grid V006, https://doi.org/https://doi.org/10.5067/MODIS/MOD15A2H.006, 2015.

National Center for Atmospheric Research: The Climate Data Guide: CERES: IGBP Land Classification., https://climatedataguide.ucar.edu/climate-data/ceres-igbp-land-classification, accessed: 2024-06-03, 2022.

Niu, G.-Y., Yang, Z.-L., Dickinson, R. E., Gulden, L. E., and Su, H.: Development of a simple groundwater model for use in climate models and evaluation with Gravity Recovery and Climate Experiment data, Journal of Geophysical Research, 112, https://doi.org/10.1029/2006jd007522, 2007.

Niu, G.-Y., Yang, Z.-L., Mitchell, K. E., Chen, F., Ek, M. B., Barlage, M., Kumar, A., Manning, K., Niyogi, D., Rosero, E., Tewari, M., and Xia, Y.: The community Noah land surface model with multiparameterization options (Noah-MP): 1. Model description and evaluation with local-scale measurements, Journal of Geophysical Research, 116, https://doi.org/10.1029/2010jd015139, 2011.

Nogueira, M., Boussetta, S., Balsamo, G., Albergel, C., Trigo, I. F., Johannsen, F., Miralles, D. G., and Dutra, E.: Upgrading Land-Cover and Vegetation Seasonality in the ECMWF Coupled System: Verification With FLUXNET Sites, METEOSAT Satellite Land Surface Temperatures, and ERA5 Atmospheric Reanalysis, J Geophys Res Atmos, 126, e2020JD034 163, https://doi.org/10.1029/2020JD034163, 2021.

Pastorello, G., Trotta, C., Canfora, E., Chu, H., Christianson, D., Cheah, Y. W., Poindexter, C., Chen, J., Elbashandy, A., Humphrey, M., Isaac, P., Polidori, D., Reichstein, M., Ribeca, A., van Ingen, C., Vuichard, N., Zhang, L., Amiro, B., Ammann, C., Arain, M. A., Ardo, J., Arkebauer, T., Arndt, S. K., Arriga, N., Aubinet, M., Aurela, M., Baldocchi, D., Barr, A., Beamesderfer, E., Marchesini, L. B., Bergeron, O., Beringer, J., Bernhofer, C., Berveiller, D., Billesbach, D., Black, T. A., Blanken, P. D., Bohrer, G., Boike, J., Bolstad, P. V., Bonal, D., Bonnefond, J. M., Bowling, D. R., Bracho, R., Brodeur, J., Brummer, C., Buchmann, N., Burban, B., Burns, S. P., Buysse, P., Cale, P., Cavagna, M., Cellier, P., Chen, S., Chini, I., Christensen, T. R., Cleverly, J., Collalti, A., Consalvo, C., Cook, B. D., Cook, D., Coursolle, C., Cremonese, E., Curtis, P. S., D'Andrea, E., da Rocha, H., Dai, X., Davis, K. J., Cinti, B., Grandcourt, A., Ligne, A., De Oliveira, R. C., Delpierre, N., Desai, A. R., Di Bella, C. M., Tommasi, P. D., Dolman, H., Domingo, F., Dong, G., Dore, S., Duce, P., Dufrene, E., Dunn, A., Dusek, J., Eamus, D., Eichelmann, U., ElKhidir, H. A. M., Eugster, W., Ewenz, C. M., Ewers, B., Famulari, D., Fares, S., Feigenwinter, I., Feitz, A., Fensholt, R., Filippa, G., Fischer, M., Frank, J., Galvagno, M., Gharun, M., et al.: The FLUXNET2015 dataset and the ONEFlux processing pipeline for eddy covariance data, Sci Data, 7, 225, https://doi.org/10.1038/s41597-020-0534-3, 2020.

Piayda, A., Dubbert, M., Werner, C., Vaz Correia, A., Pereira, J. S., and Cuntz, M.: Influence of woody tissue and leaf clumping on vertically resolved leaf area index and angular gap probability estimates, Forest Ecology and Management, 340, 103–113, https://doi.org/https://doi.org/10.1016/j.foreco.2014.12.026, 2015.

Pilotto, I. L., Rodríguez, D. A., Tomasella, J., Sampaio, G., and Chou, S. C.: Comparisons of the Noah-MP land surface model simulations with measurements of forest and crop sites in Amazonia, Meteorology and Atmospheric Physics, 127, 711–723, https://doi.org/10.1007/s00703-015-0399-8, 2015.

Rebmann, C. and Pohl, F.: Carbon, water and energy fluxes at the TERENO/ICOS ecosystem station Hohes Holz in Central Germany since 2015, https://doi.org/10.1594/PANGAEA.940760, 2023.

Ruiz-Vásquez, M., O, S., Arduini, G., Boussetta, S., Brenning, A., Bastos, A., Koirala, S., Balsamo, G., Reichstein, M., and Orth, R.: Impact of Updating Vegetation Information on Land Surface Model Performance, Journal of Geophysical Research: Atmospheres, 128, https://doi.org/10.1029/2023jd039076, 2023.

Sakaguchi, K. and Zeng, X.: Effects of soil wetness, plant litter, and under-canopy atmospheric stability on ground evaporation in the Community Land Model (CLM3.5), Journal of Geophysical Research: Atmospheres, 114, https://doi.org/10.1029/2008jd010834, 2009.

Savitzky, A. and Golay, M. J. E.: Smoothing + Differentiation of Data by Simplified Least Squares Procedures, Analytical Chemistry, 36, 1627–, https://doi.org/DOI 10.1021/ac60214a047, 1964.

Sayed, A. H.: Fundamentals of adaptive filtering, John Wiley & Sons, 2003.

Schweppe, R., Thober, S., Müller, S., Kelbling, M., Kumar, R., Attinger, S., and Samaniego, L.: MPR 1.0: a stand-alone multiscale parameter regionalization tool for improved parameter estimation of land surface models, Geoscientific Model Development, 15, 859–882, https://doi.org/10.5194/gmd-15-859-2022, 2022.

Stevens, D., Miranda, P. M. A., Orth, R., Boussetta, S., Balsamo, G., and Dutra, E.: Sensitivity of Surface Fluxes in the ECMWF Land Surface Model to the Remotely Sensed Leaf Area Index and Root Distribution: Evaluation with Tower Flux Data, Atmosphere, 11, https://doi.org/10.3390/atmos11121362, 2020.

Trabucco, A. and Zomer, R. J.: Global Aridity Index and Potential Evapo-Transpiration (ET0) Climate Database v2, CGIAR-CSI GeoPortal, 2018.

Ukkola, A. M., De Kauwe, M. G., Pitman, A. J., Best, M. J., Abramowitz, G., Haverd, V., Decker, M., and Haughton, N.: Land surface models systematically overestimate the intensity, duration and magnitude of seasonal-scale evaporative droughts, Environmental Research Letters, 11, https://doi.org/10.1088/1748-9326/11/10/104012, 2016.

University Corporation for Atmospheric Research: Noah-Multiparameterization Land Surface Model (Noah-MP®LSM), https://ral.ucar.edu/model/noah-multiparameterization-land-surface-model-noah-mp-lsm, accessed: 2024-06-04, 2023.

van den Hurk, B. J. J. M., Viterbo, P., and Los, S. O.: Impact of leaf area index seasonality on the annual land surface evaporation in a global circulation model, Journal of Geophysical Research: Atmospheres, 108, https://doi.org/10.1029/2002jd002846, 2003.

van Genuchten, M. T.: A Closed-form Equation for Predicting the Hydraulic Conductivity of Unsaturated Soils, Soil Science Society of America Journal, 44, 892–898, https://doi.org/10.2136/sssaj1980.03615995004400050002x, 1980.

Weiss, M., Baret, F., Garrigues, S., and Lacaze, R.: LAI and fAPAR CYCLOPES global products derived from VEGETATION. Part 2: validation and comparison with MODIS collection 4 products, Remote Sensing of Environment, 110, 317–331, https://doi.org/10.1016/j.rse.2007.03.001, 2007.

Wollschläger, U., Attinger, S., Borchardt, D., Brauns, M., Cuntz, M., Dietrich, P., Fleckenstein, J. H., Friese, K., Friesen, J., Harpke, A., Hildebrandt, A., Jäckel, G., Kamjunke, N., Knöller, K., Kögler, S., Kolditz, O., Krieg, R., Kumar, R., Lausch, A., Liess, M., Marx, A., Merz, R., Mueller, C., Musolff, A., Norf, H., Oswald, S. E., Rebmann, C., Reinstorf, F., Rode, M., Rink, K., Rinke, K., Samaniego, L., Vieweg, M., Vogel, H.-J., Weitere, M., Werban, U., Zink, M., and Zacharias, S.: The Bode hydrological observatory: a platform for integrated, interdisciplinary hydro-ecological research within the TERENO Harz/Central German Lowland Observatory, Environmental Earth Sciences, 76, https://doi.org/10.1007/s12665-016-6327-5, 2016.

Xiao, Z., Liang, S., Wang, J., Jiang, B., and Li, X.: Real-time retrieval of Leaf Area Index from MODIS time series data, Remote Sensing of Environment, 115, 97–106, https://doi.org/10.1016/j.rse.2010.08.009, 2011.

Xiao, Z., Liang, S., Wang, J., Xiang, Y., Zhao, X., and Song, J.: Long-Time-Series Global Land Surface Satellite Leaf Area Index Product Derived From MODIS and AVHRR Surface Reflectance, IEEE Transactions on Geoscience and Remote Sensing, 54, 5301–5318, https://doi.org/10.1109/tgrs.2016.2560522, 2016.

Xu, T., Chen, F., He, X., Barlage, M., Zhang, Z., Liu, S., and He, X.: Improve the Performance of the Noah-MP-Crop Model by Jointly Assimilating Soil Moisture and Vegetation Phenology Data, Journal of Advances in Modeling Earth Systems, 13, https://doi.org/10.1029/2020ms002394, 2021.

Yang, F., Dan, L., Peng, J., Yang, X., Li, Y., and Gao, D.: Subdaily to Seasonal Change of Surface Energy and Water Flux of the Haihe River Basin in China: Noah and Noah-MP Assessment, Advances in Atmospheric Sciences, 36, 79–92, https://doi.org/10.1007/s00376-018-8035-4, 2018.

Yang, Q., Dan, L., Lv, M., Wu, J., Li, W., and Dong, W.: Quantitative assessment of the parameterization sensitivity of the Noah-MP land surface model with dynamic vegetation using ChinaFLUX data, Agricultural and Forest Meteorology, 307, https://doi.org/10.1016/j.agrformet.2021.108542, 2021.

Yang, Z.-L. and Niu, G.-Y.: Effects of Frozen Soil on Snowmelt Runoff and Soil Water Storage at a Continental Scale, Journal of Hydrometeorology, 7, 937–952, https://doi.org/10.1175/jhm538.1, 2006.

Yang, Z.-L., Niu, G.-Y., Mitchell, K. E., Chen, F., Ek, M. B., Barlage, M., Longuevergne, L., Manning, K., Niyogi, D., Tewari, M., and Xia, Y.: The community Noah land surface model with multiparameterization options (Noah-MP): 2. Evaluation over global river basins, Journal of Geophysical Research, 116, https://doi.org/10.1029/2010jd015140, 2011.

Zhang, G., Chen, F., and Gan, Y.: Assessing uncertainties in the Noah-MP ensemble simulations of a cropland site during the Tibet Joint International Cooperation program field campaign, Journal of Geophysical Research: Atmospheres, 121, 9576–9596, https://doi.org/10.1002/2016jd024928, 2016.

Zhang, X., Yan, K., Liu, J., Yang, K., Pu, J., Yan, G., Heiskanen, J., Zhu, P., Knyazikhin, Y., and Myneni, R. B.: An Insight Into the Internal Consistency of MODIS Global Leaf Area Index Products, IEEE Transactions on Geoscience and Remote Sensing, 62, 1–16, https://doi.org/10.1109/tgrs.2024.3434366, 2024.

Zhang, Z., Xin, Q., and Li, W.: Machine Learning-Based Modeling of Vegetation Leaf Area Index and Gross Primary Productivity Across North America and Comparison With a Process-Based Model, Journal of Advances in Modeling Earth Systems, p. 25, https://doi.org/10.1029/2021MS002802, 2021.